LABORATORY INVESTIGATIONS AND ANALYTICAL AND NUMERICAL MODELING OF THE TRANSPORT OF DISSOLVED SOLUTES THROUGH SATURATED FRACTURED ROCK

by

Timothy James Callahan

Submitted in Partial Fulfillment

of the Requirements for the

Doctorate of Philosophy in Hydrology

Department of Earth and Environmental Science

New Mexico Institute of Mining and Technology

Socorro, New Mexico U.S.A.

July 2001

ABSTRACT

The objective of this research was to determine the applicability of reactive tracer data obtained from laboratory tests to larger-scale field settings. Laboratory tracer tests were used to quantify transport properties in fractured volcanic ash flow tuff from southern Nevada. In a series of experiments, a pulse containing several ionic tracers was injected into four tuff cores, each containing one induced fracture oriented along the main axis. Multiple tests were also conducted at different flow velocities. Transport data from nonreactive tracers of different diffusivity allowed the separation of the effects of hydrodynamic dispersion within the fracture and molecular diffusion between flowing and nonflowing water within the systems, which was presumed to be in the fracture and bulk porous matrix, respectively. Reactive tracers were also included to estimate the sorption capacity of the tuffs.

The experiments verified the importance of fracture/matrix and solute/solid interactions in the fractured tuffs. Using artificial tracers of different physical and chemical properties in the same test provided unique interpretations of the tests and minimized uncertainty in transport parameter estimates. Compared to separate field tests in the rock types, the laboratory experiments tended to overestimate the degree of diffusive mass transfer and underestimate sorption capacity due to the small scale and high tracer concentrations, respectively. The first result suggests that geometry

differences between lab apparatuses and field systems precluded the direct extension of laboratory-derived transport parameters to field scales. For example, smaller-scale processes such as diffusion within the stagnant water in the fractures ("free-water diffusion"), caused by fracture aperture variability, were more important at small time scales. Because free water diffusion coefficients are larger than matrix diffusion coefficients, this led to an overestimation of the amount of diffusive mass transfer. Furthermore, laboratory diffusion cell tests provided independent estimates of matrix diffusion coefficients for the tracers, and these values were similar to those estimated for the same tracers in the field tests. Thus, the value of the diffusion coefficients in the larger-scale field tests appeared to approach their asymptotic "true" values because of the larger volume of porous rock accessed during tracer testing.

The sorption capacity of the solid material was underestimated in both the laboratory and field tracer experiments. A fraction of the ion-exchanging tracer (lithium) moved through the system unretarded because the ion exchange sites on the solid phase were overwhelmed by the tracer. This happened more so in the laboratory tests due to the smaller amount of dilution in the system. These results clearly indicate that by injecting high-concentration tracers during cross-well tests, the tracer data can indicate sorption parameters smaller than those determined under lower-concentration conditions.

These results indicate that one should be cautious when applying laboratory-derived tracer data to field settings. The use of multiple tracer experiments conducted over a wide range of time scales and injection concentrations will help avoid ambiguity of the derived transport parameters.

ACKNOWLEDGMENTS

Many thanks to the members of my dissertation committee, namely Paul Reimus, the Principal Investigator of the saturated zone field and laboratory testing for the Yucca Mountain Project at Los Alamos National Laboratory, who offered me the chance to work on this project and demonstrated patience over the past five years. Paul always took time to hear my ideas and freely share his insight, keeping me on the right track. Rob Bowman provided clear guidance on how to conduct research and always offered honest opinions concerning the project and what it takes to succeed as a hydrologist. John Wilson offered countless ideas and suggestions and helped me focus on the "big-picture" aspects of the research. Brian McPherson took time to discuss ideas not only concerning research problems but career development as well. Fred Phillips offered objective opinions on the quality of the research and I am grateful to have learned from him, and from the other professors at New Mexico Tech, how to teach. I hope to pass on their enthusiasm and knowledge in the future.

I have had valuable discussions with many people during my tenure as a graduate student, and thank Roy Haggerty, Allen Shapiro, Peter Lichtner, Jake Turin, Matt Becker, and Andy Wolfsberg.

Many people have offered their friendship over the past several years, especially Rod Flores, Mike Chapin, Sam Earman, Michelle Walvoord, Charlie Ferranti, Terry

Pollock, Joe Henton, Doug Warner, Michael Palmer, Mike Skov, Doug Ware, Brent Newman, and Greg Erpenbeck. These friends have made graduate school a rewarding experience.

I thank God for all the fortune in my life, and I thank my parents, James and Jean Callahan, who provided a stable environment in which learning was not simply a means to an end.

This dissertation is dedicated to my wife, Alyssa Olson, whose love and kindness have always given me strength.

TABLE OF CONTENTS

LIST OF TABLES

Page

LIST OF FIGURES

Page

1. Introduction

1.1. Scope

The Yucca Mountain Site Characterization Project was established to determine the suitability of Yucca Mountain, Nevada, U.S.A. as a potential site for the nation's first high-level nuclear waste repository. Relevant questions include: if radionuclides were to breach the artificial and natural containment structures of the potential repository, at what rate will these materials be transported in the saturated zone underlying Yucca Mountain? Which physical and chemical mechanisms will influence the transport time?

To answer these questions, experiments were conducted on rock materials obtained from the C-Wells complex on the Nevada Test Site, 150 km northwest of Las Vegas, NV (Figure 1.1). A thorough review of the C-Wells site is provided by *Geldon* [1993]. The motivation of this work was to investigate the applicability of laboratory-derived matrix diffusion coefficients to field-scale conditions. Because environmental permitting restrictions preclude the use of radionuclides in field tracer tests, it is important to understand the scaling relationships between laboratory- and field-derived parameters for nonradioactive tracers. If such relationships can be identified, more confidence can be placed on predictions of radionuclide transport based on laboratory data.

Figure 1.1. Map of Nevada, U.S.A. and photograph of Yucca Mountain (view to the southeast). The star on the map indicates the location of Yucca Mountain.

Several rock cores were obtained from different stratigraphic horizons (all within the saturated zone) at the C-Wells site, and a fracture was mechanically induced in each of the cores. A total of twenty-one transport tests were conducted in the fractured cores. In each test, a tracer solution was injected as a pulse and the effluent concentration was monitored over the duration of the test.

Multiple ionic tracers of different molecular diffusion coefficients were used to separate the effects of dispersion in the fractures and diffusive mass transfer between the fractures and porous matrix. The fractured aquifer at the C-Wells consists of volcanic ash flow tuff units with varying degrees of welding. The aquifer can be modeled as a dual-porosity system, in which the majority of flow is through fractures with a significant volume for solute storage in the pores of the unfractured matrix.

The objectives of this study were as follows:

a) determine transport parameters for dissolved tracers in fractured media,

b) determine the applicability of laboratory-derived parameters to field scales,

c) determine the applicability of parameters obtained under high-concentration conditions to lower-concentration pollutant situations.

Each chapter of this dissertation is written as a separate manuscript, either published as a technical journal article or to be submitted as such. Chapter 2 [*Callahan et al.*, 2000] provides a review of the theory behind solute transport in a dual-porosity medium and outlines the tracer data interpretation method. The discussion emphasizes the advantages of using several single-tracer tests conducted at different flow rates, or one multiple-tracer test, to better separate the effects of hydrodynamic dispersion in fractures and molecular diffusion in the porous matrix. Chapter 3 [*Callahan et al.*, in preparation, 2001a] and Chapter 4 [*Callahan et al.*, in preparation, 2001b] describe a numerical model that accounts for competing ions in predicting reactive solute transport in single- and dual-porosity media. Chapter 5 [*Callahan et al.*, in preparation, 2001c] discusses the apparent relationship between experimental time scale and the magnitude of the mass transfer coefficient describing solute partitioning between the fracture and matrix in dual-porosity rock. Finally, Chapter 6 summarizes the conclusions and provides some recommendations for future studies of solute transport in fractured rock.

1.2. Background

Proper management of groundwater resources requires an understanding of the processes that cause water contamination and affect the remediation of polluted aquifers. One way to estimate the potential transport of contaminants is by using tracers, which are

chemicals or particles that can track the movement of water in a flow system such as an aquifer and are easily detected. Testing involves injecting tracers and then monitoring the tracer concentrations as a function of location and/or time. Measuring tracers as a function of location requires a sampling array that covers a representative area of the system. This allows for monitoring of the spatial distribution of a tracer plume over time. Contaminated aquifers in unconsolidated porous media have been characterized at numerous field sites using a sampling array method where contaminant plumes migrated under natural-gradient conditions. Some examples are the Borden site, Ontario [*Sudicky*, 1986; *MacKay et al.*, 1986; *Freyberg*, 1986; *Roberts et al.*, 1986]; the Cape Cod site, Massachusetts [*LeBlanc et al.*, 1991; *Garabedian et al.*, 1991; *Brusseau and Srivastava*, 1999]; the Columbus Air Force Base, Mississippi [*Boggs et al.*, 1992; *Harvey and Gorelick*, 2000]; the Rocky Mountain Arsenal, Colorado [*Thorbjarnarson and MacKay*, 1997]; and the Vestskoven site, Denmark [*Sonnenborg et al.*, 1996; *Engesgaard and Traberg*, 1996]. However, the large number of sampling locations required in an array often restricts this method to shallow systems. Another field tracer investigation method involves conducting forced-gradient cross-well tests in which tracer responses are measured at one location as a function of time. The transport parameters are estimated by generating a tracer "breakthrough curve" (BTC) at the observation point (e.g., the pumping well) as a function of time (Figure 1.2). Examples of these types of experiments are the Horkheimer Insel site, Germany [*Ptak and Schmid*, 1996], Béthune, France [*Garnier et al.*, 1985; *Maloszewski and Zuber*, 1990; *Moench*, 1995], the Lange Bramke basin, Germany [*Maloszewski et al.*, 1999], the Finnsjön research area, Sweden [*Kimura and Munakata*, 1992], Funen, Denmark [*Sidle et al.*, 1998; *Broholm et al.*, 2000], the

Chalk River site, Ontario [*Novakowski et al.*, 1985; *Raven et al.*, 1988; *Novakowski,* 1992; *Novakowski and Lapcevic,* 1994; *Lapcevic et al.*, 1999], the Stripa Mine site, Sweden [*Birgersson and Neretnieks,* 1990; *Abelin et al.*, 1991; *Birgersson et al.*, 1993; *Abelin et al.*, 1994], the Oak Ridge National Laboratory [*Cook et al.*, 1996; *Jardine et al.*, 1999], Pahute Mesa, Nevada [*Reimus and Haga,* 1999], and the Yucca Mountain Site, Nevada [*Reimus et al.*, 1998; 1999]. All of the studies above except the study by *Ptak and Schmid* [1996] were conducted in fractured rock systems. Because it is difficult to estimate the location of the fractures, emplacement of a sampling array is usually inefficient. Point-to-point tracer methods (e.g., cross-well tests) are more easily managed than sampling arrays and allow for efficient collection of tracer transport data.

Figure 1.2. Examples of tracer breakthrough curves.

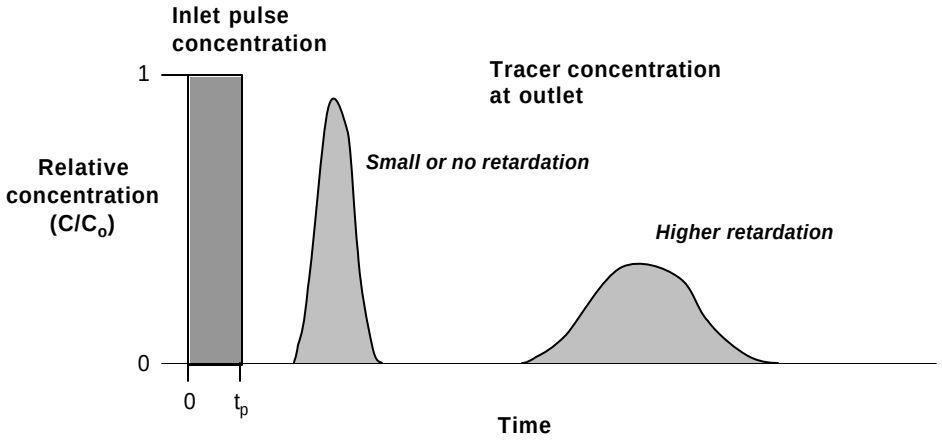

One of the main factors controlling transport of materials in the subsurface is the degree of flow heterogeneity. The distribution of hydraulic conductivities or permeabilities strongly influences the movement of contaminants over large distances in porous media. Heterogeneity tends to be greater in fractured rock aquifers, making the

interpretation and prediction of contaminant transport more difficult. Interpretations of transport responses in fractured aquifers have included several different modeling approaches, including discrete fracture networks, equivalent porous continuum models, and dual-continuum ("dual-porosity" or "dual-porosity/dual-permeability") models [*Neuzil and Tracy*, 1981; *Narasimhan*, 1982; *Huyakorn et al.*, 1983; *Moensch*, 1984; *Tsang*, 1995; *Maloszewski et al.*, 1999; *Lichtner*, 2000; *Callahan et al.*, 2000]. For the discrete network model, fracture connectivity is the most important parameter, yet it is also the most difficult to estimate in the field. In the equivalent porous continuum approach, transport occurs in a representative equivalent volume (REV) of fractured rock that is treated as a porous medium with given heterogeneity parameters. In the dual-continuum approach, solutes are assumed to be advectively transported predominantly in fractures with a considerable storage volume in the pores adjacent to the fractures, or to be transported by advection in both the fractures and the pores but at different rates (Figure 1.3). Regardless of whether solutes are advected within the porous rock surrounding the fractures, contaminant mass is assumed to access the entire system. Thus, the two most important transport parameters in the dual-continuum approach are the advective velocity and the coefficient of mass transfer between the advective and nonadvective domains.

Because of the high costs associated with field transport experiments, laboratory tests are often conducted to study contaminant transport in representative rock samples. Another advantage to laboratory experiments is the ability to constrain test interpretations by controlling flow geometry and by isolating the effects of certain transport

mechanisms, which can make the overall process of parameter estimation easier and the test interpretations less ambiguous.

Figure 1.3. The dual-continuum (dual-porosity or dual-porosity/dual-permeability) model. The variables v_f and v_m [L T^{-1}] refer to the linear velocity in the fracture and the matrix, respectively. D_m [L^2 T^{-1}] is the coefficient of diffusion in the porous matrix, and B [L] is the fracture aperture (assumed constant).

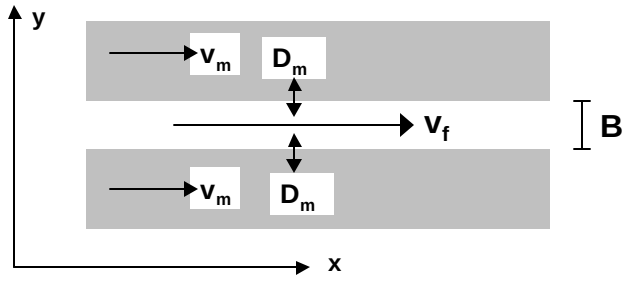

References

Abelin, H., L. Birgesson, J. Gidlund, and I. Neretnieks, A large-scale flow and tracer experiment in granite, 1. Experimental design and flow distribution, *Water Resour. Res., 27* (12), 3107-3117, 1991.

Abelin, H., L. Birgesson, H. Widén, T. Ågren, L. Moreno, and I. Neretnieks, Channeling experiments in crystalline fractured rocks, *J. Contam. Hyd., 15*, 129-158, 1994.

Birgersson, L. and I. Neretnieks, Diffusion in the matrix of granitic rock: Field test in the Stripa Mine, *Water Resour. Res., 26* (11), 2833-2842, 1990.

Birgersson, L., L. Moreno, I. Neretnieks, H. Widén, and T. Ågren, A tracer migration experiment in a small fracture zone in granite, *Water Resour. Res., 29* (12), 3867-3878, 1993.

Boggs, J. M., S. C. Young, L. M. Beard, L. W. Gelhar, K. R. Rehfeldt, and E. E. Adams, Field study of dispersion in a heterogeneous aquifer, 1, Overview and site description, *Water Resour. Res., 28*(12), 3281-3291, 1992.

Broholm, K., B. Nilsson, R. C. Sidle, and E. Arvin, Transport and biodegradation of creosote compounds in a clayey till, a field experiment, *J. Contam. Hyd., 41*, 239-260, 2000.

Brusseau, M. L. and R. Srivastava, Nonideal transport of reactive solutes in heterogeneous porous media, 4. Analysis of the Cape Cod natural-gradient field experiment, *Water Resour. Res., 35,* 1113-1125, 1999.

Callahan, T. J., P. W. Reimus, R. S. Bowman, and M. J. Haga, Using multiple experimental methods to determine fracture/matrix interactions and dispersion in saturated fractured volcanic tuff, *Water Resour. Res., 36*(12), 3547-3558, 2000.

Callahan, T. J., P. W. Reimus, P. C. Lichtner, and R. S. Bowman, Interpreting Asymmetric Transport Patterns of High Concentration Ionic Tracers in Porous Media, in preparation, 2001a.

Callahan, T. J., P. W. Reimus, P. C. Lichtner, and R. S. Bowman, Multicomponent Effects on the Transport of Cations Undergoing Ion Exchange in Saturated, Fractured Rock, in preparation, 2001b.

Callahan, T. J., P. W. Reimus, and R. S. Bowman, Influence of Solute Residence Time on Matrix Diffusion in Fractured, Saturated Rock, in preparation, 2001c.

Cook, P. G., D. K. Solomon, W. E. Sanford, E. Busenberg, L. N. Plummer, and R. J. Poreda, Inferring shallow groundwater flow in saprolite and fractured rock using environmental tracers, *Water Resour. Res., 32*(6), 1501-1509, 1996.

Engesgaard, P. and R. Traberg, Contaminant transport at a waste residue deposit, 2, Geochemical transport modeling, *Water Resour. Res., 32*(4), 939-951, 1996.

Freyberg, D. L., A natural gradient experiment on solute transport in a sand aquifer, 2, Spatial moments and the advection and dispersion of nonreactive tracers, *Water Resour. Res., 22*, 2031-2046, 1986.

Garabedian, S. P., D. R. LeBlanc, L. W. Gelhar, and M. A. Celia, Large-scale natural gradient tracer test in sand and gravel, Cape Cod, Massachusetts, 2, Analysis of spatial moments for a nonreactive tracer, *Water Resour. Res., 27,* 911-924, 1991.

Garnier, J. M., N. Crampon, C. Préaux, G. Porel, and M. Vreulx, Traçage pa ^{13}C, ^{2}H, I^-, et uranine dans la nappe de la craie sénonienne en écoulement radial convergent (Béthune, France), *J. Hydrol., 78*, 379-392, 1985.

Geldon, A. L., Preliminary hydrogeologic assessment of boreholes UE-25c#1, UE-25c#2, and UE-25c#3, Yucca Mountain, Nye County, Nevada, *Water-Resources Investigations Report 92-4016*, United States Geological Survey, Denver, CO, 1993.

Harvey, C. and S. M. Gorelick, Rate-limited mass transfer or macrodispersion: Which dominates plume evolution at the Macrodispersion Experiment (MADE) site? *Water Resour. Res., 36*(3): 637-650, 2000.

Huyakorn, P. S., B. H. Lester, and C. R. Faust, Finite element techniques for modeling groundwater flow in fractured aquifers, *Water Resour. Res., 19*, 1019-1035, 1983.

Jardine, P. M., W. E. Sanford, J.-P. Gwo, O. C. Reedy, D. S. Hicks, J. S. Riggs, and W. B. Bailey, Quantifying diffusive mass transfer in fractured shale bedrock, *Water Resour. Res., 35*, 2015-2030, 1999.

Kimura, H. and M. Munakata, Validation studies of tracer tests in a fracture zone at the Finnsjön research area, *Adv. Water Resour., 15*, 63-74, 1992.

Lapcevic, P. A., K. S. Novakowski, and E. A. Sudicky, The interpretation of a tracer experiment conducted under conditions of natural groundwater flow, *Water Resour. Res., 35*, 2301-2312, 1999.

LeBlanc, D. R., S. P. Garabedian, K. M. Hess, L. W. Gelhar, R. D. Quadri, K. G. Stollenwerk, and W. W. Wood, Large-scale natural gradient tracer test in sand and gravel, Cape Cod, Massachusetts, 1, Experimental design and observed tracer movement, *Water Resour. Res., 27*, 895-910, 1991.

Lichtner, P. C., Critique of dual continuum formulations of multicomponent reactive transport in fractured porous media, Dynamics of Fluids in Fractured Rock, B. Faybishenko, P. A. Witherspoon, and S. M. Benson (eds.), *Geophys. Mon. 122*, 281-298, Amer. Geophys. Union, 2000.

MacKay, D. M., D. L. Freyberg, and P. V. Roberts, A natural gradient experiment on solute transport in a sand aquifer, 1, Approach and overview of plume movement, *Water Resour. Res., 22*, 2017-2029, 1986.

Maloszewski, P. and A. Zuber, Mathematical modeling of tracer behavior in short-term experiments in fissured rocks, *Water Resour. Res. 26*, 1517-1528, 1990.

Maloszewski, P., A. Herrmann, and A. Zuber, Interpretations of tracer tests performed in fractured rock of the Lange Bramke basin, Germany, *Hydrogeol. J., 7*, 209-218, 1999.

Moensch, A. F., Double-porosity models for a fissured groundwater reservoir with fracture skin, *Water Resour. Res., 20* (7), 831-846, 1984.

Moensch, A. F., Convergent radial dispersion in a double-porosity aquifer with fracture skin: Analytical solution and application to a field experiment in fractured chalk, *Water Resour. Res., 31* (8), 1823-1835, 1995.

Narasimhan, T. N., Multidimensional numerical simulation of fluid flow in fractured porous media., *Water Resour. Res., 18*, 1235-1247, 1982.

Neuzil, C. E. and J. V. Tracy, Flow through fractures, *Water Resour. Res., 17,* 191-199, 1981.

Novakowski, K. S., G. V. Evans, D. A. Lever, and K. G. Raven, A field example of measuring hydrodynamic dispersion in a single fracture, *Water Resour. Res., 21*, 1165-1174, 1985.

Novakowski, K. S., The analysis of tracer experiments conducted in divergent radial flow fields, *Water Resour. Res., 28* (12), 3215-3225, 1992.

Novakowski, K. S. and P. A. Lapcevic, Field measurement of radial solute transport in fractured rock, *Water Resour. Res., 30*, 37-44, 1994.

Ptak, T. and G. Schmid, Dual-tracer transport experiments in a physically and chemically heterogeneous porous aquifer: effective transport parameters and spatial variability, *J. Hydrol., 183*, 117-138, 1996.

Raven, K. G., K. S. Novakowski, and P. A. Lapcevic, Interpretation of field tracer tests of a single fracture using a transient solute storage model, *Water Resour. Res., 24*, 2019-2032, 1988.

Reimus, P. W., M. J. Haga, T. J. Callahan, I. Anghel, H. J. Turin, and D. Counce, C-Holes update report: Reinterpretation of the reactive tracer test in the Bullfrog Tuff and results of laboratory experiments, Yucca Mountain Site Characterization Project

Milestone Report SP32E2M4SZ, Los Alamos National Laboratory, Los Alamos, NM, 1998.

Reimus, P. W. and M. J. Haga, Analysis of tracer responses in the BULLION forced-gradient experiment at Pahute Mesa, Nevada, *Los Alamos National Laboratory Report LA-13615-MS*, Los Alamos, NM, 1999.

Reimus, P. W., A. Adams, M. J. Haga, A. Humphrey, T. Callahan, I. Anghel, and D. Counce, Results and interpretation of hydraulic and tracer testing in the Prow Pass Tuff at the C-Holes, *Yucca Mountain Site Characterization Project Milestone Report SP32E2M4SZ*, Los Alamos National Laboratory, Los Alamos, NM, 1999.

Roberts, P. V., M. N. Goltz, and D. M. MacKay, A natural gradient experiment on solute transport in a sand aquifer, 3, Retardation estimates and mass balances for organic solutes, *Water Resour. Res., 22*, 2047-2058, 1986.

Sidle, R. C., B. Nilsson, M. Hansen, and J. Fredericia, Spatially varying hydraulic and solute transport characteristics of a fractured till determined by field tracer tests, Funen, Denmark, *Water Resour. Res., 34*(10), 2515-2527, 1998.

Sonnenborg, T. O., P. Engesgaard, and D. Rosbjerg, Contaminant transport at a waste residue deposit, 1, Inverse flow and nonreactive transport modeling, *Water Resour. Res., 32*(4), 939-951, 1996.

Sudicky, E. A., A natural gradient experiment on solute transport in a sand aquifer: Spatial variability of hydraulic conductivity and its role in the dispersion process, *Water Resour. Res., 22*, 2069-2082, 1986.

Thorbjarnarson, K. W. and D. M. MacKay, A field test of tracer transport and organic contaminant elution in a stratified aquifer at the Rocky Mountain Arsenal (Denver, CO, U.S.A.), *J. Contam. Hyd. 24*, 287-312, 1997.

Tsang, Y. W., Study of alternative tracer tests in characterizing transport in fractured rocks, *Geophys. Res. Letters, 22* (11), 1421-1424, 1995.

2. Using Multiple Experimental Methods to Determine Fracture/Matrix Interactions and Dispersion of Nonreactive Solutes in Saturated Volcanic Tuff

(Callahan, T. J., P. W. Reimus, R. S. Bowman, and M. J. Haga, *Water Resour. Res.*, *32*(12), 3547-3558, 2000.)

Timothy J. Callahan[1,2], Paul W. Reimus[1], Robert S. Bowman[2], and Marc J Haga[1]

[1]Environmental Science and Waste Technology Group, Los Alamos National Laboratory, Los Alamos, NM 87545

[2]Department of Earth and Environmental Science, New Mexico Institute of Mining and Technology, Socorro, NM 87801

Abstract. The objective of this research was to investigate the effects of matrix diffusion on solute transport in fractured volcanic tuff. Two tuff cores were studied, one with a matrix porosity of 0.27 and the other of 0.14. The matrix permeabilities of the cores were 4.7×10^{-15} and 7.8×10^{-19} m^2, five and nine orders of magnitude less than the respective fracture permeabilities. This suggested that the cores could be modeled as dual porosity systems with no flow in the matrix but significant solute storage capacity. Two types of tracer tests were conducted in each fractured core: 1) iodide was injected in separate experiments at different flow rates and 2) two tracers of different matrix diffusion coefficients (bromide and pentafluorobenzoate [PFBA]) were injected in another test. A difference in the maximum concentrations of the solutes and the extended tailing of the breakthrough curves were assumed indicative of diffusive mass transfer

between the fracture and the porous matrix of the cores. Interpreting the results from both methods allowed the identification of matrix diffusion and dispersion effects within the fracture by simultaneously fitting the data sets (with known constraints) using a relatively simple conceptual model. Estimates of mass transfer coefficients for the fractured cores were also obtained.

2.1. Introduction

Because solute transport is controlled by both the physical nature of the flow system and the characteristics of the solutes (velocity, dispersivity, water saturation, sorption behavior, diffusion coefficient), it is often difficult to determine the importance of each parameter or process. Several previous studies have shown that hydrodynamic dispersion in a single fracture can cause significant spreading or "tailing" of solutes during transport through fractured media [*Tsang et al*., 1988; *Johns and Roberts*, 1991; *Dronfield and Silliman*, 1993]. However, solute tailing can also be indicative of diffusive mass transfer between mobile water in fractures and immobile water in the surrounding porous matrix [*Grisak and Pickens*, 1980; *Grisak et al.*, 1980; *Tang et al.*, 1981; *Neretnieks et al.*, 1982; *Maloszewski and Zuber*, 1985; *Moreno and Tsang*, 1991; *Maloszewski and Zuber*, 1993; *Haggerty and Gorelick*, 1995; *Lapcevic et al.*, 1999; *Maloszewski et al.*, 1999]. The fact that both processes can have a similar influence on solute breakthrough curves in fractured media makes it difficult to distinguish between the two in tracer transport tests. The motivation of the current research is to develop and demonstrate a consistent method of tracer transport testing and data analysis that provides unique estimates of both hydrodynamic dispersion and matrix diffusion in fractured rock.

A single axial fracture was induced in two intact cores of volcanic tuff and the cores were then saturated with water, resulting in systems that were used to study solute transport in saturated fractures contained within a porous but relatively impermeable matrix. A flow interruption method was also used [*Reedy et al.*, 1996; *Brusseau et al.*, 1997] to verify the presence of diffusive mass transfer between the fracture and matrix. Separate samples of each core were used for matrix diffusion coefficient, porosity, and permeability measurements. These experiments provided independent estimates of the matrix diffusion coefficients of the different solutes used in the fractured core experiments.

The dual porosity conceptual model accurately described solute transport through the fractured cores and captured the importance of fracture/matrix interactions. The solute breakthrough curves follow a -1.5 slope in log space, which is probably due to diffusive mass transfer between the fracture and the surrounding porous matrix. However, the independent matrix diffusion coefficient measurements for Br^- and PFBA in the same rock types were smaller than those calculated from the fractured core tracer tests. It is possible that some degree of fracture flow channeling occurred within the fractured cores, resulting in overestimates of the mass transfer coefficients. It is theorized that this was an artifact of the short time scale of the laboratory tracer tests, and during field tests, it is likely that the longer solute residence times will diminish the importance of free water diffusion on tracer transport.

2.2. Theory

2.2.1. Conceptual model

One-dimensional advection and dispersion in the fractures was assumed with a diffusive fracture/matrix interaction orthogonal to flow direction. Diffusion into the matrix was assumed perpendicular to the flow direction in the fracture. This is commonly known as the dual porosity model (Figure 2.1). The solute residence time in the fracture was assumed large enough that molecular diffusion homogenized the concentration profile across the fracture aperture [*Hull et al*., 1987]. This was verified by comparing the calculated diffusion distances $\sqrt{2Dt}$ (where D is the free water diffusion coefficient and t is the solute residence time in the fracture) with the average fracture apertures calculated from tracer tests. The diffusion distance was always greater than the apertures. Under these conditions, dispersion in the fractures should be independent of the flow rate. In this simplified model, the fracture aperture was assumed uniform and constant throughout the fracture (i.e., an average over the fracture domain). The dispersion term then captures the effects of flow channeling caused by the variable apertures in the fracture [*Thompson*, 1991].

Figure 2.1. Conceptual model of a dual porosity system for solute transport in fractured tuff cores (adapted from Maloszewski and Zuber, 1985).

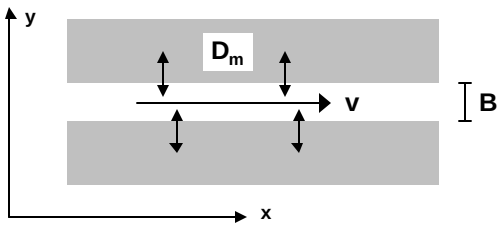

2.2.2. Mathematical model for fracture transport

Tang et al. [1981] describe solute transport though dual porosity media as using the following governing equations

$$\frac{\partial C_f}{\partial t} = D_f \frac{\partial^2 C_f}{\partial x^2} - v_f \frac{\partial C_f}{\partial x} + \frac{n_m D_m}{b n_f} \frac{\partial C_m}{\partial y}\bigg|_{y=b} \tag{2.1}$$

$$\frac{\partial C_m}{\partial t} = D_m \frac{\partial^2 C_m}{\partial y^2}. \tag{2.2}$$

The coordinate system (x, y) used in this discussion relates to Figure 2.1. The aqueous phase concentration in the fracture is C_f [M L^{-3}]; in the matrix, it is C_m [M L^{-3}]. The hydrodynamic dispersion coefficient in the fracture is D_f [L^2 T^{-1}], v_f [L T^{-1}] is the average solute velocity in the fracture, and b [L] is the fracture half aperture. The matrix diffusion coefficient, D_m [L^2 T^{-1}] describes the effective diffusion of a solute in the pores of the matrix. Similar to the pore water diffusion coefficient of *Ohlsson and Neretnieks* [1998], it does not include the matrix porosity n_m [-] but it does implicitly include tortuosity factors. The term n_f is the porosity within the fractures, taken to be unity in all cases for the mechanically induced fractures of this study.

The water-saturated, dual-porosity rock cores were subject to the same initial and boundary conditions as in *Tang et al*. [1981] except here a pulse of tracer solution was injected where

$$C_f\left(x = 0, 0 < t < t_p\right) = C_o, \tag{2.3}$$

where t_p [T] is the tracer injection pulse duration and C_o [M L^{-3}] is the concentration of the pulse. The fracture and pore water were assumed to be free of solute and an infinite matrix orthogonal to the fracture was assumed (i.e., tracer behavior was not influenced by

the radial boundaries of the fractured rock cores). The validity of this last assumption is discussed in section 2.4.1.

Following *Tang et al*. [1981], the Laplace transforms of (2.1) and (2.2) yield the following ordinary differential equations

$$s\overline{C_f} = D_f \frac{\partial^2 \overline{C_f}}{\partial x^2} - v_f \frac{\partial \overline{C_f}}{\partial x} + \frac{n_m D_m}{b} \frac{\partial \overline{C_m}}{\partial y}\bigg|_{y=b} \tag{2.4}$$

$$s\overline{C_m} = D_m \frac{\partial^2 \overline{C_m}}{\partial y^2}, \tag{2.5}$$

where s [T^{-1}] is the transform variable for Laplace space. The overbar denotes the Laplace transform of the corresponding concentration variable. The combined solution of (2.4) and (2.5) for a nonreactive solute can be found in *Tang et al.* [1981]. From the combined solution we define the terms *MTC* (mass transfer coefficient) as $MTC = (n_m/B)^2 * D_m$ [T^{-1}], where $B = 2b$; $t = (x/v_f)$ [T] as the mean solute residence time in the fracture; and $Pe = (x * v_f)/D_f$ [-] as the Peclet number. These parameters are used to compare tracer transport data for either different solutes in the same test or multiple tests using the same solute.

To interpret the tracer transport data, a semi-analytical algorithm was used, following the theory of *Tang et al.* [1981]. At least two data sets generated from tracer tests in the same fractured core were fitted together to obtain estimates of t, Pe, and the *MTC*. These three parameters were allowed to float to obtain a best least-squares fit to the data sets. In the case of a tracer test involving two nonsorbing solutes with different free water diffusion coefficients, the ratio of diffusion coefficients was fixed, based on independent diffusion coefficient data. For cases in which one nonsorbing solute is used in multiple tracer tests conducted at different flow rates, the ratio of solute residence

times was fixed for the different tests. For example, one tracer test was conducted at an average flow rate of 20.11 mL hr^{-1} and a later test was at 2.01 mL hr^{-1}, therefore the ratio of residence times was 0.01 because flow rate and residence time are inversely proportional for a system of constant volume.

This approach yields much more constrained parameter estimates than the analysis of a single tracer data set. Dispersion and matrix diffusion often result in similar effects on tracer breakthrough curves, as they both tend to increase the second moment of tracer responses. However, only matrix diffusion can cause significant changes in the shape of a breakthrough curve as a function of either the solute residence time in the system or the matrix diffusion coefficient. By using multiple nonsorbing solutes of different diffusion coefficients in the same test, or conducting experiments at different flow rates with the same tracer in the same fracture, we were able to separate the effects of dispersion and matrix diffusion in the fractured cores.

2.3. Methods

2.3.1. Fractured Rock Cores

2.3.1.1. Apparatus. Intact rock cores from the Crater Flat Tuff Formation were collected from the C-Wells field site, 1.5 km SE of Yucca Mountain, NV (Table 2.1). The lithologic units sampled were Miocene age ash flow tuff [*Geldon*, 1993]. Core 1 was of the upper flow zone and core 2 was of the central flow zone, both from the Prow Pass Tuff Member of the Crater Flat Tuff Formation. The samples were obtained from depth intervals (below surface) of 532.3 – 533.4 m and 553.0 – 553.8 m, respectively. Core 1 was 0.161 m long and had a matrix porosity of 0.27. Core 2 was 0.173 m long and

Table 2.1. Petrographic descriptions of the cores used for this study.

	Core/Wafer 1	Core/Wafer 2
Stratigraphic Unit	Crater Flat Tuff Formation, Prow Pass Tuff Member, upper flow zone	Crater Flat Tuff Formation, Prow Pass Tuff Member, central flow zone
Core Interval (m below surface)	532.3 - 533.4	553.0 – 553.8
Dimensions of core used for dynamic transport experiments	Length = 0.161 m Diameter = 0.095 m	Length = 0.173 m Diameter = 0.095 m
Lithologic Description	Pink-white, mod.-welded ash flow tuff. Crystal-poor (< 2% of matrix). Crystals 0.5 mm in length. Quartz, feldspar, and traces of golden-altered biotite. Lithic frag. Are few, < 4% of matrix, light to dark brown and angular. Avg. lithic frag. length is ≈ 25 mm. Abundant white pumice (≈ 30% of matrix), rounded shape, unaltered; avg. length 20 mm.	Coral to pink-red, densely welded ash flow tuff. Crystals ≈ 5% of matrix; crystal size < 1 mm long. Crystals include feldspars, quartz, biotite, and hornblende. Lithic frag. < 8% of the matrix, light to dark brown in color and angular to rounded. Avg. frag. length < 5 mm. About 30% white pumice; unaltered and rounded in shape, avg length 10 mm.

its matrix porosity was 0.14. Both samples were 0.095 m in diameter. Matrix porosity measurements were made on three representative samples of each core by measuring the difference between the wet and dry weights and dividing by the volumes of the samples. Smaller representative samples were used because the lack of sensitivity of analytical balances under heavy loads prevented us from obtaining accurate wet and dry weights of the large cores used for transport testing.

Nonfractured core samples were selected because of the scarcity of naturally fractured cores suitable for testing. One axial fracture was induced mechanically in each of the cores using a 1.5-kg hammer and a chisel with a 10-cm wide blade. Each fracture propagated through the core resulting in separation. We took care to avoid rock fragment loss from the fracture surfaces. Because of the induced nature, there were no secondary mineral coatings or alteration products in the fractures

After the fractures were created, the ends of the cores were planed off using a standard diamond-tipped rock saw. Preparation for the tracer transport experiments involved fitting the ends of each core with specially-machined acrylic end plates (11.5-cm diameter) designed to route the injectate and effluent into and out of the fracture (Figure 2.2). The recessed "D-spacing" pattern on the underside of the end plates was filled with a clear caulk (Lexel, Sashco Sealants, Brighton, CO; the use of brand or product names is for identification purposes and does not constitute endorsement by Los Alamos National Laboratory). This allowed the plates to be sealed to the ends of the core thus minimizing the inlet and outlet volumes on each core to 1.5 mL and 1 mL for core 1 and core 2, respectively.

The outer cylindrical surface of each core was then treated with the caulk, especially along the fracture traces along the sides of the cores to prevent fracture leakage. The cores were set aside overnight to allow the caulk to dry. The inner surfaces of 12.5-cm diameter acrylic cylinders were roughened using 120 grit aluminum oxide C-weight sandpaper to facilitate adhesion of epoxy to the and used to attach each core to the cylinders. The resulting apparatus had an annulus of 1.5 cm around each core (Figure 2.2), which was filled with a two-part epoxy at a resin: hardener ratio of 5:1 by weight.

Figure 2.2. Schematic diagram of the fractured rock core apparatus. Three flow ports on each end of the core allowed access to the inlet and outlet regions; the central flow ports were used to connect the cores to the syringe pump and fraction collector via 0.8-mm diameter tubing.

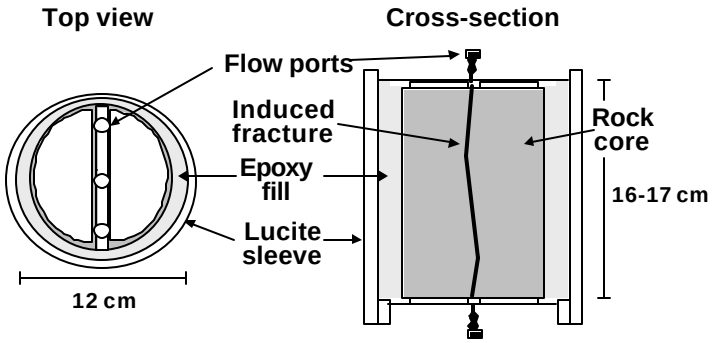

After a two-day curing period, compressed CO_2 gas was slowly injected into each core by way of the middle flow port for about one hour. Most of the resident air was assumed to be displaced from the fracture and the near-fracture porous matrix, and that most of the CO_2 would dissolve in water, thus expediting water saturation. The rock cores were then placed in a 18.9-L polyetherimide vacuum chamber and submersed in filtered groundwater from well J-13 near Yucca Mountain (Table 2.2). The system was evacuated ($P \approx -85$ kPa) using a vacuum pump to aid water saturation of the core samples. This saturation step continued for at least one month for each sample. Saturation was considered complete when gas bubbles ceased to emanate from the cores. This check of water saturation was only by observation. The effectiveness of this technique was verified by the tracer data. Separation of the solutes signified that diffusive mass transfer was a function of diffusion coefficient rather than imbibition of water (and solutes) into the matrix.

Table 2.2. Chemical composition of the water samples used in the diffusion cell and fractured rock core experiments. All analyses in mg L^{-1} (except pH).

	J-13 well water[a]	$NaHCO_3$ water[b]	Prow Pass water[b]
B	0.13		0.12
Br^-			0.02
Ca^{2+}	11.3		3.25
Cl^-	7		5.9
F			2.16
Fe	0.02		0.08
HCO_3^-	124	141	137
K^+	5		2.9
Li^+	0.040		0.074
Mg^{2+}	≤ 0.010		0.09
Na^+	44	54	58.6
Si^{4+} (as H_4SiO_4)	30		20.8
SO_4^{2-}	19		18.5
pH	7.8 – 8.1[†]	7.7 – 8.0	8.0

[a]Fuentes et al. [1989].

[b]This study. The Prow Pass water was sampled in the field during a pump test.

2.3.1.2. Fracture Permeability Measurements. After constructing the fractured rock core apparatus, the integrity of each column was tested by imposing a 2-m head of water above the columns using a large reservoir and plastic tubing. No leaks were detected in either core apparatus as water flowed through the fracture. The constant head of water was used to supply flow in a manner similar to a constant head permeameter test. This method was used due to the relatively high hydraulic conductivities of the fractures [*Freeze and Cherry*, 1979]. The cubic law was employed [*Domenico and Schwartz*, 1990] to estimate the hydraulic fracture aperture in each core

$$Q = \frac{\rho g}{\mu} \frac{B_h^2}{12} A \frac{dh}{dx} \qquad \text{where} \qquad A = B_h w . \tag{2.6}$$

Here, Q is the volumetric flow rate through a fracture of cross-sectional area A; B_h and w are the hydraulic aperture and the width of the fracture, respectively; ρ is the density of water; μ is the dynamic viscosity of water; g is the gravitational constant (9.8 m s^{-2}); and dh/dx is the hydraulic gradient across the length of the fracture. The ρ and μ of water were assumed to be 1000 kg m^{-3} and 0.001 kg m^{-1} s^{-1}, respectively. To calculate the fracture permeabilities of the cores, the following formula was used [*Freeze and Cherry*, 1979]

$$k = \frac{B_h^2}{12} . \tag{2.7}$$

2.3.1.3. Tracer Transport Experiments. Tracer preparation consisted of dissolving either sodium iodide (NaI, Mallinckrodt, Inc., St. Louis, MO) or a mixture of lithium bromide (LiBr, Fisher Scientific, Hampton, NH) and pentafluorobenzoate (PFBA, Oakwood Products, W. Columbia, SC) in filtered J-13 well water (Tables 2.3 and 2.4). Lithium bromide was selected because lithium exhibits weak sorption to the tuffs. For the Br^-/PFBA solution, the pH decreased to about 3 upon addition of the PFBA (due to deprotonation of carboxylic acid groups), so we buffered it using a 50% by volume sodium hydroxide solution (NaOH, Mallinckrodt Baker, Inc., Phillipsburg, NJ). The final pH was between 7.7 and 8.3 (the pH of the well J-13 water was 7.6 – 8.2). These tracer solutions were deaerated before injection. The tracer concentrations are listed in Tables 2.3 and 2.4 for cores 1 and 2, respectively. Iodide was used as a single tracer in experiments conducted at different flow rates to measure the amount of matrix diffusion

as a function of solute residence time in the fractured cores. Bromide and PFBA were used together in one experiment to measure the relative difference of matrix diffusion as a function of their diffusion coefficients. The free water diffusion coefficient for bromide is 21.5 x 10^{-10} m^2 s^{-1} [*J. L. Wilson et al*., pers. comm., 1999]; for PFBA it is 7.6 x 10^{-10} m^2 s^{-1} [*Benson and Bowman*, 1996].

Because the focus of this paper is on comparative transport of multiple solutes in fractured rock, control experiments in artificial fractures were not conducted. Tracer transport experiments and visualization studies in artificial fractures have been conducted elsewhere [for example, *Brown*, 1987; *Wels and Smith*, 1994; *Wels et al.*, 1996; *Brown et al.*, 1998; *Detwiler et al.*, 1999]. The concern of this study was the separation of matrix diffusion and dispersion effects by generating multiple tracer data sets in the same flow system. The tracer data verify that the flow conditions in all tests were comparable.

Tracer was injected into each fractured rock core using two 60-mL capacity plastic syringes and two single-rotor syringe pumps. Two syringes were plumbed into each core in order to inject tracer volumes of 55 – 80 mL for each tracer test. Translucent polytetrafluoroethylene (PTFE) of 0.8-mm inner diameter tubing was used to connect the syringes to the column apparatus via the middle flow port on the lower end of the column (Figure 2.2). The tracer injections were conducted from bottom to top of the fractures to avoid gravitational flow effects. The tubing was wrapped in opaque self-adhesive tape to inhibit microbial growth within the apparatus.

Table 2.3. Experimental conditions for the fracture transport tests, core 1 (upper flow zone sample, Prow Pass Tuff Member of the Crater Flat Tuff Formation, NV).

Core 1, Upper flow zone, Prow Pass Tuff Member				
Core length, L (m)	Core width, w (m)		Matrix porosity, n_m (-)	
0.16	0.10		0.27	
Hydraulic aperture, B_h (m)[a]		0.14×10^{-3}		
Experimental Parameters	I^- Test 1	I^- Test 2	I^- Test 3	Br^-/PFBA test
Volumetric flow rate, Q (mL hr^{-1})	2.01	20.11	8.30	6.39
Injection duration, t_p (hr)	29.9	2.87	7.26	11.53
Injection concentration, C_o (mg L^{-1})	1000.	1000.	1000.	2528 (Br^-) 766 (PFBA)
Flow interruption period, time since start of injection (hr)	NA[b]	NA[b]	NA[b]	43.95 – 63.95
Flow rate after restart, Q (mL hr^{-1})	NA[b]	NA[b]	NA[b]	6.46
Mass recovery (%)	86	96	94	89 (Br^-) 95 (PFBA)

[a]Determined from a constant head permeameter method.

[b]Not applicable; flow was not interrupted during these tests.

After injection of the tracer pulse, a 260-mL capacity syringe pump was used to flush the core with deaerated, tracer-free well J-13 water at approximately the same flow rate as during the tracer injection (Tables 2.3 and 2.4). This continued until the effluent concentration was less than 1% of the injection concentration.

Effluent from the cores was separated into 8-mL capacity sample vials using a programmable fraction collector. The collection time interval was set to provide 2 – 6 mL of effluent per vial, with smaller volumes collected early in the tests and larger volumes later in the tests. These sample volumes were necessary because of the small fracture volumes, estimated to be 10 – 15 and 11 – 12 mL for cores 1 and 2, respectively. A total of four tracer tests were conducted in each fracture; three separate I^- injections, each at a

different flow rate, and one Br^-/PFBA injection. Mass recovery was nearly complete in all tests (Tables 2.3 and 2.4). The fractures were flushed with tracer-free groundwater after each test in order to remove as much of the tracer mass as possible. Tracer concentrations were measured before starting the next test and initial concentrations were accounted for before data interpretation.

Table 2.4. Experimental conditions for the fracture transport tests, core 2 (central flow zone sample, Prow Pass Tuff Member of the Crater Flat Tuff Formation, NV).

Core 2, Central flow zone, Prow Pass Tuff Member				
Core length, L (m)	Core width, w (m)		Matrix porosity, n_m (-)	
0.17	0.10		0.14	
Hydraulic aperture, B_h (m)[a]	0.13×10^{-3}			
Experimental Parameters	I^- Test 1	I^- Test 2	I^- Test 3	Br^-/PFBA test
Volumetric flow rate, Q (mL hr^{-1})	19.93	49.59	11.74	5.96
Injection duration, t_p (hr)	4.0	1.5	6.2	11.94
Injection concentration, C_o (mg L^{-1})	1000	1000	1000	2528 (Br^-) 766 (PFBA)
Flow interruption period, time since start of injection (hr)	NA[b]	NA[b]	NA[b]	42.93 – 62.93
Flow rate after restart, Q (mL hr^{-1})	NA[b]	NA[b]	NA[b]	5.95
Mass recovery (%)	89	98	84	90 (Br^-) 95 (PFBA)

[a]Determined from a constant head permeameter method.

[b]Not applicable; flow was not interrupted during these tests.

During the Br^-/PFBA experiments, a flow interruption was conducted at late time by simply closing in the columns and stopping the pump. After twenty hours (for both tests), the pump was restarted and flow continued through the columns at roughly the

same flow rate (Tables 2.3 and 2.4). The fraction collection interval was decreased after resuming flow in order to measure the tracer response to the flow transient.

2.3.2. Diffusion Cells

2.3.2.1. Apparatus. Separate samples from the same wells and depth intervals as the fractured rock cores were used for diffusion cell experiments. The diffusion cell samples were generated by making parallel radial cuts through the cores, resulting in cylindrical "wafers" of uniform thickness. These wafers were 0.0098 m and 0.0123 m thick for cores 1 and 2, respectively. Like the fractured rock cores, both diffusion wafers were 0.095 m in diameter. The respective matrix porosities were 0.27 and 0.14 for wafers 1 and 2 (also the same as the fractured rock cores). Intact core samples were selected in order to avoid the preferential flow or diffusion paths associated with fractures. Using the same two-part epoxy mentioned above, the cylindrical surface of each rock wafer was fitted with an acrylic sleeve. After a two-day curing time, the samples were submersed in sodium bicarbonate ($NaHCO_3$) water (Table 2.2) using the same saturation procedure as for the fractured rock cores. The sodium bicarbonate water was used for convenience and was similar in chemistry to the well J-13 water. The sodium bicarbonate solution was undersaturated with respect to silica in the diffusion wafers; however, the rate of silica dissolution is extremely low at 25°C. (According to *Brady and Walther* [1989], the rate of both pure quartz and low albite dissolution is about 10^{-12} mol m^{-2} s^{-1} in solutions of 0.001 M ionic strength, 25°C, and a pH of 8.) The saturation step continued for at least two weeks for each core. After the samples were saturated with water, the final diffusion cell apparatus was constructed, consisting of two Plexiglas reservoirs separated by the

rock wafer (Figure 2.3). Advection did not occur through the wafers because orienting the inlet and outlet points were oriented at the same elevation. In previous test wafers, advection did occur which was evident from the lack of separation of the Br^- and PFBA breakthrough curves. The data presented here verify that advection did not occur in wafers 1 and 2.

Figure 2.3. Schematic diagram of the diffusion cell apparatus. The collection reservoir was continuously flushed by the syringe pump, providing effluent to the automatic fraction collector.

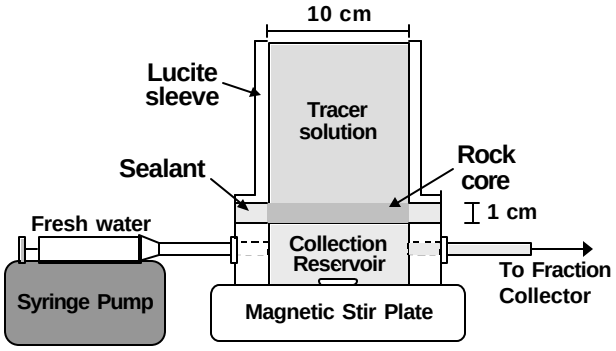

2.3.2.2. Matrix Permeability Measure ments. The matrix permeabilities of the diffusion cell samples were measured in a manner similar to a falling head permeameter test. The falling head method was assumed most appropriate due to the expected low permeabilities of the intact diffusion cell samples [*Freeze and Cherry*, 1979]. After measuring the hydraulic conductivity of each wafer, the following equation was used to calculate permeability

$$k = \frac{K m}{r g}. \qquad (2.8)$$

2.3.2.3. Diffusion Experiments. One diffusion cell experiment was conducted in each sample to determine the matrix diffusion coefficients of Br^- and PFBA. The I^- matrix diffusion coefficient was not measured during these experiments, but I^- and Br^- have very similar diffusion coefficients [*Newman*, 1973]. A solution containing dissolved LiBr and PFBA was poured into the upper reservoir. The lower reservoir was filled with tracer-free sodium bicarbonate water (Figure 2.3). Both solutions were deaerated before the start of the tests. The lower reservoir was kept well mixed using a magnetic stir bar and stir plate and flushed continuously at an initial flow rate of 8.0 mL hr^{-1}. The flow rate was decreased to 1.5 mL hr^{-1} after the first 250 hours to increase the fraction collection time and the sample size. The effluent was collected using the same type of vials as for the fracture tests in a programmable fraction collector (Model FC-220, Gilson, Inc., Middleton, WI).

2.3.3. Tracer Analysis

2.3.3.1. Iodide. The effluent from the fracture tracer tests was measured for I^- using an ion-selective electrode and a combination millivolt/pH meter and was compared to I^- standards prepared via dilution of the tracer solution in a log (concentration) series. The detection limit of the electrode was estimated to be ≤ 0.05 mg L^{-1} I^-. Background I^- concentration in the $NaHCO_3$ and J-13 waters was less than the detection limit. The error of the ion-selective electrode was two to four percent for all tests. Instrument drift was corrected for by analyzing the 10 mg L^{-1} standard every tenth sample and adding (or subtracting) the amount of drift per sample to the millivolt readings.

2.3.3.2. Br^-/PFBA. Ion chromatography (IC) was used to analyze the samples from both the fracture tracer tests and the diffusion cell experiments for Br^- and PFBA using a Dionex (Sunnyvale, CA) model 4500 chromatograph. In the analytical laboratory, automated sample injection was used for Br^- analysis whereas PFBA analysis was conducted via manual injection. Detection limits were ≤ 0.04 mg L^{-1} and ≤ 0.02 mg L^{-1} for Br^- and PFBA, respectively. The background concentration of Br^- was 0.02 in the well J-13 water; for PFBA it was less than the detection limit. The average error of measurement was approximately 5%. Independent standards and blanks were used during analysis for quality assurance.

Because I^- analysis was relatively fast, at least two I^- experiments were conducted in each core to estimate the fracture volume of the cores. This allowed us to plan the later Br^-/PFBA tests with regard to appropriate flow rate and fraction collection interval.

2.4. Results and Discussion

2.4.1. Fractured Rock Cores

2.4.1.1. Hydraulic Tests. The hydraulic apertures were 0.14×10^{-3} m for core 1 and 0.13×10^{-3} m for core 2. The hydraulic apertures were less than the calculated tracer apertures (Tables 2.5 and 2.6), which is similar to the results found in other studies [*Tsang*, 1992]. Using the aperture values and (2.7) above, the fracture permeabilities were calculated to be 1.6×10^{-9} m^2 for core 1 and 1.4×10^{-9} m^2 for core 2. These values were roughly five and nine orders of magnitude greater than the matrix permeabilities (as determined from the diffusion wafers, below) for the respective cores. This suggests that

the dual porosity concept was the simplest model that could describe solute transport in the fractured cores.

Table 2.5. Modeling results for the fracture transport tests, core 1.

Core 1, Upper flow zone, Prow Pass Tuff Member				
Modeling Parameters[a]	I^- Test 1	I^- Test 2	I^- Test 3	Br^-/PFBA test
Solute mean residence time, t (hr)	5.3	0.53	1.3	2.8
Peclet number, Pe		16		3.0
Mass transfer coefficient, $MTC = \left(\frac{n_m}{B} \right)^2 D_m$ (hr^{-1})		0.201 (I^-)		0.255 (Br^-) 0.085 (PFBA)
Fracture aperture, B (m)[b]		0.70×10^{-3}		1.16×10^{-3}
Dispersivity in fracture, $a = \frac{L}{Pe}$ (m)		10.4×10^{-3}		53.7×10^{-3}
Matrix diffusion coefficient, D_m ($\times 10^{-10}$ m^2 s^{-1})[c]		3.7 (I^-)		12.9 (Br^-) 4.3 (PFBA)

[a]The three I^- data sets were fit simultaneously assuming Pe was the same for the three tests and t was inversely proportional to the volumetric flow rate. The Br^- and PFBA data were fit simultaneously by constraining the D_m ratio for Br^-:PFBA to 3:1.

[b]Based on the relationship $B = \frac{Qt}{Lw}$, where t is the solute mean residence time.

[c]Determined from the MTC using the measured n_m and the calculated B.

Table 2.6. Modeling results for the fracture transport tests, core 2.

Core 2, Central flow zone, Prow Pass Tuff Member				
Modeling Parameters[a]	I^- Test 1	I^- Test 2	I^- Test 3	Br^-/PFBA test
Solute mean residence time, t (hr)	0.60	0.24	1.02	2.0
Peclet number, Pe	23			15
Mass transfer coefficient, $MTC = \left(\frac{n_m}{B}\right)^2 D_m$ (s^{-1})	11.4×10^{-6} (I^-)			0.032 (Br^-) 0.011 (PFBA)
Fracture aperture, B (m)[b]	0.72×10^{-3}			0.72×10^{-3}
Dispersivity in fracture, $a = \frac{L}{Pe}$ (m)	7.5×10^{-3}			11.5×10^{-3}
Matrix diffusion coefficient, D_m ($\times 10^{-10}$ m^2 s^{-1})[c]	3.1 (I^-)			2.4 (Br^-) 0.8 (PFBA)

[a]The three I^- data sets were fit simultaneously assuming Pe was the same for the three tests and t was inversely proportional to the volumetric flow rate. The Br^- and PFBA data were fit simultaneously by constraining the D_m ratio for Br^-:PFBA to 3:1.

[b]Based on the relationship $B = \frac{Qt}{Lw}$, where t is the solute mean residence time.

[c]Determined from the MTC using the measured n_m and the calculated B.

2.4.1.2. Tracer Data Interpretation Procedure. Using the data from either the three I^- tests or the one Br^-/PFBA test for each sample, the semi-analytical method from *Tang et al.* [1981] was employed to simultaneously fit the experimental data up to the flow interruptions for each fractured tuff core sample. This provided values for t; Pe, and the MTC [$(n_m/B)^2 * D_m$]. This method was used to interpret the data generated under constant flow rate conditions. The best-fitting parameters were then fixed in a numerical computer code RETRAN to generate the model curves seen in Figures 2.4 – 2.8. RETRAN is an alternating-direction finite difference algorithm that mimics the semi-analytical method and can be used for conditions of varying flow velocity [*Reimus et al.*,

1999]. RETRAN was used here in a forward mode to produce breakthrough curves based on the parameters determined from the semi-analytical method.

To verify the infinite matrix assumption for solute transport in the cores, the following equation was used

$$x_D = \sqrt{2D_m t}\ , \qquad (2.9)$$

where x_D is the diffusion distance from the fracture into the matrix (D_m and t defined previously). For the case where $D_m = 10^{-9}$ m^2 s^{-1} and t = 10 hr, $x_D \approx 0.009$ m, about six times less than the half-diameter of the cores. This calculation illustrates that during the tracer experiments only a very small fraction of the total volume of the cores were accessed. Saturation was verified by 1) the lack of air bubble evolution from the cores under strong vacuum and 2) the consistent separation of the tracer breakthrough curves as a function of diffusion coefficient. If imbibition of water into the porous matrix was the dominating transport process, the separation of the breakthrough curves of the different tracers would have been much less.

Two procedures were used to interpret the fracture transport data. For the three I^- experiments in each core, t was constrained to be inversely proportional to flow rate and all other parameters were assumed to be identical for each data set. For the Br^-/PFBA fracture tests, both the Br^- and PFBA data sets were simultaneously fitted assuming a D_m ratio of 3:1 based on information from the diffusion cell tests and the free water diffusion coefficients. As mentioned in section 3.1.3, the free water diffusion coefficient for Br^- and PFBA are 21.5 x 10^{-10} m^2 s^{-1} and 7.6 x 10^{-10} m^2 s^{-1}, respectively. All other transport parameters were assumed identical for Br^- and PFBA in each test.

Figure 2.4. Effects of varying the Peclet number, *Pe* for a single data set. The open circles are PFBA data from the fractured rock core test in core 1. The three curves are RETRAN predictions using only the one tracer data set and systematically varying the Peclet number (*Pe*) while allowing the residence time (t), fracture aperture (B), and the mass transfer coefficient (*MTC*) to float. The curves for *Pe* = 10 and 100 are nearly identical.

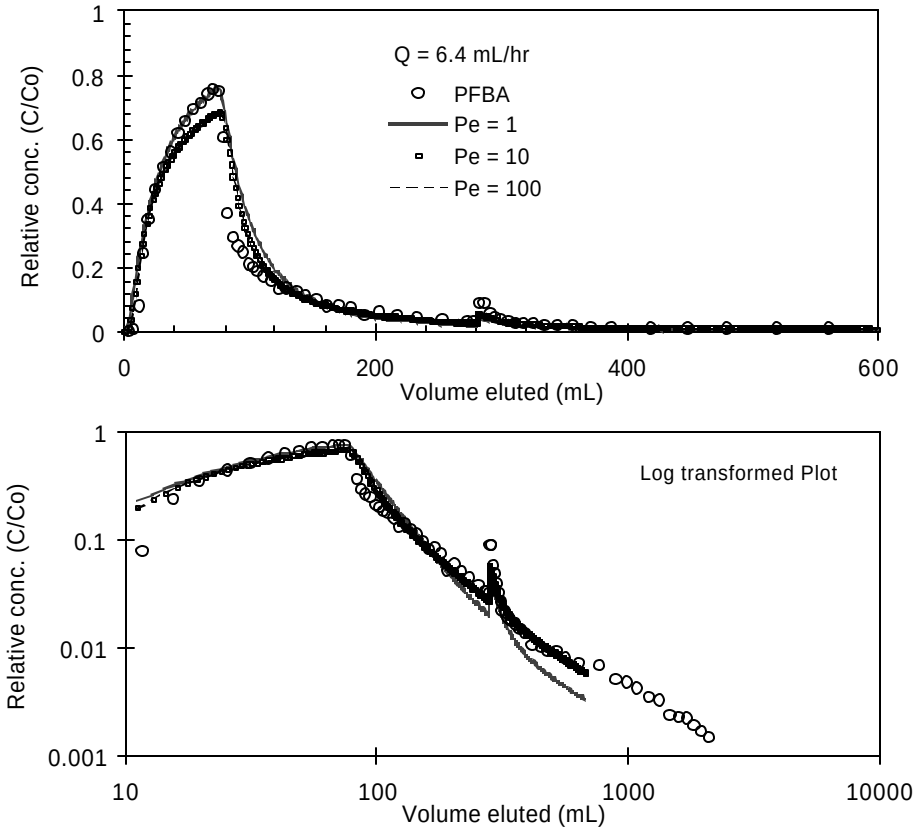

Figure 2.5. Experimental and modeling results from the three I^- transport tests, core 1. All three data sets were used to simultaneously fit t, Pe and MTC. Data are relative to injection concentration.

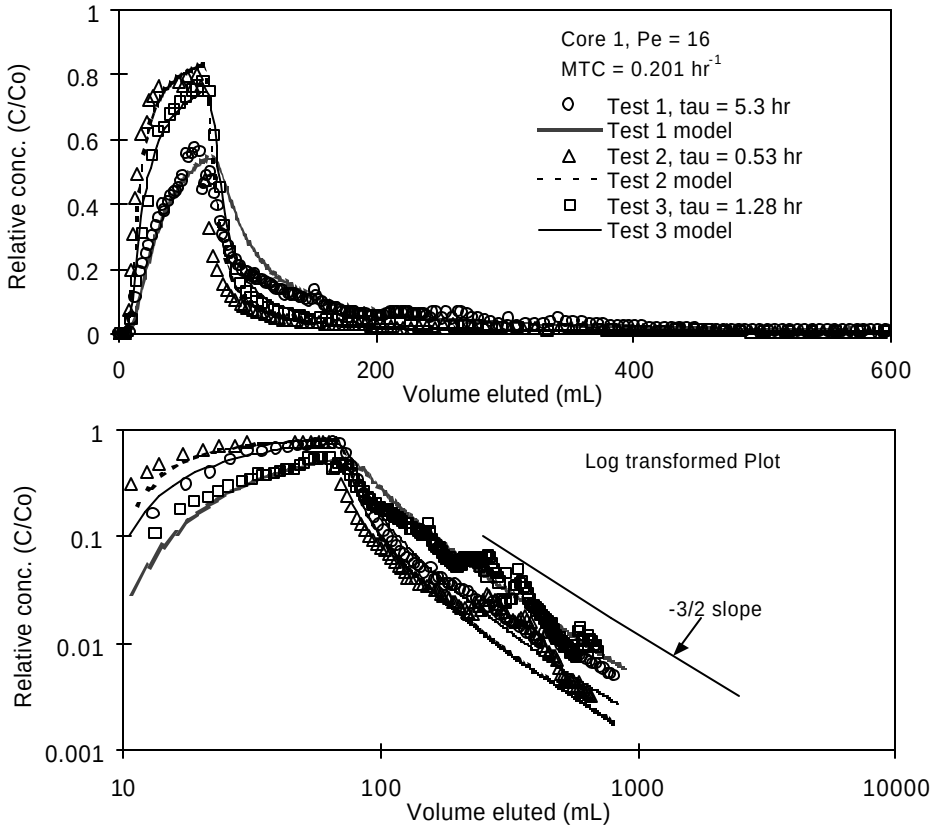

Figure 2.6. Experimental and modeling results from the PFBA/Br^- transport test, core 1. Both data sets were used to simultaneously fit t, *Pe* and *MTC*. Data are relative to injection concentration.

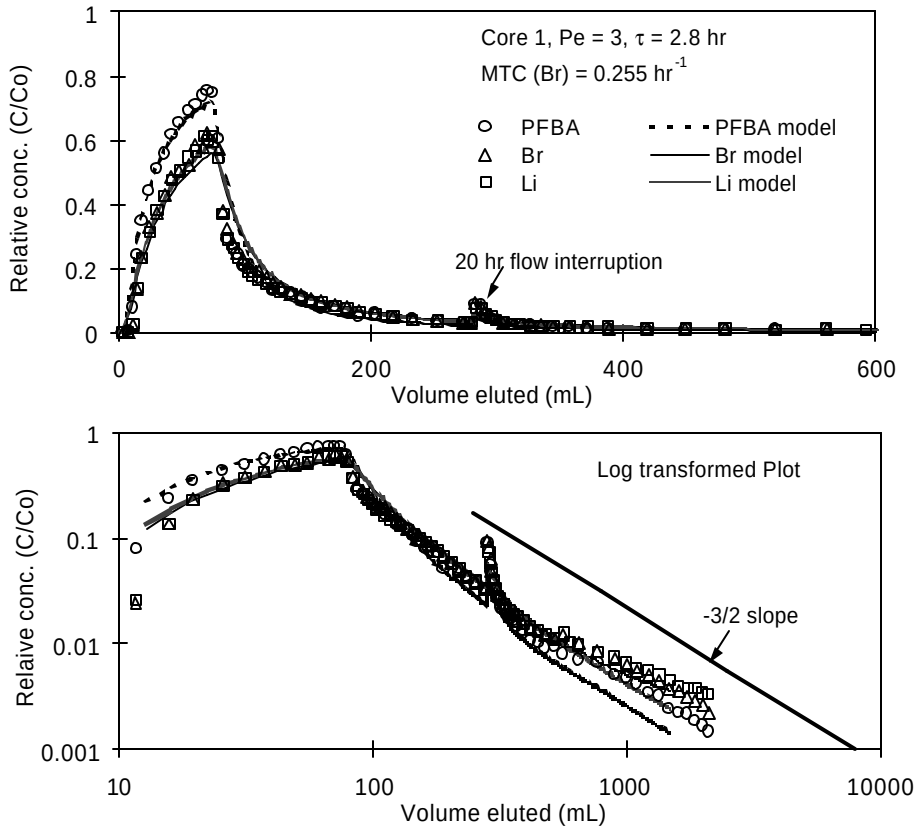

Figure 2.7. Experimental and modeling results from the three I^- transport tests, core 2. All three data sets were used to simultaneously fit t, Pe and MTC. Data are relative to injection concentration.

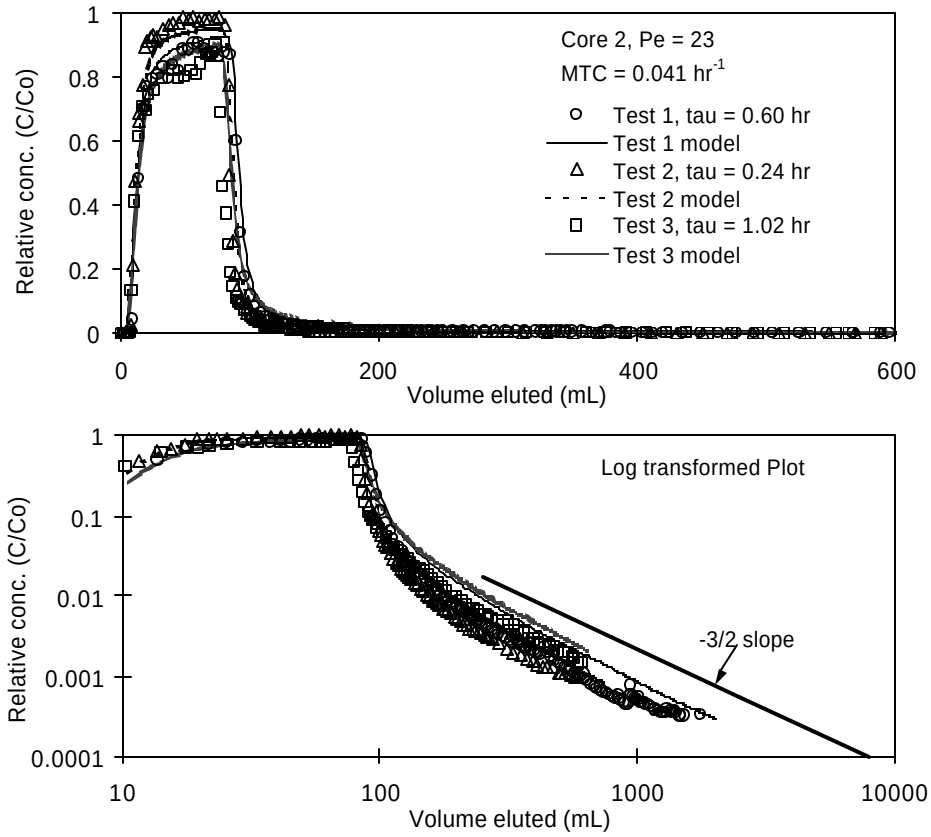

Figure 2.8. Experimental and modeling results from the PFBA/Br^- transport test, core 2. Both data sets were used to simultaneously fit t, *Pe* and *MTC*. Data are relative to injection concentration.

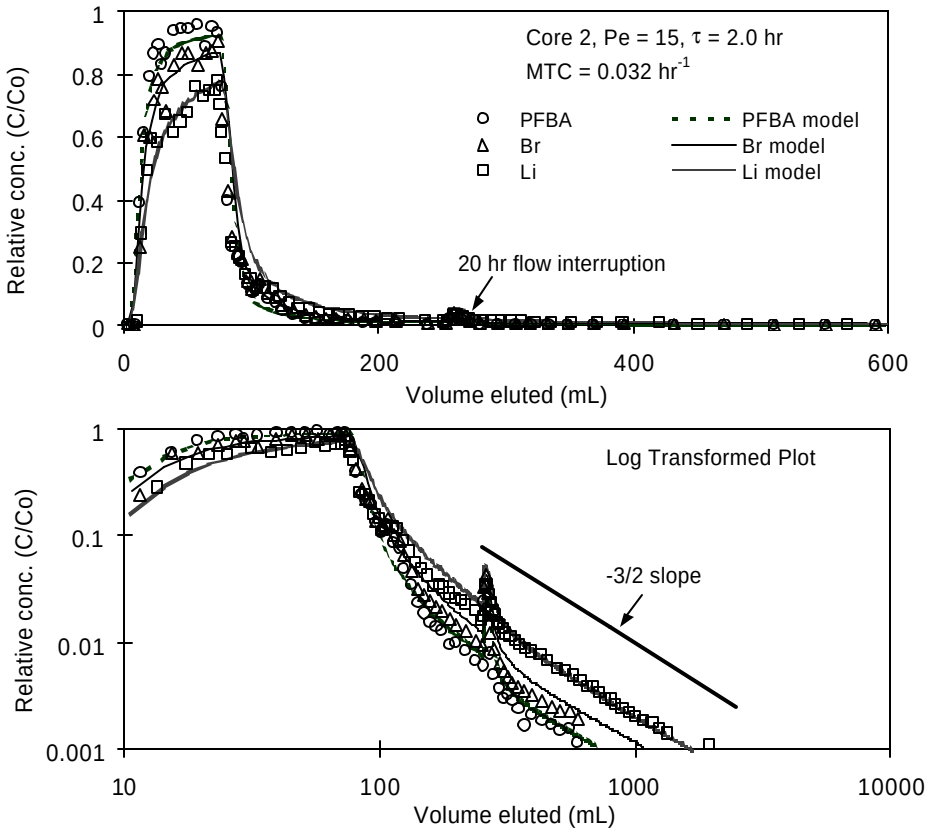

To investigate the advantages of simultaneously interpreting multiple data sets, a single tracer data set was fitted using the semi-analytical method of *Tang et al.* [1981] three times by assuming *Pe* equal to 1, 10, and 100 and allowing t and *MTC* to float in each case. Similar fits were obtained regardless of which *Pe* was used (Figure 2.4). The values of t and the *MTC* were also different depending on the *Pe* used in the fitting procedure. For *Pe* = 1, the *MTC* = 0.0144 hr^{-1}. Increasing *Pe* to 10 produced an *MTC* of 0.436 hr^{-1}, and increasing it further to 100 gave an *MTC* of 1.44 hr^{-1}. The resulting fits are all quite similar, especially for the two higher *Pe* cases. Assuming that both dispersion

and matrix diffusion influenced tracer transport, it is evident that the processes could not be separated by analyzing only one tracer response.

2.4.1.3. Tracer Transport Results. The experimental and modeling results for the tracer tests in core 1 are listed in Tables 2.3 and 2.5 and shown in Figures 2.5 and 2.6. The corresponding data for core 2 are listed in Tables 2.4 and 2.6 and Figures 2.7 and 2.8. The maximum relative concentrations were different for the two solutes and the tails of the breakthrough curves exhibited a -1.5 slope in log space. Both phenomena are assumed indicative of diffusive mass transfer in dual porosity media [*Maloszewski and Zuber*, 1985; *Maloszewski and Zuber*, 1993; *Tsang*, 1995; *Maloszewski et al.*, 1999]. The amount of mass transfer between the fracture and the porous matrix was dependent on 1) fracture residence times, as seen from the I^- data, 2) matrix diffusion coefficients (Br^-/PFBA data), and 3) matrix permeabilities (comparing the two core samples). There was much more analytical deviation at low concentrations with the ion-selective electrode method for the I^- tests than the IC method for the Br^-/PFBA tests. This is most apparent when the data are plotted in log space.

For core 1, the mass transfer coefficient (*MTC*) from the I^- tests was 0.201 hr^{-1} compared to 0.255 hr^{-1} for Br^- from the Br^-/PFBA test (Table 2.5). Because the matrix diffusion coefficient for Br^- was constrained to be three times larger than PFBA, the *MTC* for PFBA was 0.085 hr^{-1}. The calculated *Pe* was 16 from the I^- tests and 3.0 from the Br^-/PFBA test. All three I^- experiments were conducted before the Br^-/PFBA test; during the latter experiment, the amount of water in the void space of the inlet had increased (by displacing air that had previously occupied the space), and it is possible that this

increased the volume of the injection manifold resulted in larger apparatus-induced dispersion (thus the smaller value of *Pe*). This may have also caused the erroneously large fracture residence time for the Br^-/PFBA experiment (Table 2.5).

For core 2, the *MTCs* were 0.041 hr^{-1} (I^- data sets) and 0.032 hr^{-1} (Br^-). The *Pe* calculated from the I^- data was 23 and from the Br^-/PFBA data *Pe* was 15, which is relatively good agreement. The inlet and outlet volumes for this sample were much smaller than in core 1 and therefore apparatus-induced dispersion should have been minimized.

The purpose of the flow interruption step at late times was to provide further verification of the dual porosity concept for the fractured rock cores. Figure 2.6 shows that the response was qualitatively matched yet underpredicted by RETRAN. This suggests that the method of *Tang et al.* [1981] overestimated the amount of mass transfer back into the fracture prior to the flow interruption; to conserve mass balance, the model underpredicted the concentration increase after the flow interruption. Conversely, the model fits match the data well for core 2 (Figure 2.8). Perhaps more importantly, the flow interruption procedure confirmed the importance of matrix diffusion as a limiting process on tracer transport in both fractured rock cores.

2.4.2. Diffusion Cells

2.4.2.1. Falling Head Permeameter Results. The matrix permeabilities for cores 1 and 2 were 4.7 x 10^{-15} and 7.8 x 10^{-19} m^2, respectively. These values were five and nine orders of magnitude less than the estimated fracture permeabilities for the respective

cores. This verified the applicability of the dual porosity conceptual model to solute transport in the fractured volcanic tuff samples.

2.4.2.2. Diffusion Data Interpretation Procedure. To estimate matrix diffusion coefficients, one-dimensional diffusion was assumed to be the only transport mechanism in the wafers. The one-dimensional diffusion equation was used

$$\frac{\partial C}{\partial t} = D_m \frac{\partial^2 C}{\partial x^2}. \tag{2.10}$$

The equations describing the tracer concentrations in the upper and the lower reservoirs were:

$$\frac{\partial C_u}{\partial t} = \frac{n_m p\ r^2 D_m}{V_u} \left.\frac{\partial C}{\partial x}\right|_{x=0} \tag{2.11}$$

$$\frac{\partial C_l}{\partial t} = -\frac{n_m p\ r^2 D_m}{V_l} \left.\frac{\partial C}{\partial x}\right|_{x=l} - \frac{Q}{V_l} C_l. \tag{2.12}$$

The concentration in the upper and lower reservoirs were C_u and $C_{l,}$ respectively; V_u and V_l were the volumes of the upper and lower reservoirs, r was the radius of the rock wafer, l was the diffusion distance (i.e., the thickness of the wafer), and Q was the flush rate through the lower reservoir.

A finite-difference method that allowed the user to specify changes in the flush rate with time was used to solve (2.10). The resulting simulations were iteratively matched to the data to obtain the matrix diffusion coefficient estimates for each solute.

2.4.2.3. Diffusion Cell Results. Table 2.7 lists the experimental and modeling results for matrix diffusion coefficients for both rock wafers. The data are shown

graphically in Figures 2.9 and 2.10. For wafer 1, the matrix diffusion coefficients were 6.0 x 10^{-10} m^2 s^{-1} and 1.9 x 10^{-10} m^2 s^{-1} for Br^- and PFBA, respectively. Results for the same ions in wafer 2 were 0.4 x 10^{-10} m^2 s^{-1} and 0.13 x 10^{-10} m^2 s^{-1}. The matrix permeabilities for the samples were 4.7 x 10^{-15} and 7.8 x 10^{-19} m^2, respectively. This positive correlation between matrix diffusion coefficient and permeability has been demonstrated in several other rock types from the C-Wells field site [*Reimus et al.*, 1999].

Table 2.7. Experimental conditions and results from the diffusion cell experiments for wafers 1 and 2.

	Wafer 1, upper flow zone	Wafer 2, central flow zone
Experimental Parameters		
Reservoir flush rate (mL hr^{-1})	0.8 – 8.0	0.8 – 6.0
Injection concentration (mg L^{-1})	399 (Br-) 1326 (PFBA)	1677 (Br-) 1069 (PFBA)
Modeling Parameters		
Br- (x 10^{-10} m^2 s^{-1})	6.0	0.4
PFBA (x 10^{-10} m^2 s^{-1})	1.9	0.13
Br^-: PFBA ratio	3.2	3.1

The value for the Br^- matrix diffusion coefficient was about three times greater than that for PFBA, similar to the ratio of the published free water diffusion coefficients. This result verified that advection through the diffusion wafers was negligible, as any advection would have resulted in a smaller difference between the breakthrough curves of the two tracers.

Figure 2.9. Experimental and modeling results for diffusion cell test, wafer 1. Data are relative to injection concentration.

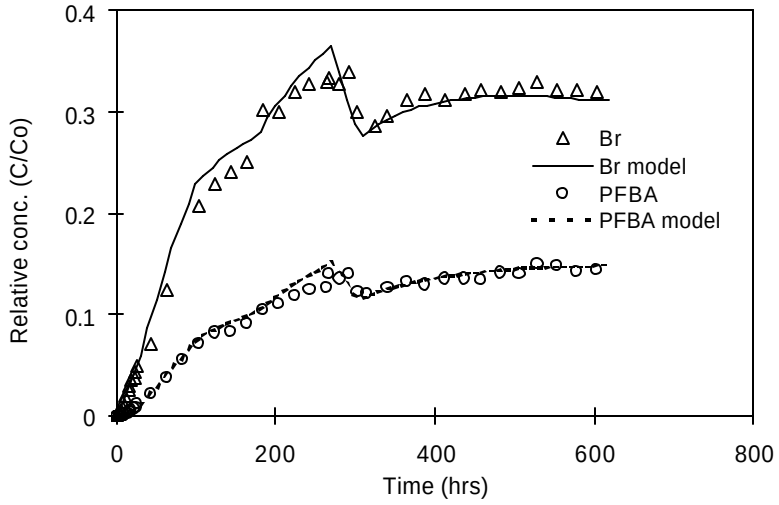

Figure 2.10. Experimental and modeling results for diffusion cell test, wafer 2. Data are relative to injection concentration.

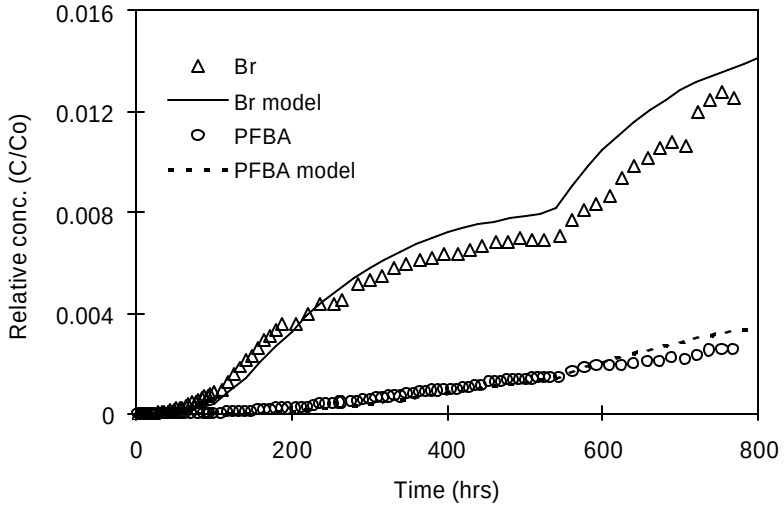

2.4.3. Comparing Fractured Rock Core and Diffusion Cell Data

If the conceptualization of fracture-matrix interaction is correct, the matrix diffusion coefficients calculated for Br^- and PFBA from the fracture transport tests and

the diffusion cell tests should have been the same. Comparisons between the different types of experiments can be made in two ways: 1) Using the matrix porosity measurement n_m and the calculated fracture aperture B from the relationship $B = \frac{Qt}{Lw}$ to calculate D_m from the MTC $\left[\left(\frac{n_m}{B}\right)^2 D_m\right]$ and comparing this value to the estimated D_m from the corresponding diffusion cell test; or the opposite technique 2) using the estimated D_m from the diffusion cell test to calculate B from the MTC and compare to the value from $B = \frac{Qt}{Lw}$. Either a larger D_m (method 1) or a smaller B (method 2) from the fitted MTC would indicate a greater amount of mass transfer in the fractured rock cores than would be predicted using the diffusion cell D_m value. Comparing the two estimates of B may provide insights into flow channeling and surface roughness within the fractures. Another concern is the large difference in the geometry of the two media. Although the diffusion wafers and the fractured cores are the same diameter (0.095 cm), the diffusion wafers are only about 0.01 m in length, much smaller than the fractured rock cores (0.016 m and 0.017 m long for core 1 and core 2, respectively). Yet the diffusion distance in the fractured cores was at most 0.009 m (as calculated above), which is on the same order as the diffusion wafer thickness.

However, the matrix diffusion coefficients determined from the two methods were not the same. For core 1, the matrix diffusion coefficient for Br^- calculated from the fractured core tracer test was 12.9 x 10^{-10} m^2 (Table 2.5), about two times greater than the Br^- value of 6.0 x 10^{-10} determined from the diffusion cell test (Table 2.7). For core 2, the matrix diffusion coefficient for Br^- calculated from the fractured rock core was 2.4 x 10^{-10}

$m^2\ s^{-1}$ (Table 2.6), six times greater than the diffusion cell result of $0.4 \times 10^{-10}\ m^2\ s^{-1}$ (Table 2.7). These differences may have been due to 1) a larger fracture surface area than would be calculated assuming parallel plates, due to the roughness of the fracture, 2) solute diffusion into stagnant free water in the fractures, or 3) the geometric difference between the two apparatuses. The first two hypotheses could directly explain an apparently larger amount of mass transfer between the fracture and matrix than predicted from diffusion cell data. This result may be most important for rocks of low matrix permeability (e.g., $7.8 \times 10^{-19}\ m^2$ for wafer 2) and hence low matrix diffusion. When the matrix diffusion coefficients estimated from the diffusion cell tests are inserted into the *MTC* determined from the fracture transport tests, the effective aperture *B* for core 1 is calculated to be $\sqrt{2}$ times less than that obtained from $B = \frac{Qt}{Lw}$. For core 2, the difference was $\sqrt{6}$ times less. Thus, the effective fracture surface area to volume ratio was either $\sqrt{2}$ or $\sqrt{6}$ times greater for the respective cores than that calculated from the length, width, and mean solute residence time. Previous researchers [*Brown et al.*, 1998; *Wan et al.*, 2000] have demonstrated that flow channeling occurs in casts of natural fractures. Models describing solute transport in channelized flow systems have been proposed to explain tracer transport data [*Tsang et al.*, 1988; *Johns and Roberts*, 1991]. Diffusion of solutes from flow channels into stagnant regions within fractures has also been suggested for fractured rock systems [*Raven et al.*, 1988; *National Research Council*, 1996; *Grenier et al.*, 1998; *Wallach and Parlange*, 1998]. Free water diffusion should proceed at a rate faster than matrix diffusion, and mass transfer between the flowing water in channels and stagnant water within the fracture would have been interpreted as matrix diffusion by our model. This may be the most likely explanation for

the overestimation of matrix diffusion coefficients in the fractures. This process may be more important in short-term laboratory experiments than in field studies. At the field scale, matrix diffusion would likely dominate over diffusion into stagnant water in dual porosity media due to the much larger volume of porous matrix relative to stagnant water in fractures.

2.5. Conclusions

This study has demonstrated the importance of using multiple experimental methods and multiple solutes of differing diffusion coefficients together to estimate transport parameters in fractured, dual porosity media. It is apparent that analyzing tracer tests using only one solute leads to nonunique results for these parameters. By analyzing multiple tracer data sets, the processes of matrix diffusion and dispersion within a fracture were effectively separated and the parameter estimates were much more constrained.

The results of the laboratory experiments confirm that matrix diffusion serves to increase the transport time of solutes in dual porosity media by spreading mass away from the advecting region of the fractures, thus utilizing the capacitance of the porous matrix. In log space, the decrease in solute concentration with volume eluted follows a -1.5 slope, often assumed indicative of diffusive mass transfer into an infinite domain. However, the results of these short-term tests were probably influenced to some degree by free water diffusion into stagnant water within the fractures, which may explain why the matrix diffusion coefficients estimated from the fracture transport tests were consistently larger than those measured in the diffusion cell tests. In field experiments,

where the solute residence times are usually much larger than in laboratory experiments, the influence of free water diffusion within fractures should be minimal. That is, the relative volume of porous matrix should be much larger than that of the stagnant water in fractures.

Notation

a hydrodynamic dispersivity in fracture [L]

m dynamic viscosity of water [M L^{-1} T^{-1}]

r density of water [M L^{-3}]

t mean solute residence time in fracture [T]

B tracer fracture aperture [L]

B_h hydraulic fracture aperture [L]

C solute concentration in the aqueous phase (subscript *f* for fracture, *m* for matrix) [M L^{-3}]

C_o solute concentration of injection pulse [M L^{-3}]

$\overline{C}$ Laplace transform of solute concentration in the aqueous phase (subscript *f* for fracture, *m* for matrix) [M L^{-3}]

D_f hydrodynamic dispersion coefficient in fracture [L^2 T^{-1}]

D_m effective matrix diffusion coefficient in pore water [L^2 T^{-1}]

dh/dx hydraulic gradient [-]

g gravitational acceleration constant [L T^{-2}]

K hydraulic conductivity of fractured rock cores (fracture or matrix) [L T^{-1}]

k permeability of the fractured rock cores (fracture or matrix) [L^2]

L fracture length [L]

l thickness (length) of diffusion wafers [L]

MTC mass transfer coefficient for diffusive transport between fracture and matrix [T^{-1}];

$$MTC = \left(\frac{n_m}{B} \right)^2 D_m$$

n_f porosity within a fracture; for an open fracture, $n_f = 1$ [-]

n_m porosity of matrix material; fraction of pore volume to total volume [-]

Pe Peclet number [-]; $Pe = \frac{v_f L}{D_f} = \frac{L}{a}$ where $D_f = a\ v_f$

Q volumetric flow rate [$L^3\ T^{-1}$]

q specific discharge through fracture [$L\ T^{-1}$]

r radius of diffusion cell wafer [L]

s transform variable for Laplace space [T^{-1}]

t_p time of solute injection pulse [T]

V_u volume of diffusion cell tracer reservoir [L^3]

V_l volume of diffusion cell flush reservoir [L^3]

v_f velocity of water flowing in fractures [$L\ T^{-1}$]

w fracture width [L]

Acknowledgments. Financial support for this work was provided by the U.S. Department of Energy, Office of Civilian Radioactive Waste Management, as part of the Yucca Mountain Site Characterization Project. We wish to thank Kent Novakowski, Roy Haggerty, Lucy Meigs, John Wilson, Fred Phillips, Brian McPherson, and an anonymous reviewer for their helpful comments. We also thank Dale Counce for the sample analyses.

References

Benson, C. F. and R. S. Bowman, Erratum in: Tri- and tetrafluorobenzoates as nonreactive tracers in soil and groundwater, *Soil Sci. Soc. Am. J., 60*, 1780, 1996.

Brady, P. V. and J. V. Walther, Controls on silicate dissolution rates in neutral and basic pH solutions and 25°C, *Geochim. Cosmochim. Acta, 53*, 2823-2830.

Brown, S. R., Fluid flow through rock joints: The effect of surface roughness, *J. Geophys. Res., 92* (B2), 1337-1347, 1987.

Brown, S., A. Caprihan, and R. Hardy, Experimental observation of fluid flow channels in a single fracture, *J. Geophys. Res., 103* (B3), 5125-5132, 1998.

Brusseau, M. L., Q. Hu, and R. Srivastava, Using flow interruption to identify factors causing nonideal contaminant transport, *J. Contam. Hyd., 24*, 205-219, 1997.

Detwiler, R. L., S. E. Pringle, and R. J. Glass, Measurement of fracture aperture fields using transmitted light: An evaluation of measurement errors and their influence on simulations of flow and transport through a single fracture, *Water Resour. Res., 35*, 2605-2617, 1999.

Domenico, P. A. and W. Schwartz, Physical and chemical hydrogeology, John Wiley and Sons, New York, 1990.

Dronfield, D. G. and S. E. Silliman, Velocity dependence of dispersion for transport through a single fracture of variable roughness, *Water Resour. Res., 29*, 3477-3483, 1993.

Freeze, R. A. and J. A. Cherry, *Groundwater*, Prentice-Hall, Inc., Upper Saddle River, NJ, 1979.

Fuentes, H. R., W. L. Polzer, E. H. Essington, and B. D. Newman, Characterization of reactive tracers for C-Wells Field Experiment I: Electrostatic sorption mechanism, lithium, *Los Alamos National Laboratory Report, LA-11691-MS*, Los Alamos, NM, 1989.

Geldon, A. L., Preliminary hydrogeologic assessment of boreholes UE-25c#1, UE-25c#2, and UE-25c#3, Yucca Mountain, Nye County, Nevada, *Water-Resources Investigations Report 92-4016*, United States Geological Survey, Denver, CO, 1993.

Grenier C., E. Mouche, and E. Tevissen, Influence of variable fracture aperture on transport of non-sorbing solutes in a fracture: a numerical investigation, *J. Contam. Hyd., 35*, 305-313, 1998.

Grisak, G. E. and J. F. Pickens, Solute transport through fractured media, 1. The effect of matrix diffusion, *Water Resour. Res., 16*, 719-730, 1980.

Grisak, G. E., J. F. Pickens, and J. A. Cherry, Solute transport through fractured media. 2. Column study of fractured till, *Water Resour. Res., 16*, 731-739, 1980.

Haggerty, R. and S. Gorelick, Multiple-rate mass transfer for modeling diffusion and surface reactions in media with pore-scale heterogeneity, *Water Resour. Res., 31*(10), 2383-2400, 1995.

Hull, L. C., J. D. Miller, and T. M. Clemo, Laboratory and simulation studies of solute transport in fracture networks, *Water Resour. Res., 23*, 1505-1513, 1987.

Johns, R. A. and P. V. Roberts, A solute transport model for channelized flow in a fracture, *Water Resour. Res., 27*, 1797-1808, 1991.

Lapcevic, P. A., K. S. Novakowski, and E. A. Sudicky, The interpretation of a tracer experiment conducted under conditions of natural groundwater flow, *Water Resour. Res., 35*, 2301-2312, 1999.

Maloszewski, P. and A. Zuber, On the theory of tracer experiments in fissured rocks with a porous matrix, *J. Hydrol., 79*, 333-358, 1985.

Maloszewski, P. and A. Zuber, Tracer experiments in fractured rocks: Matrix diffusion and the validity of models, *Water Resour. Res., 29*, 2723-2735, 1993.

Maloszewski, P., A. Herrmann, and A. Zuber, Interpretations of tracer tests performed in fractured rock of the Lange Bramke basin, Germany, *Hydrogeol. J., 7*, 209-218, 1999.

Moreno, L. and C.-F. Tsang, Multiple-peak response to tracer injection tests in single fractures: a numerical study, *Water Resour. Res., 27* (8), 2143-2150, 1991.

National Research Council, Committee on Fracture Characterization and Fluid Flow, Rock Fractures and Fluid Flow: Contemporary Understanding and Applications, National Academy Press, Washington, D.C., 1996.

Neretnieks, I., T. Eriksen, and P. Tahtinen, Tracer movement in a single fissure in granitic rock: Some experimental results and their interpretation, *Water Resour. Res., 18*, 849-858, 1982.

Newman, J. S., Electrochemical Systems, Prentice-Hall, Englewood Cliffs, NJ, 1973.

Ohlsson, Y. and I. Neretnieks, Some evidence for surface ion mobility in rock, *J. Contam. Hyd., 35*, 91-100, 1998.

Raven, K. G., K. S. Novakowski, and P. A. Lapcevic, Interpretation of field tracer tests of a single fracture using a transient solute storage model, *Water Resour. Res., 24*, 2019-2032, 1988.

Reedy, O. C., P. M. Jardine, G. V. Wilson, and H. M. Selim, Quantifying the diffusive mass transfer of nonreactive solutes in columns of fractured saprolite using flow interruption, *Soc. Sci. Am. J., 60*, 1376-1384, 1996.

Reimus, P. W., A. Adams, M. J. Haga, A. Humphrey, T. Callahan, I. Anghel, and D. Counce, Results and interpretation of hydraulic and tracer testing in the Prow Pass Tuff at the C-Holes, *Yucca Mountain Project Milestone SP32E7M4*, Los Alamos National Laboratory, Los Alamos, NM, 1999.

Tang, D. H., E. O. Frind, and E. A. Sudicky, Contaminant transport in fractured porous media: Analytical solution for a single fracture, *Water Resour. Res., 17*, 555-564, 1981.

Thompson, M. E., Numerical simulation of solute transport in rough fractures, *J. Geophys. Res., 96* (B3), 4157-4166, 1991.

Tsang, Y. W., Usage of "equivalent apertures" for rock fractures as derived from hydraulic and tracer tests, *Water Resour. Res., 28*, 1451-1455, 1992.

Tsang, Y. W., Study of alternative tracer tests in characterizing transport in fractured rocks, *Geophys. Res. Lett., 22*, 1421-1424, 1995.

Tsang, Y. W., C.-F. Tsang, I. Neretnieks, and L. Moreno, Flow and tracer transport in fractured media: A variable aperture channel model and its properties, *Water Resour. Res., 24*, 2049-2060, 1988.

Wallach, R. and J.-Y. Parlange, Modeling transport in a single crack by the dual-porosity concept with a boundary layer at the interface, *J. Contam. Hyd., 34*,121-138, 1998.

Wan, J., T. K. Tokunaga, T. R. Orr, J. O'Niell, and R. W. Connors, Glass casts of rock fracture surfaces: A new tool for studying flow and transport, *Water Resour. Res., 36(1)*, 355-360, 2000.

Wels, C. and L. Smith, Retardation of sorbing solutes in fractured media, *Water Resour. Res., 30,* 2547-2563, 1994.

Wels, C., L. Smith, and T. T. Vandergraaf, Influence of specific surface area on transport of sorbing solutes in fractures: An experimental analysis, *Water Resour. Res., 32*, 1943-1954, 1996.

3. Interpreting Asymmetric Transport Patterns of High Concentration Ionic Tracers in Porous Media

(In preparation for submission to *Journal of Environmental Quality*)

Timothy J. Callahan[1,2], Paul W. Reimus[1], Peter C. Lichtner[3], and Robert S. Bowman[2]

[1]Environmental Science and Waste Technology Group, Los Alamos National Laboratory, Los Alamos, NM 87545

[2]Department of Earth and Environmental Science, New Mexico Institute of Mining and Technology, Socorro, NM 87801

[3]Hydrology, Geochemistry and Geology Group, Los Alamos National Laboratory, Los Alamos, NM 87545

Abstract. It is common practice to describe reactive contaminant transport in complex field situations using a linear sorption (K_D) model. Estimates of K_D are often obtained from laboratory or field tracer tests where a pulse of tracer solution is injected at high concentrations to ensure adequate detection at the sampling point(s). We discuss the potential inaccuracies associated with using K_Ds derived from high-concentration tracer tests to describe transport of ionic solutes in lower-concentration contaminant plumes.. We conducted column tracer tests in crushed rock using lithium as a dissolved cationic tracer. When injected at high concentrations, the lithium produced asymmetric breakthrough curves due to ion-exchange with the other cations in the system (sodium and calcium). Using a simple K_D value without accounting for competitive ion effects did not fully explain the lithium breakthrough curves and tended to underpredict retardation of lithium. Using ion exchange theory and a simplified three-component system, we were

able to accurately describe the asymmetric elution behavior. We conclude that, for ion exchanging species, K_Ds derived from high-concentration tracer tests will tend to underpredict contaminant retardation, and that ion exchange models will allow more accurate extrapolations from high concentration tracer tests to lower concentration contaminant plumes.

3.1. Introduction

Transport data obtained from the injection and recovery of tracer materials is often used in both surface water and groundwater hydrology studies to estimate system properties such as travel time, dispersion, and chemical reactions of pollutants. These transport data are often used without considering the applicability of the experimentally-derived information to natural contaminant conditions. Linear sorption models are often used to explain the transport of reactive tracers. In the case of cations such as lithium ion, the amount of retardation is a function of its concentration [*Fetter*, 1993; *Appelo and Postma*, 1993; *Reimus et al.*, 1999] as well as the concentration of other cations in the system. Here, we use an ion-exchange approach to describe asymmetric transport behavior of lithium that was due to its high concentration in the tracer pulse.

It is well known that solute partitioning between the aqueous and solid phases can be a function of contaminant concentration. However, the effects other ions in solution have on transport behavior are often overlooked. Several previous studies have employed a multicomponent approach to describe reactive transport in porous media [*Charbeneau*, 1981; *Valocchi et al.*, 1981a; b; *Appelo and Williamsen*, 1987; *Charbeneau*, 1988; *Appelo et al.*, 1990; *Griffioen et al.*, 1992; *Appelo et al.*, 1993; *Mansell et al.*, 1993; *Appelo and*

Postma, 1993; *Appelo*, 1994; *Cerník et al.*, 1994; *Lichtner*, 1995; *Appelo*, 1996; *Bond*, 1997; *LeGallo et al.*, 1998; *TebesStevens et al.*, 1998; *Vulava*, 1998; *TebesStevens and Valocchi*, 2000; *Voegelin et al.*, 2000]. Reviews of multicomponent models are found in *Liu and Narasimhan* [1989], *Yeh and Tripathi* [1989], and *Lichtner* [1996]. Predictive models such as HYDROGEOCHEM [*Yeh and Tripathi*, 1988], PHREEQC [*Parkhurst*, 1995], FEREACT [*TebesStevens et al.*, 1998], and FEHM [*Robinson et al.*, 2000] have been used to describe multiple-species transport in geologic media, especially those species that are affected by chemical or biological reactions. However, these computer programs often are computationally intensive and have numerous fitting parameters, resulting in nonunique solutions of the transport parameters. Here, we propose a simplified method of interpreting transport behavior of a solute, lithium, that is assumed to be dominated by cation exchange.

In this study, the transport of ionic tracers was studied by injecting pulses of tracer solutions into columns containing crushed and sieved ash flow tuff from the C-Wells site in Nevada [*Reimus et al.*, 1999]. The initial purpose was to estimate the sorption characteristics of the solid material with respect to lithium ion (Li^+), providing the Yucca Mountain Site Characterization Project with transport data for this sorbing ion [*Reimus et al.*, 1999]. However, interpreting the transport behavior of the bromide (Br^-) and Li^+ tracers using a linear retardation factor was inadequate. Therefore, the effects of ion exchange equilibria for the ternary ion system $Li^+\backslash Na^+\backslash Ca^{2+}$ were investigated, based on the groundwater geochemistry at the field site. The objective was to determine the ability of an ion exchange model to describe Li^+ transport data and the implications of ion exchange equilibria to high concentration field tracer tests.

3.2. Theory

Appelo and Postma [1993] provide a review of multicomponent transport theory, and their Table 5.5 lists equations for the exchange of various cations for sodium in a soil matrix. The equation describing a cation exchanging with a sodium ion on a negatively-charged monovalent surface exchange site *X* is

$$\frac{1}{z_i} i^{z_i+} + NaX \leftrightarrow \frac{1}{z_i} iX_{z_i} + Na^+ \qquad K_{i\backslash Na} = \frac{[iX_{i_i}]^{1/z_i}[Na^+]}{[i^{z_i+}]^{1/z_i}[NaX]}, \qquad (3.1)$$

where i is the exchanging cation of valence z_i and the equilibrium exchange coefficient is $K_{i\backslash Na}$, [*Appelo and Postma*, 1993; *Appelo*, 1996]. The brackets refer to molar concentration, either in the liquid (Na^+) or on the solid (NaX). Equilibrium equations such as these implicitly account for charge balance in the system. Finite difference numerical methods that simulate solute transport [*Callahan et al.*, 2000] were used in conjunction with mass action equations of the form in (3.1) to fully describe multicomponent transport. The transport equations listed in *Callahan et al.* [2000] pertain to a dual-porosity system, but the equations were simplified here because single-porosity conditions were assumed for the columns (i.e., all water was assumed to be mobile). It was determined that aqueous complexation did not appreciably affect the model simulations. Therefore, only free ion species were considered.

Ion exchange equilibria relationships were added to the Reactive Transport code (RETRAN), an implicit alternating-direction finite difference algorithm that provides approximate solutions to the advection dispersion equation [*Reimus et al.*, 1999]. This expanded version of RETRAN is called the Reactive Transport Multicomponent code (RETRAN-M). Adapting the approach of *Appelo and Postma* [1993] and *Appelo* [1994], the mass action equations for Li^+, Na^+, and Ca^{2+} exchange in RETRAN-M are

$$Li^+ + NaX \leftrightarrow LiX + Na^+ \qquad K_{Li\backslash Na} = \frac{[LiX][Na^+]}{[NaX][Li^+]} \qquad (3.2)$$

$$Li^+ + 0.5CaX_2 \leftrightarrow LiX + 0.5Ca^{2+} \qquad K_{Li\backslash Ca} = \frac{[LiX][Ca^{2+}]^{0.5}}{[CaX_2]^{0.5}[Li^+]} \qquad (3.3)$$

$$Na^+ + 0.5CaX_2 \leftrightarrow NaX + 0.5Ca^{2+} \qquad \frac{K_{Li\backslash Ca}}{K_{Li\backslash Na}} = \frac{[NaX][Ca^{2+}]^{0.5}}{[CaX_2]^{0.5}[Na^+]}, \qquad (3.4)$$

Also included in the model was the cation exchange capacity (CEC)-mass balance equation for this three component system

$$CEC = [LiX] + [NaX] + 0.5[CaX_2], \qquad (3.5)$$

The ion exchange parameters $K_{Li\backslash Na}$, $K_{Li\backslash Ca}$, and CEC are fitting parameters in RETRAN-M for experiments in which the effluent is not monitored for Na^+ and Ca^{2+} concentrations; thus the problem is inherently nonunique. The model can be calibrated using tracer (Li^+) transport data by altering the values of $K_{Li\backslash Na}$, $K_{Li\backslash Ca}$, and CEC in RETRAN-M for each tracer test to provide the best fit to a set of Li^+ transport data. However, equally good model fits can be obtained by assuming a two-component system (e.g., Li^+/Na^+). Furthermore, there exists more than one combination to the ion exchange parameters and the CEC value for each tracer data set.

3.3. Methods

A rock sample was obtained from the C-Wells complex at the Nevada Test Site. The sample was taken as core from well UE25c #2 at a depth interval of 733.7 m - 735.4 m below surface, in the Bullfrog Tuff Member of the Crater Flat Tuff Formation. This interval of the Bullfrog Tuff is categorized by *Geldon* [1993] as the central flow zone, based on hydraulic testing of the saturated zone at the C-Wells. The rock lithology,

quantitative X-ray diffraction (QXRD) results, Li^+ batch sorption data, and Li^+ CEC results are presented by *Callahan* [2001]. The central Bullfrog Tuff contributed 93% of all flow into borehole UE25c #2 during open hole pump testing, based on flow logs [*Geldon*, 1993].

The core sample obtained for these tests was broken into ≤ 1-cm pieces using a 2-kg hammer on a cobalt-nickel alloy plate. The pieces were then crushed using a standard jaw crusher (Retsch, type BBO, GmbH & Co., Haan, Germany) and an agate ball mill (Retsch, type RMO, GmbH & Co., Haan, Germany) and wet sieved to a size fraction of 75 - 500 μm (A.S.T.M.E.-11 specification sieves, Fisher Scientific, Hampton, NH). Water from well J-13, 4 km southeast of the C-Wells site, filtered using a 0.2 μm membrane filter, was used to wet sieve the crushed tuff. Wells UE25 c#2 and J-13 both produce sodium-calcium-bicarbonate waters that have a similar chemical composition. Chemical analyses of the well waters are shown in Table 3.1.

Table 3.1. Water chemistry for well J-13 and well UE25c #2, Nevada Test Site, as reported in *Fuentes et al.* [1989]. Values in mg L^{-1} (except pH).

Species	J-13 well water	UE 25 c#2 water
B	0.13	ND[a]
Br^-	< 0.02[b]	ND
Ca^{2+}	11.3	11
Cl^-	7	7
Fe	0.02	ND
HCO_3^-	124	142
K^+	5	2
Li^+	0.040	0.11
Mg^{2+}	≤ 0.010	0.38
Na^+	44	55
Si^{4+} (as H_4SiO_4)	30	25
SO_4^{2-}	19	22
pH	7.8 – 8.1[b]	7.8

[a]ND: not determined.

[b]Determined from tracer experiments in this study.

Two glass columns, each 91.4 cm long and 0.62 cm in diameter, were filled with water from well J-13 and then packed with the crushed tuff of the particle size range described above. Column 1 was used for tests 1 and 2 and column 2 was used for test 3. The resulting porosity was calculated by measuring the difference in weight of the water-saturated tuff and the dry material, and then dividing that quantity by the volume of the column. The porosities in columns 1 and 2 were 0.56 and 0.57, respectively.

The tracer solutions for tests 1, 2, and 3, containing 249 mg L^{-1} (2.9 meq L^{-1}), 292 mg L^{-1} (3.4 meq L^{-1}), and 73.9 mg L^{-1} (0.85 meq L^{-1}) LiBr, respectively, were prepared in filtered J-13 well water. Table 3.2 lists the complete experimental information. A fraction collector (Model FC-220, Gilson, Inc., Middleton, WI) was used to collect 2.4-mL

samples of the effluent from each column in plastic test tubes. The samples were analyzed using an ion chromatograph (IC) for both Li^+ and Br^-. The detection limits were 0.10 mg L^{-1} for Li^+ and 0.005 mg L^{-1} for Br^-. The original purpose of the tests was to determine a linear sorption coefficient (K_D) for Li^+ and this volcanic tuff. The concentration of other cations in solution was assumed to be irrelevant. Thus, the effluent was not analyzed for any other solutes.

Table 3.2. List of experimental parameters.

Experimental Parameters	Test 1	Test 2	Test 3
Column porosity	0.566	0.566	0.573
Column dry bulk density (g mL^{-1})	1.453	1.453	1.310
Dry weight of solids in column (g)	40.12	40.12	36.15
Column pore volume (mL)	15.64	15.64	15.82
Volumetric flow rate (mL hr^{-1})	9.73	2.20	2.20
Volume of tracer pulse (mL)	49.5	44.8	44.4
Tracer composition (meq L^{-1} LiBr)	2.9	3.4	0.85
Groundwater composition (meq L^{-1} $NaHCO_3$+$Ca(HCO_3)_2$)	2.7	2.7	2.7
Percent recovery (Li^+, Br^-)	105 100	106 100	109 100
$t_{1/2}$, time for Br^- to reach C/C_o = 0.5 (in pore volumes)	1.10	1.08	1.07

The hydrodynamic properties for each column were first estimated using the Br^- transport data and experimental parameters listed in Table 3.2. Values of the equilibrium constants $K_{Li\backslash Na}$ and $K_{Li\backslash Ca}$ were estimated assuming that the flow properties also applied to the cations in the respective experiments. Because the effluent was not analyzed for Na^+ and Ca^{2+} during the experiments, the optimal values of the ion exchange parameters

$K_{Li\backslash Na}$, $K_{Li\backslash Ca}$, and CEC were determined using the model-independent parameter estimation code PEST [*Dougherty,* 1999]. The "best-fit" results were the combination of the three parameters for all three tests that produced the smallest sum-of-squares differences of the model predictions to the Li^+ transport data. As mentioned previously, these parameters were only one set of a large number of possible solutions. The problem was inherently nonunique due to the lack of Na^+ and Ca^{2+} transport data for these experiments.

3.4. Results and Discussion

The amount of Li^+ injected in the tracer pulses for tests 1 and 2 were 49% and 53% of the total cations in solution, respectively, whereas in test 3 the amount of Li^+ was only 22% of the total cations in solution. The rising portion of the Li^+ BTC was explained quite well using a simple retardation approach (Figure 3.1), but the tail was not matched using this approach. Also, the asymmetric elution pattern for Li^+ in test 1 (Figures 3.1, 3.2) and test 2 (Figure 3.3) was not as evident in test 3 (Figure 3.4). This behavior can be explained as follows. First, the tracer pulse of Li^+ moved through the column and exchanged for Na^+ and Ca^{2+}, which resulted in the delay in the Li^+ breakthrough curve (BTC) relative to Br^-. Second, the high concentration of Li^+ relative to the total cations in solution in tests 1 and 2 caused the early elution of Li^+ from the column in order to maintain mass and charge balance in the system. It follows that the less pronounced secondary plateau in test 3 was due to the lower concentration of Li^+ relative to the total cations in solution. Figures 3.2-3.4 show the BTCs for the three tests with the numerical simulations incorporating the mass action equations (3.2) – (3.5) listed above. The

multicomponent model provided a much better fit to the asymmetric Li^+ BTCs than the linear retardation factor approach.

Figure 3.1. Transport data (symbols) from test 1 with model fits (lines) using a linear retardation approach for Li^+.

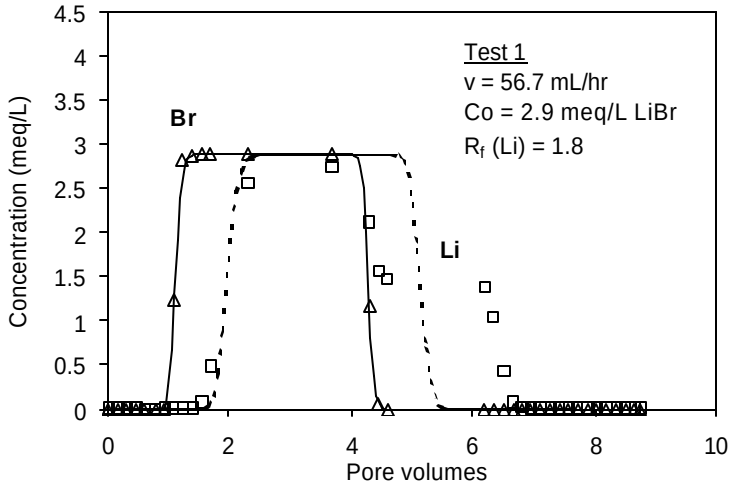

Figure 3.2. Transport data (symbols) from test 1 with model fits (lines) using an ion exchange approach for Li^+. Model fits for Na^+ and Ca^{2+} are based on the least sum-of-squares differences for all three tests, as determined from the optimization method PEST [*Dougherty*, 1999].

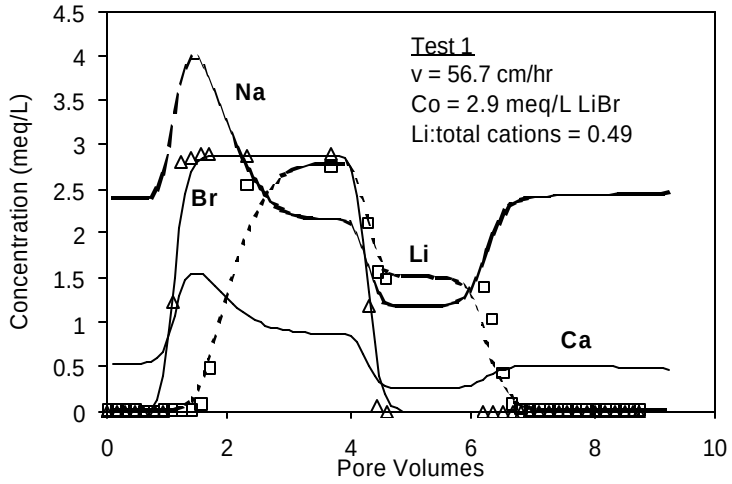

Figure 3.3. Transport data (symbols) from test 2 with model fits (lines) using an ion exchange approach for Li^+. Model fits for Na^+ and Ca^{2+} are based on the least sum-of-squares differences for all three tests, as determined from the optimization method PEST [*Dougherty*, 1999].

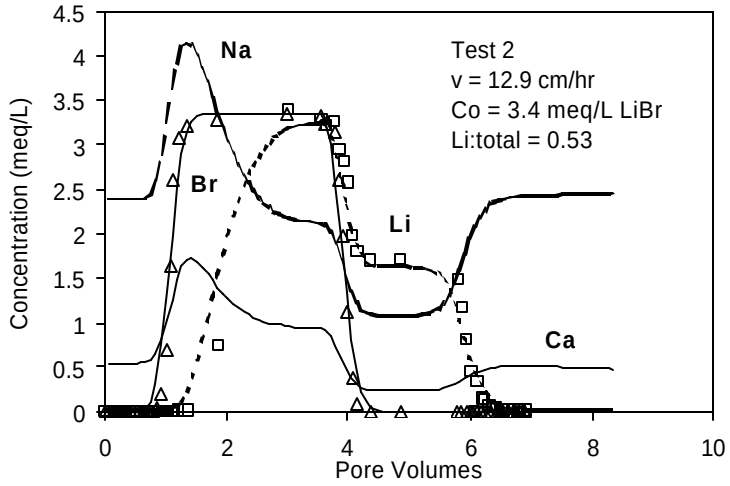

Figure 3.4. Transport data (symbols) from test 3 with model fits (lines) using an ion exchange approach for Li^+. Model fits for Na^+ and Ca^{2+} are based on the least sum-of-squares differences for all three tests, as determined from the optimization method PEST [*Dougherty*, 1999].

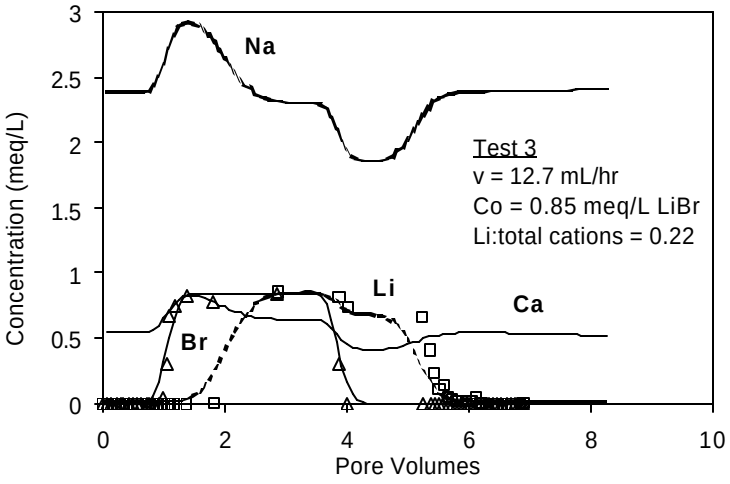

Table 3.3. List of best-fit model parameters. The retardation factors were determined for Li^+ from the rising portion of the BTC using an analytical solution of the 1-D advection-dispersion equation for reactive solutes.

Modeling Parameters	Test 1	Test 2	Test 3
Retardation factor[a]	1.8	2.0	2.3
Solute residence time (hr)	1.8	7.6	7.6
Peclet number	375	225	1025
Best-fit selectivity parameters[b]			
CEC (meq kg^{-1})		36.5	
$K_{Li\backslash Na}$		0.4306	
$K_{Ca\backslash Na}$		11.16	
Selectivity coefficients, *Appelo and Postma* [1993]	$K_{Li\backslash Na}$ 0.833 - 1.05		$K_{Ca\backslash Na}$ 1.67 - 3.33

[a]Based on the separation of the rising fronts of the Br^- and Li^+ breakthrough curves.

[b]Combination of parameter values maintaining the smallest sum-of-squares differences obtained from PEST.

Table 3.3 lists the model parameter estimates for the three tests. The modeling results using the ion exchange approach matched the tracer data quite well for all three tests. The rising portions of the Li^+ curves in all three tests were delayed by a factor of about two, matched using the linear retardation model. However, the K_D values fail to explain the Li^+ tailing behavior. The declining portion of the Li^+ curves in tests 1 and 2 initially follow the declining portion of the Br^- curves. As the tracer-free groundwater moved through the columns, Na^+ and Ca^{2+} in the solutions exchanged with the sorbed Li^+, and the column attained a new equilibrium state. The Li^+ curves reached a plateau of relatively constant concentration that continued during the elution of about two pore volumes. The heights of these Li^+, Na^+, and Ca^{2+} plateaus between about 4 and 6 pore volumes reflected these new equilibrium conditions in the columns. The plateaus

persisted until all the Li^+ was desorbed and flushed from the system (based on the approximately 100% recovery of injected Li^+ in all three tests). The duration of the plateaus was dictated by the ion exchange equilibria, the CEC of the media, and the mass of Li^+ introduced to the system. If either the mass of Li^+ injected was larger or the CEC of the rock were larger, the duration of the plateaus would have been longer.

The values obtained from the PEST optimization procedure (all three tests optimized simultaneously) were $K_{Li\backslash Na} = 0.431$, $K_{Li\backslash Ca} = 11.2$, and CEC = 36.5 meq kg^{-1} for all three experiments. This value for CEC was the same as that measured in cation exchange capacity tests for Li^+ on another sample of this core [*Anghel et al.*, 2000]. We assumed that the packing of the columns was the same within the range of analytical uncertainty, therefore the best-fit values for $K_{Li\backslash Na}$, $K_{Li\backslash Ca}$, and CEC for all three tests were determined simultaneously. However, because $K_{Li\backslash Na}$ and $K_{Li\backslash Ca}$ are indirectly related through Na^+-Ca^{2+} exchange, there does not exist a unique solution to these parameters. Transport data for Na^+ and Ca^{2+} are necessary to constrain the problem and arrive at a unique solution for $K_{Li\backslash Na}$ and $K_{Li\backslash Ca}$. Unfortunately, the effluent collected during the tracer tests was analyzed only for Li^+ and Br^-. Thus, the values of $K_{Li\backslash Na}$ and $K_{Li\backslash Ca}$ were optimized for all three tests simultaneously using PEST which minimized the sum of squares differences between the model and the Li^+ data.

These modeling efforts indicate the importance of other cations in solution on the transport of a cationic tracer species. The ion exchange model produced good fits to the data and underscore the importance of considering electroneutrality (charge balance) requirements in a system where multiple cations participate in ion exchange. For example, Figure 3.5 shows numerical predictions of tracer experiments with flow

conditions the same as in test 2 but at various LiBr concentrations. When the fraction of the tracer cation relative to the total cations in the system approaches unity, the separation of the Br^- and Li^+ BTCs after the peak concentrations becomes smaller due to mass and charge balance requirements. It is also important to note that the apparent retardation of Li^+ decreases with increasing concentration; i.e., the separation of the rising limbs of the Br^- and Li^+ breakthrough curves is substantially decreased (compare Figure 3.5a and Figure 3.5d). While our results emphasize multicomponent transport patterns during pulse injections, this decreased tracer separation would also be important when conducting tracer tests involving a step injection (continuous tracer injection); the retardation coefficient deduced from tests of higher tracer concentration would be smaller than at lower concentration conditions. Thus, tracer data obtained from a high-concentration experiment would tend to underestimate the apparent retardation of a cationic species at lower concentrations.

Figure 3.5. Simulated breakthrough curves (semilog scale) for the conditions of test 2 at various Li^+: total cations ratios for the tracer injectate; (b) shows the same data (symbols) and simulations (lines) as Figure 3.3.

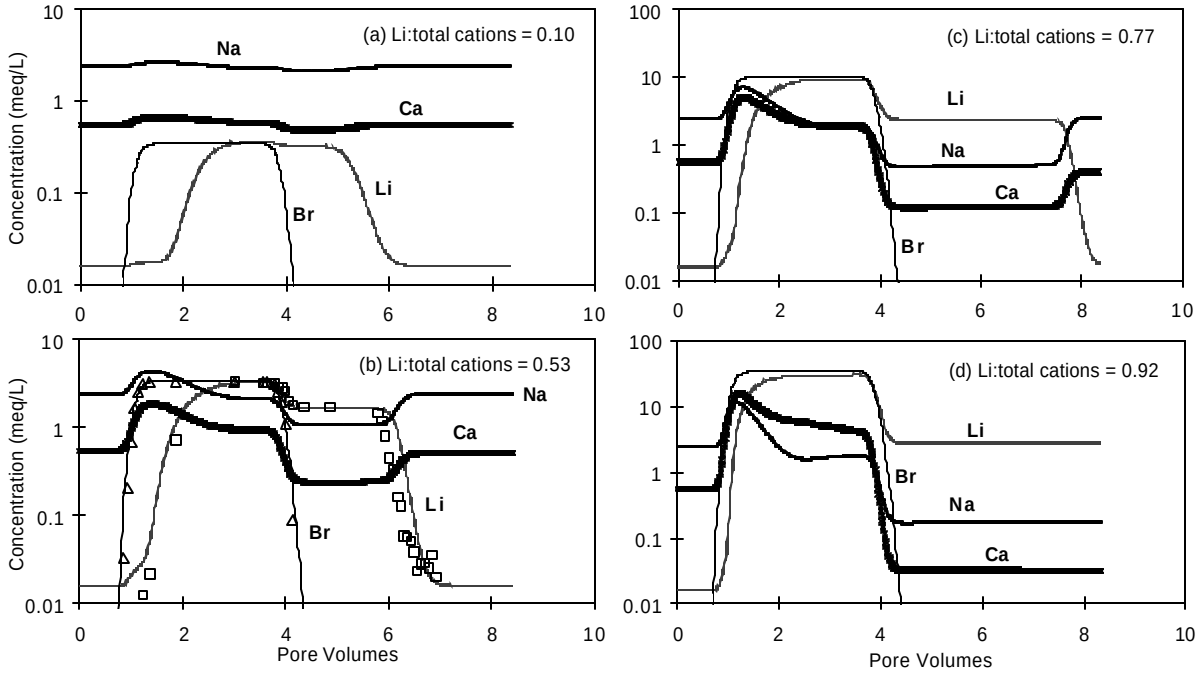

3.5. Conclusions

The transport of lithium ion through columns of crushed rock was affected by its concentration relative to the other cations in solution. In three tracer experiments, the fraction of Li^+ relative to the total cation equivalents in solution was 49%, 53%, and 22%, respectively. Ion exchange was assumed to be the primary mechanism influencing Li^+ transport, which caused the transport of Li^+ to be retarded relative to bromide, but this retardation was less than would be predicted from a linear retardation ("K_D") model. The Li^+ tracer response was most likely a function of the CEC of the medium as well as the relatively low concentration of the other cations in solution (Na^+ and Ca^{2+}). A portion of the Li^+ moved through the column unretarded because of the finite number of cation

exchange sites on the solid phase and the fact that the solid and solution reached equilibrium before injection of Li^+ ceased. The resulting breakthrough curves from the three column experiments were modeled effectively using a numerical method that accounted for cation exchange reactions.

It is common to inject large masses of tracers to ensure detectable concentrations at the sampling point(s). These data highlight potential complexities when interpreting field tracer tests in which tracer concentrations greatly exceed the resident ion concentrations. A substantial fraction of a reactive solute may be transported faster than predicted using a single-component (K_D) approach. That is, the apparent retardation of a cationic species during a high concentration tracer test would be smaller than that at lower concentrations. A conceptual model that incorporates ion exchange equilibria is required to explain and predict the transport of cations under high concentration conditions.

Acknowledgments. Financial support for this work was provided by the U.S. Department of Energy, Office of Civilian Radioactive Waste Management, as part of the Yucca Mountain Site Characterization Project. This paper greatly benefited from discussions with John Wilson, Fred Phillips, and Brian McPherson. We also thank Armando Furlano for conducting the column tests and Darlene Linzey for the sample analyses.

References

Anghel, I., H. J. Turin, and P. W. Reimus, Lithium sorption to Yucca Mountain Tuffs, *Los Alamos Unrestricted Report LA-UR-00-2998*, Los Alamos National Laboratory, Los Alamos, N.M., 2000.

Appelo, C. A. J., Some calculations on multicomponent transport with cation-exchange in aquifers, *Ground Water, 32*(6), 968-975, 1994.

Appelo, C. A. J., Multicomponent ion exchange and chromatography in natural systems. In: P. C. Lichtner, C. I. Steefel, and E. H. Oelkers (Editors), Reactive Transport in Porous Media. *Rev. Mineral., 34*, 193-227, 1996.

Appelo, C. A. J. and D. Postma, Geochemistry, Groundwater and Pollution, A. A. Balkema, Rotterdam, 1993.

Appelo, C. A. J. and A. Willemsen, Geochemical calculations and observations on salt water intrusions, I., *J. Hyd., 94*, 313-330, 1987.

Appelo, C. A. J., A. Willemsen, H. E. Beekman, and J. Griffioen, Geochemical calculations and observations on salt water intrusions, II., *J. Hyd., 120*, 225-250, 1990.

Appelo, C. A. J., J. A. Hendriks, and M. van Veldhuizen, Flushing factors and a sharp front solution for solute transport with multicomponent ion exchange, *J. Hyd., 146*, 89-113, 1993.

Bond, W. J., Competitive exchange of K^+, Na^+, and Ca^{2+} during transport through soil, *Aust. J. Soil Res., 35*, 739-752, 1997.

Callahan, T. J., Laboratory investigations and analytical and numerical modeling of the transport of dissolved solutes through fractured rock, unpublished Ph.D. dissertation, New Mexico Institute of Mining and Technology, Socorro, 2001.

Callahan, T. J., P. W. Reimus, R. S. Bowman, and M. J Haga, Using multiple experimental methods to determine fracture/matrix interactions and dispersion of nonreactive solutes in saturated volcanic rock, *Water Resour. Res.*, *36*(12), 3547-3558, 2000.

Cerník, M., K. Barmettler, D. Grolimund, W. Rohr, M. Borkovec, and H. Sticher, Cation transport in natural porous media on laboratory scale: multicomponent effects, *J. Contam. Hyd.*, *16*, 319-337, 1994.

Dougherty, J., PEST: Model-independent parameter estimation, Third edition, *Watermark Computing*, Brisbane, Austral., 1999.

Fuentes, H. R., W. L. Polzer, E. H. Essington, and B. D. Newman, Characterization of reactive tracers for C-Wells Field Experiment I: Electrostatic sorption mechanism, lithium, *Los Alamos National Laboratory Report, LA-11691-MS*, Los Alamos, NM, 1989.

Geldon, A. L., Preliminary hydrogeologic assessment of boreholes UE25c #1, UE25c #2, and UE25c #3, Yucca Mountain, Nye County, Nevada, *U.S. Geol. Surv. Water-Resour. Invest. Rep.*, *92-4016*, Denver, CO, 1993.

Griffioen, J., C. A. J. Appelo, and M. van Veldhuizen, Practice of chromatography: Deriving isotherms from elution curves, *Soil Sci. Soc. Am. J.*, *56*(5), 1429-1437, 1992.

LeGallo, Y., O. Bildstein, and E. Brosse, Coupled reaction-flow modeling of diagenetic changes in reservoir permeability, porosity and mineral compositions, *J. Hydrol.*, *209*(1-4), 366-388, 1998.

Lichtner, P. C., Principles and practice of reactive transport modeling, *Mat. Res. Soc. Symp. Proc.*, *353*, 117-130, 1995.

Lichtner, P. C., Continuum formulation of multicomponent-multiphase reactive transport, in Reactive Transport in Porous Media, P. C. Lichtner, C. I. Steefel, and E. H. Oelkers (eds.), *Rev. Mineral., 34*, 1-81, 1996.

Liu, C. W. and T. N. Narasimhan, Redox-controlled, multiple-species reactive chemical transport. 1. Model development, *Water Resour. Res.*, *25*(5), 869-882, 1989.

Parkhurst, D. L., User's guide to PHREEQC - A computer program for speciation, reaction-path, advective transport, and inverse geochemical calculations, *U.S. Geol. Surv. Water Resour. Invest. Rep., 95-4227*, Denver, CO, 1995.

Reimus, P. W., A. Adams, M. J. Haga, A. Humphrey, T. Callahan, I. Anghel, and D. Counce, Results and interpretation of hydraulic and tracer testing in the Prow Pass Tuff at the C-Holes, *Yucca Mountain Site Characterization Project Milestone Report SP32E2M4SZ*, Los Alamos National Laboratory, Los Alamos, NM, 1999.

Robinson, B. A., H. S. Viswanathan, and A. J. Valocchi, Efficient numerical techniques for modeling multicomponent ground-water transport based upon simultaneous solution of strongly coupled subsets of chemical components, *Adv. Water Resour., 23*, 307-324, 2000.

TebesStevens, C., A. J. Valocchi, J. M. VanBriesen, B. E. Rittmann, Multicomponent transport with coupled geochemical and biological reactions: Model description and example simulations, *J. Hydrol., 209*, 8-26, 1998.

TebesSteves, C. L. and A. J. Valocchi, Calculation of reaction parameter sensitivity coefficients in multicomponent subsurface transport models, *Adv. Water Resour., 23*, 591-611, 2000.

Valocchi, A. J., R. L. Street, and P. V. Roberts, Transport of ion-exchanging solutes in groundwater: Chromatographic theory and field simulation, *Water Resour. Res., 17*, 1517-1527, 1981a.

Valocchi, A. J., P. V. Roberts, G. A. Parks, and R. L. Street, Simulation of the transport of ion-exchanging solutes using laboratory-determined chemical parameter values, *Ground Water, 19*, 600-607, 1981b.

Voegelin, A., V. M. Vulava, F. Kuhnen, and R. Kretzschmar, Multicomponent transport of major cations predicted from binary adsorption experiments, *J. Contam. Hyd., 46*, 319-338, 2000.

Yeh, G. T. and V. S. Tripathi, HYDROGEOCHEM: A coupled model of hydrological transport and geochemical equilibrium of multi-component systems, *Rep. ORNL-6371*, Oak Ridge Nat. Lab., Oak Ridge, Tenn., 1988.

Yeh, G. T. and V. S. Tripathi, A critical evaluation of recent developments of hydrogeochemical transport models of reactive multichemical components, *Water Resour. Res., 25*, 93-108, 1989.

4. Multicomponent Effects on the Transport of Cations Undergoing Ion Exchange in Fractured Media

(In preparation for submission to the Int'l. Groundwater Symposium, co-sponsors: Int'l. Assoc. Hydrol. Sci.; Am. Soc. Civ. Eng.; Env. Water Resour. Inst.; Amer. Geophys. Union, Mar. 25-28, 2002)

Timothy J. Callahan[1,2], Paul W. Reimus[1], Peter C. Lichtner[3], and Robert S. Bowman[2]

[1]Environmental Science and Waste Technology Group, Los Alamos National Laboratory, Los Alamos, NM 87545

[2]Department of Earth and Environmental Science, New Mexico Institute of Mining and Technology, Socorro, NM 87801

[3]Hydrology, Geochemistry and Geology Group, Los Alamos National Laboratory, Los Alamos, NM 87545

Abstract. We developed a simple ion-exchange model to describe the transport of a cation (lithium) in fractured rock cores. The hydrodynamics of the system was characterized by injecting two nonsorbing anions having different diffusion coefficients. A numerical method based on a dual-porosity transport model was used to describe advection in the fractures and molecular diffusion in the porous matrix, taking into account species-dependent diffusion coefficients. Although the arrival and rise in concentration of lithium during the tests could be explained quite well with a simple matrix retardation factor, the observed "tailing" of lithium was less than predicted, especially in rock types having a relatively high cation exchange capacity. By explicitly accounting for ion exchange reactions as well as charge balance in the dual-porosity

model, simulations of lithium transport in the fractured rocks were much improved. We conclude that accounting for ion exchange and charge balance is necessary to properly interpret reactive transport experiments in fractured media, particularly when the injection concentrations of cations are high relative to the groundwater, and when the cation exchange capacity of the rock type is large.

4.1. Introduction

Transport in fractured media is often described using the dual-continuum approach in which solutes or particles advect at different rates in two continua, often fractures and unfractured porous matrix. This conceptual model has been used previously by *Barenblatt et al.* [1960]; *Grisak and Pickens* [1980]; *Grisak et al.* [1980]; *Neretnieks* [1980]; *Bibby* [1981]; *Maloszewski and Zuber* [1983; 1985]; *Berkowitz et al.* [1988]; *Maloszewski and Zuber* [1990; 1993]; *Tsang* [1995]; *Ostensen* [1998]; *Wallach and Parlange* [1998; 2000]; *Corapcioglu and Wang* [1999]; *Jardine et al.* [1999]; and *Maloszewski et al.* [1999]. The dual-porosity model is one form of the dual-continuum concept, in which mass advects mainly or exclusively within the fractures with negligible or no advection occurring in the surrounding unfractured porous tuff matrix. However, solutes can access the matrix by molecular diffusion. Previously, the dual-porosity model was shown to accurately describe the transport of nonreactive solutes in fractured volcanic tuff cores [*Callahan et al.*, 2000]. Initial attempts to model the transport of a reactive solute (lithium ion) using a simple linear retardation model were inaccurate, especially for rock types of high sorption capacity. We hypothesized that the high concentration of Li^+ injected in the cores (relative to the other cations in the system,

predominantly sodium and calcium) resulted in asymmetric chromatographic separation of the solute breakthrough curves (BTCs). This assumption is based on a previous study of Li^+ transport in laboratory columns containing crushed samples of similar volcanic tuff [*Callahan et al.*, 2001], in which three columns containing crushed volcanic tuff were injected with a pulse of LiBr solution and the effluent was monitored for Li^+ and Br^- concentrations. The resulting BTC for Li^+ was a function of the ratio of Li^+ to the other cations in the system (Na^+ and Ca^{2+}) as well as the cation exchange capacity (CEC) of the crushed tuff.

The phenomenon of asymmetric chromatographic separation in high concentration tracer tests has been reported elsewhere [*Valocchi et al.,* 1981a; b; *Charbeneau*, 1988; *Appelo et al.*, 1990; *Appelo and Postma*, 1993; *Appelo et al.*, 1993; *Mansell et al.*, 1993; *Cerník et al.*, 1994; *Appelo*, 1994; *Bond*, 1997; *Vulava*, 1998]. The purpose of this study was to determine whether a multicomponent approach, which included ion exchange equilibria, could better describe the transport behavior of Li^+ in the fractured tuff cores. A better understanding of multicomponent effects in fractured media could lead to more accurate assessment of transport in contaminated aquifers, especially when predicting contaminant transport based on the behavior of tracers injected at high molar concentrations.

4.2. Theory

Solute transport in saturated, fractured volcanic tuff can be described using the dual-porosity concept if the hydraulic conductivity of the fractures is appreciably greater than that of the bulk unfractured tuff (i.e., two or more orders of magnitude greater)

[*Tang et al.*, 1981; *Maloszewski and Zuber*, 1983; *Callahan et al.*, 2000]. The governing equations for a dual-porosity system are

$$R_f \frac{\partial C_f}{\partial t} = D_f \frac{\partial^2 C_f}{\partial x^2} - v_f \frac{\partial C_f}{\partial x} + \frac{n_m D_m}{b n_f} \frac{\partial C_m}{\partial y}\bigg|_{y=b} \tag{4.1}$$

$$R_m \frac{\partial C_m}{\partial t} = D_m \frac{\partial^2 C_m}{\partial y^2}, \tag{4.2}$$

where R_f [-] is the retardation factor for solute in the fracture, C_f [M L^{-3}] is the solute concentration in the fracture, D_f [L^2 T^{-1}] is the hydrodynamic dispersion in the fracture, x [L] is the flow distance within the fracture, v_f [L T^{-1}] is the fluid velocity in the fracture, n_f [dimensionless] is the porosity within the fracture (unity for open fractures), n_m [dimensionless] is the porosity of the matrix, D_m [L^2 T^{-1}] is the molecular diffusion coefficient of the solute within the matrix, b [L] is the half-aperture of the fracture ($B=2b$ is the total fracture aperture), R_m is the retardation factor for solute in the porous matrix, C_m [M L^{-3}] is the solute concentration in the porous matrix, y [L] is the diffusion distance between the fracture and the matrix, and t is time (Figure 4.1). Advection occurs in the fracture, and the aperture is assumed to be constant. Transport in the matrix is due to molecular diffusion. The boundary condition for the porous matrix in a system with one fracture is

$$C_m(y \to \infty, t) = 0 \tag{4.3}$$

For the volcanic tuffs studied here, the ratios of fracture to matrix permeability were 10^5 to 10^9, measured using a falling-head permeameter technique. During the tracer experiments, the solute residence times in the fractures were long enough to allow molecular diffusion to distribute the solute mass across the aperture of the fractures;

therefore advection in the fractures was assumed to be one-dimensional [*Hull et al.*, 1987; *Callahan et al.*, 2000].

Figure 4.1. Schematic drawing of the dual-continuum (dual-porosity or dual-porosity/dual-permeability) model.

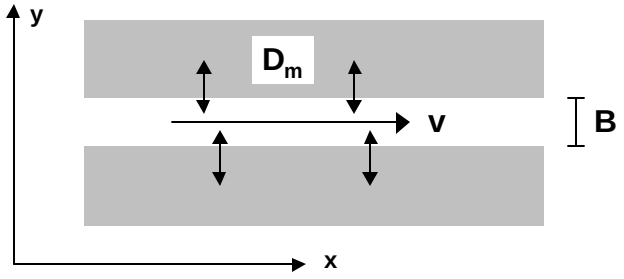

Using a Laplace transform inversion technique within the Reactive Transport Laplace Transform Inversion code (RELAP) [*Reimus and Haga*, 1999], the time variables in (4.1) and (4.2) were removed, resulting in ordinary differential equations. The dimensionless form of the combined solution of the equations in Laplace space shows that the three parameters dictating transport of nonreactive solutes through a dual-porosity system are the mass transfer coefficient ($MTC = (n_m/B)^2 * D_m$); the Peclet number ($Pe = (x * v_f)/D_f$); and the mean solute residence time ($t = x/v_f$) as parameters that dictate solute transport. These parameters can be estimated for a dual-porosity medium either by collecting transport data for one nonreactive solute in multiple tracer tests or from one experiment using multiple nonreactive solutes of different diffusion coefficients [*Callahan et al.*, 2000]. Here, the latter method was used; data for the nonreactive solutes bromide ion and pentafluorobenzoate (PFBA) were analyzed to provide estimates of the above transport parameters. These estimates were then fixed in the Reactive Transport Multicomponent code (RETRAN-M), which accounts for cation exchange of the reactive

solute lithium and charge balance while obtaining numerical solutions to the advection-dispersion equation. The ion exchange mass action equations for lithium exchanging with sodium and lithium exchanging with calcium (exchange coefficients were $K_{Li\backslash Na}$ and $K_{Li\backslash Ca}$, respectively) are described by *Callahan et al.* [2001]. Also used in the numerical model was the cation exchange capacity coefficient, CEC. The numerical model was calibrated using these three parameters as well as the transport parameters τ, Pe, and MTC obtained from the nonsorbing solute responses using the inverse method RELAP.

4.3. Methods

The solute transport experiments were conducted following the procedure in *Callahan et al.* [2000]. Four separate cores of volcanic tuff were obtained from the C-Wells tracer test complex near Yucca Mountain, Nevada. The rock types were ash flow tuffs with varying degrees of welding. Cores 1, 2, and 3 were from the upper, central, and lower flow zones of the Prow Pass Tuff Member, respectively. Core 4 was from the lower flow zone of the Bullfrog Tuff Member. Both the Prow Pass and Bullfrog Tuff are part of the Crater Flat Tuff Formation [*Geldon*, 1993; *Callahan*, 2001]. The mineralogy was determined using quantitative X-ray diffraction (QXRD). Core 4 (lower flow zone of the Bullfrog Tuff) contained the highest percentage of clay and zeolite minerals, 9 ± 3 wt. % smectite, 4 ± 1 wt % clinoptilolite, and 13 ± 1 wt. % analcime. (The complete QXRD results can be found in the electronic file "QXRD.XLS" on the compact disc attached to *Callahan* [2001]). A single fracture was mechanically induced in each of the four cores. The cores were laid on a cement floor and a four-pound hammer and chisel were used to induced a fracture lengthwise. The cores were then encased in an epoxy and Plexiglas column apparatus following the procedure of *Callahan et al.* [2000].

A steady-state flow field was established in each core by continuously injecting degassed, filtered groundwater obtained from well J-13, approximately 4 km SE of the C-Wells site [*Fuentes et al.*, 1989; *Geldon*, 1993]. The C-Wells water and J-13 well water are dominated by sodium, calcium, and bicarbonate ions and are chemically similar [*Fuentes et al.*, 1989]. A pulse of tracer solution containing LiBr, PFBA, and sodium iodide (NaI) dissolved in well J-13 water was injected into the cores. After injection of the tracer pulse, continuous injection of tracer-free well J-13 water was resumed. The effluent was monitored for the tracer ions as well as for Na^+ and Ca^{2+} using ion chromatography (IC) for Br^- and PFBA analysis and inductively-coupled plasma atomic emission spectrometry (ICP-AES) for analysis of Li^+, Na^+, and Ca^{2+}. The detection limits were 0.05 mg L^{-1} for Li^+ and Ca^{2+}, 0.5 mg L^{-1} for Na^+, 0.04 mg L^{-1} for Br^-, and 0.02 mg L^{-1} for PFBA. Flow was interrupted at late times in each test to verify the physical nonequilibrium between the water in the fractures and in the porous matrix of the tuff cores [*Brusseau et al.*, 1997]. The experimental conditions for the tracer tests are in *Callahan* [2001]. One tracer test each was conducted for cores 2, 3, and 4; core 1 was tested twice under similar flow conditions to study the reproducibility of the tracer parameters.

4.4. Results and Discussion

4.4.1. Core 1 Results

The ion-exchange parameters $K_{Li\backslash Na}$, $K_{Li\backslash Ca}$, and CEC were determined by visually fitting the model results from RETRAN-M to the transport data for each test. Modeling results for the two tests conducted on core 1 are shown in Table 4.1 and Figures 4.2 and

4.3. Two experiments were conducted in this core under similar flow conditions to determine reproducibility, and the figures illustrate that the transport behavior of the solutes were nearly identical. For test 1, the best-fit results for $K_{Li\backslash Na}$ and $K_{Li\backslash Ca}$ were 0.005 and 0.079, respectively; for test 2 $K_{Li\backslash Na}$ was 0.008 and $K_{Li\backslash Ca}$ was 0.103. These values obtained from RETRAN-M are essentially identical due to the relative insensitivity of the model to $K_{Li\backslash Na}$ and $K_{Li\backslash Ca}$. The best-fit CEC value for each test was 19.9 meq kg^{-1}, the same as that measured in cation exchange capacity experiments on a separate crushed sample of this rock unit [*Anghel et al.*, 2000]. Figure 4.4 shows comparisons to the best-fit results and the data for core 1, test 1. The three simulations were generated using the same experimental and modeling parameters, except that for each successive simulation, one ion exchange parameter was increased by a factor of five while holding the other two parameters constant. Figure 4.4 shows that the sensitivity of RETRAN-M increases in order of $K_{Li\backslash Ca}$, $K_{Li\backslash Na}$, and CEC. Because the ion exchange equilibria depends on $[Ca^{2+}]$ to a power half that of $[Na^{+}]$ and $[Li^{+}]$ [*Callahan et al.*, 2001], the problem is less sensitive to changes in $K_{Li\backslash Ca}$.

Table 4.1. Best-fit model parameters for the fracture transport tests, cores 1 and 2. Core descriptions are given in *Callahan* [2001].

Modeling Parameters[a]	Core 1, test 1	Core 1, test 2	Core 2
Porosity of matrix	0.27	0.27	0.14
Volumetric flow rate, Q (mL hr^{-1})	4.0	4.0	6.0
Solute mean residence time, t (hr)	8.2	7.5	2.0
Peclet number, *Pe*	3.0	1.7	15
Dispersivity in fracture, $a = \frac{L}{Pe}$ (m)	53.7 x 10^{-3}	94.7 x 10^{-3}	11.5 x 10^{-3}
Li^+ Retardation factor, R (-)[b]	2.1	2.4	4.3
Li^+ Partition coefficient, K_D (L kg^{-1})	0.15	0.20	0.20
Mass transfer coefficient,	0.0533 (Br^-)	0.067 (Br^-)	0.0317 (Br^-)
$MTC = (n_m^2/B^2)D_m$ (hr^{-1})	0.0178 (PFBA)	0.033 (PFBA)	0.0106 (PFBA)
Fracture aperture, B (m)[c]	2.12 x 10^{-3}	1.96 x 10^{-3}	0.72 x 10^{-3}
Matrix diffusion coefficient, D_m	9.0 (Br^-)	9.6 (Br^-)	2.4 (Br^-)
(x 10^{-10} m^2 s^{-1})[d]	3.0 (PFBA)	3.2 (PFBA)	0.8 (PFBA)
CEC (meq kg^{-1}), Measured	19.9	19.9	43.2
CEC (meq kg^{-1}), Fitted	19.9	19.9	129.6
$K_{Li\backslash Na}$[e]	0.005	0.008	10.0
$K_{Ca\backslash Na}$[e]	0.079	0.103	100.0

[a]The Br^- and PFBA data were fit simultaneously by constraining the D_m ratio for Br^-:PFBA to 3:1. The matrix diffusion coefficient for Li^+ was assumed to be 2/3 of the value for Br^-.

[b]Calculated from the Li^+ transport data from rising portion of the BTC using the Reactive Transport Laplace Transform Inversion code (RELAP) [*Reimus and Haga*, 1999].

[c]Based on the relationship $B = (Q\,t)/(L\,w)$, where t is the solute mean residence time.

[d]Determined from the MTC using the measured n_m and the calculated B.

[e]Equilibrium ion exchange coefficients, determined from best fit to the Li^+, Na^+, and Ca^{2+} data for each test.

Figure 4.2. Transport data and RETRAN-M modeling results, core 1, test 1.

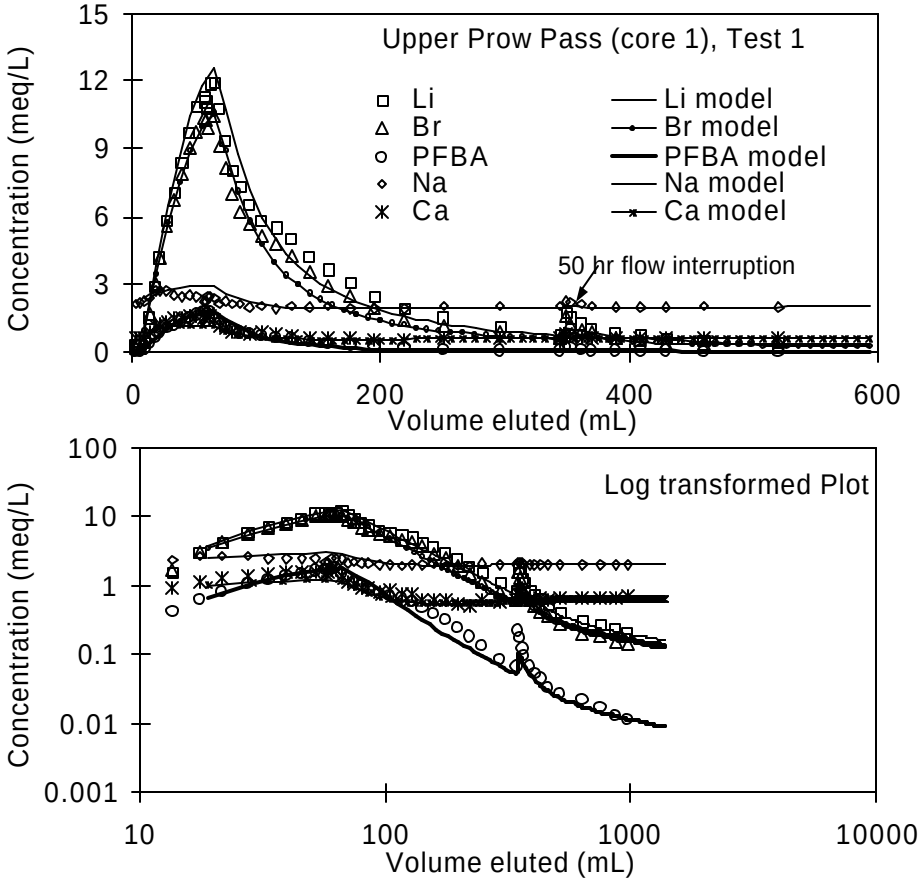

Figure 4.3. Transport data and RETRAN-M modeling results, core 1, test 2.

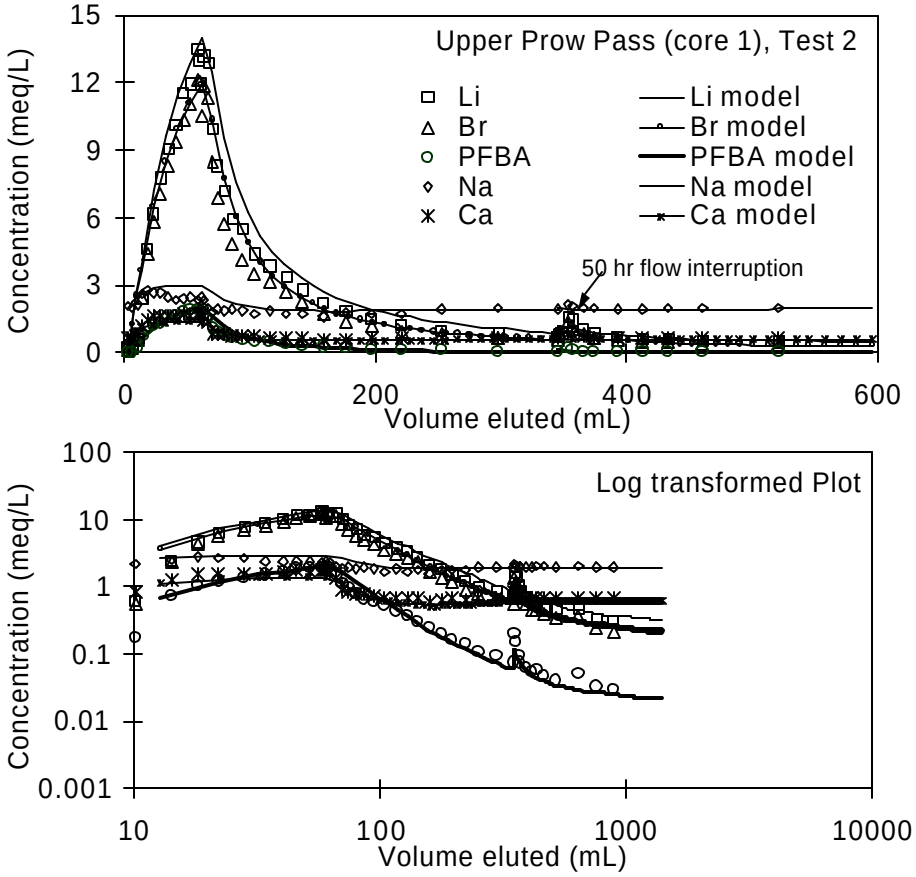

Figure 4.4. Sensitivity of ion-exchange model to (a) $K_{Li\backslash Na}$, (b) $K_{Li\backslash Ca}$, and (c) CEC for core 1, test 1. Best fit values were $K_{Li\backslash Na}$ = 0.005, $K_{Li\backslash Ca}$ = 0.08, CEC = 19.9 meq kg^{-1}. While holding the other two parameters constant, the value of $K_{Li\backslash Na}$ in (a) was changed to 0.025, $K_{Li\backslash Ca}$ in (b) to 0.40, and CEC to 100 meq kg^{-1} in (c).

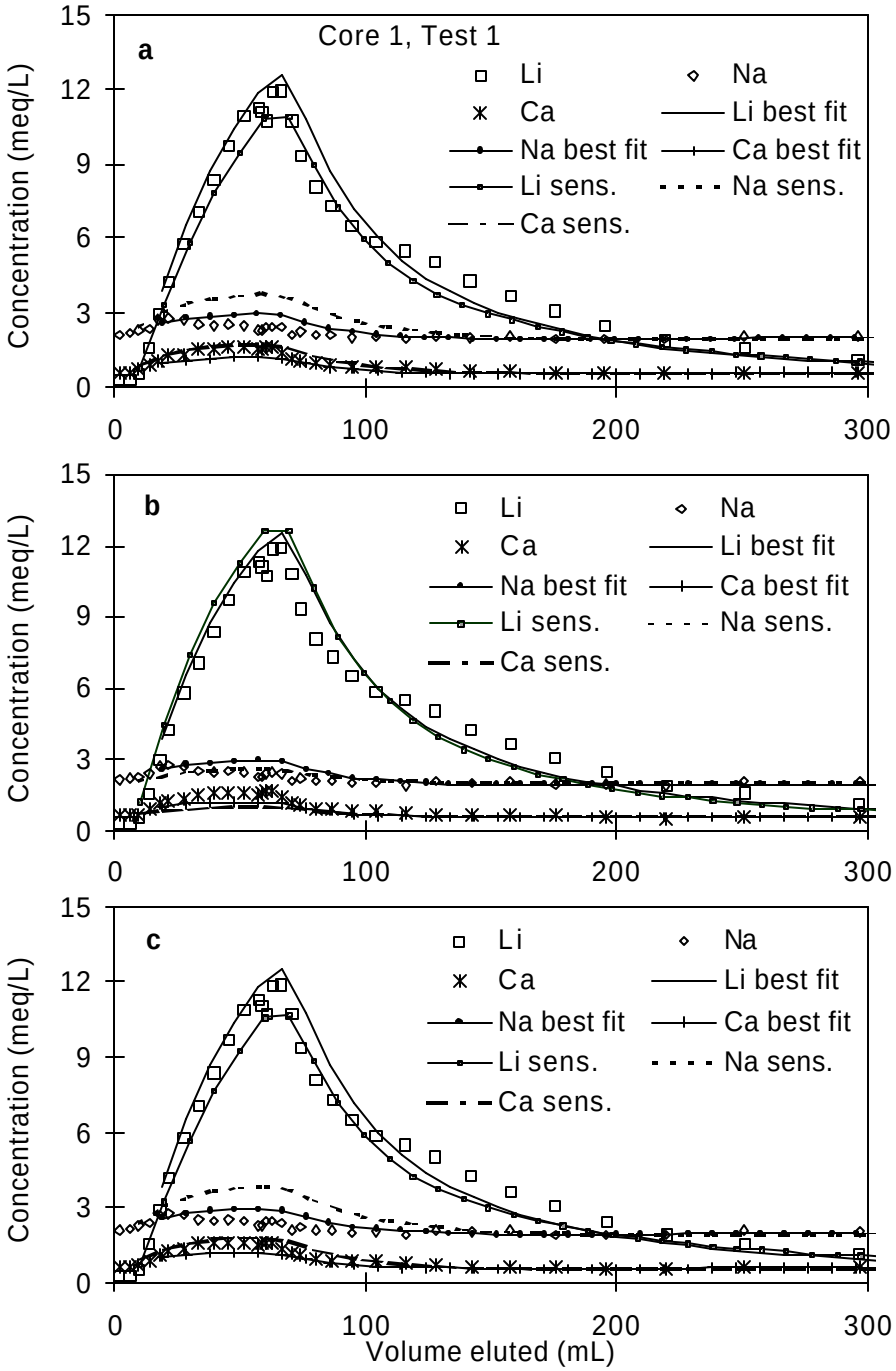

4.4.2. Core 2 results

Results from core 2 are listed in Table 4.1 and Figure 4.5. The best-fit results for the ion exchange parameters $K_{Li\backslash Na}$ and $K_{Li\backslash Ca}$ were 10.0 and 100.0, respectively; the CEC best-fit value was 129.6 meq kg^{-1}. The model simulations show a good match to the Li^+ and Na^+ data; however the model did not match the Ca^{2+} data very well, as seen in the log-log plot of Figure 4.5. Sodium hydroxide (NaOH) was added to the tracer solution to adjust the pH to 7.8 (dissociation of the PFBA resulted in an initial pH of about 3). Therefore, ion exchange was dominated by exchange between Li^+ and Na^+ in this tracer test. On the other hand, in the two experiments in core 1, Li^+ was the only cation added to the tracer solution (the pH of the tracer solutions for the core 1 tests was buffered using LiOH). Both Na^+ and Ca^{2+} were present at background concentrations (2 meq L^{-1} and 0.65 meq L^{-1}, respectively) in these experiments.

Figure 4.5. Transport data and RETRAN-M modeling results, core 2.

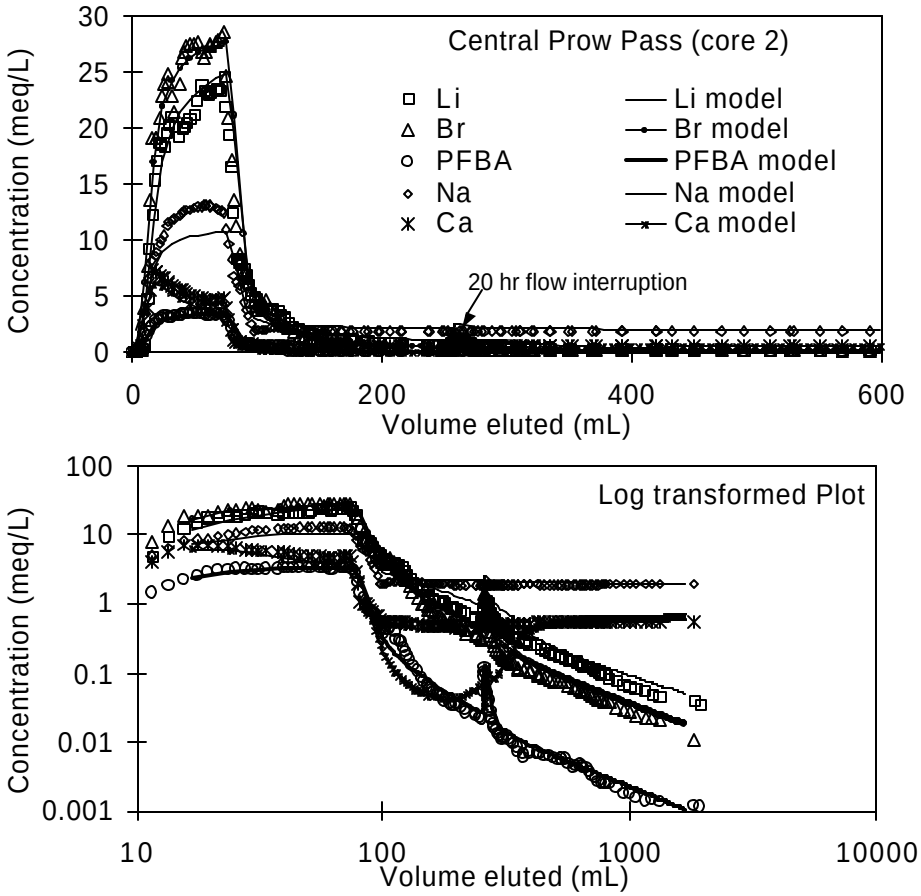

4.4.3. Core 3 results

Table 4.2 lists the modeling results for the transport test conducted in core 3 and Figure 4.6 shows the tracer data and model simulations. The best-fit model results for $K_{Li\backslash Na}$ and $K_{Li\backslash Ca}$ were 0.5 and 1.12, respectively. The model fits matched the Li^+ and Na^+ data, but for the Ca^{2+} data, the model approximated the BTC pattern but was lower in magnitude. This result is similar to that for core 2. The best-fit CEC value was 3.19 meq kg^{-1}, ten times less than the measured value [*Anghel et al.*, 2000]. This was the only test in which the measured CEC value was greater than that deduced from the fractured tuff core transport data. It is important to note for this experiment, HCO_3^-, I^-, OH^-, and Cl^-,

balanced the cations but their BTCs were not shown for clarity of the graph. This applied to the other experiments as well, but the tracer test in core 3 was the only one to exhibit charge imbalance (cations > anions). The reason for this charge imbalance is unclear.

Table 4.2. Best-fit model parameters for the fracture transport tests, cores 3 and 4. Core descriptions are listed in *Callahan* [2001].

Modeling Parameters[a]	Core 3	Core 4
Porosity of matrix	0.29	0.30
Volumetric flow rate, Q (mL hr^{-1})	11.4	4.9
Solute mean residence time, t (hr)	0.8	4.2
Peclet number, *Pe*	17.5	46.
Dispersivity in fracture, $a = \frac{L}{Pe}$ (m)	6.63 x 10^{-3}	4.72 x 10^{-3}
Li^+ Retardation factor, R (-)[b]	1.2	6.9
Li^+ Partition coefficient, K_D (L kg^{-1})	0.037	0.95
Mass transfer coefficient,	0.183 (Br^-)	0.0767 (Br^-)
$MTC = (n_m^2/B^2)D_m$ (hr^{-1})	0.0611 (PFBA)	0.0256 (PFBA)
Fracture aperture, B (m)[c]	0.82 x 10^{-3}	1.00 x 10^{-3}
Matrix diffusion coefficient, D_m	4.13 (Br^-)	2.4 (Br^-)
(x 10^{-10} m^2 s^{-1})[d]	1.38 (PFBA)	0.8 (PFBA)
CEC (meq kg^{-1}), Measured	31.9	180
CEC (meq kg^{-1}), Fitted	3.19	270
$K_{Li\backslash Na}$[e]	0.50	9.0
$K_{Ca\backslash Na}$[e]	1.12	32.9

[a]The Br^- and PFBA data were fit simultaneously by constraining the D_m ratio for Br^-:PFBA to 3:1. The matrix diffusion coefficient for Li^+ was assumed to be 2/3 of the value for Br^-.

[b]Calculated from the Li^+ transport data from rising portion of the BTC using the Reactive Transport Laplace Transform Inversion code (RELAP) [*Reimus and Haga*, 1999].

[c]Based on the relationship $B = (Q\ t)/(L\ w)$, where t is the solute mean residence time.

[d]Determined from the MTC using the measured n_m and the calculated B.

[e]Equilibrium ion exchange coefficients, determined from best fit to the Li^+, Na^+, and Ca^{2+} data for each test.

Figure 4.6. Transport data and RETRAN-M modeling results, core 3.

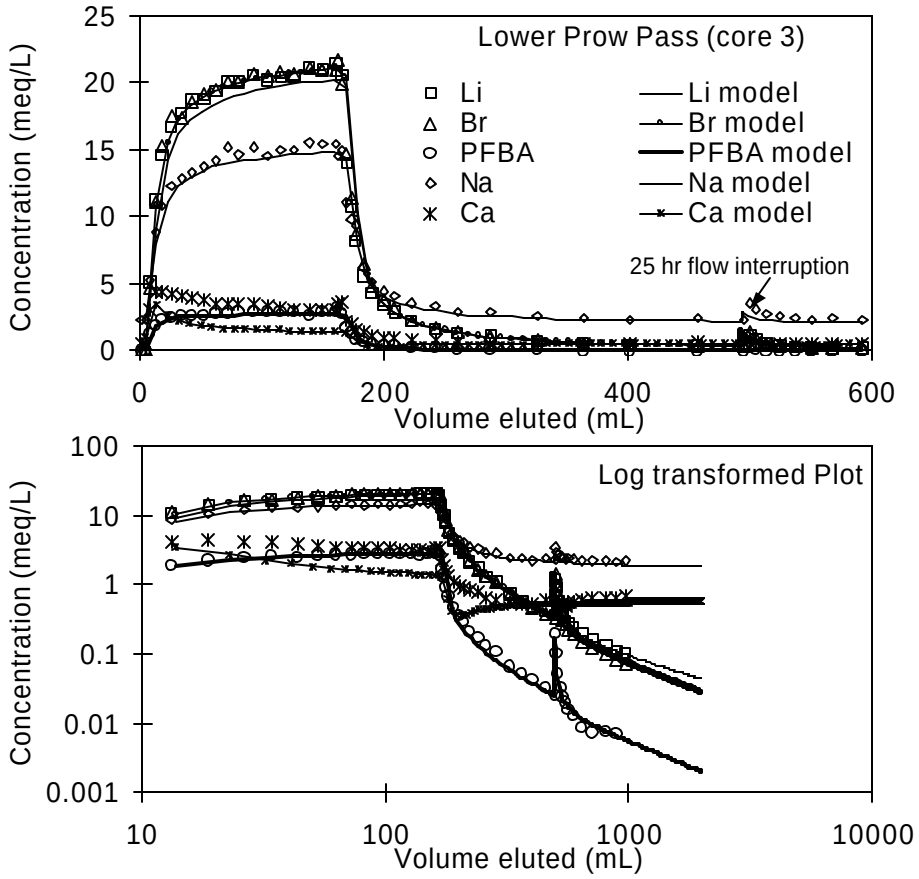

4.4.4. Core 4 results

Data obtained from the transport test in core 4 indicate a higher sorption capacity for Li^+ relative to the other three rock types. Experimental and best-fit model results are shown in Table 4.2 and Figure 4.7. Figure 4.8 shows the model results from both the single-component and ion-exchange models for Li^+ transport with the Li^+ data. This core exhibited the most asymmetric Li^+ BTC. Quantitative X-ray diffraction measurements on crushed samples of this rock type show significant fractions of clay and zeolite minerals [*Anghel et al.*, 2000]. In core 4, there was 9 ± 3 wt. % smectite, 13 ± 3 wt. % analcime, and 4 ± 1 wt. % clinoptilolite. The other rock types contained $\leq 2 \pm 1$ wt. % of these

minerals. The values of the ion exchange parameters $K_{Li\backslash Na}$, $K_{Li\backslash Ca}$, and CEC were much greater for this core compared to the other three, as was the Li^+ K_D value.

Figure 4.7. Transport data and RETRAN-M modeling results, core 4.

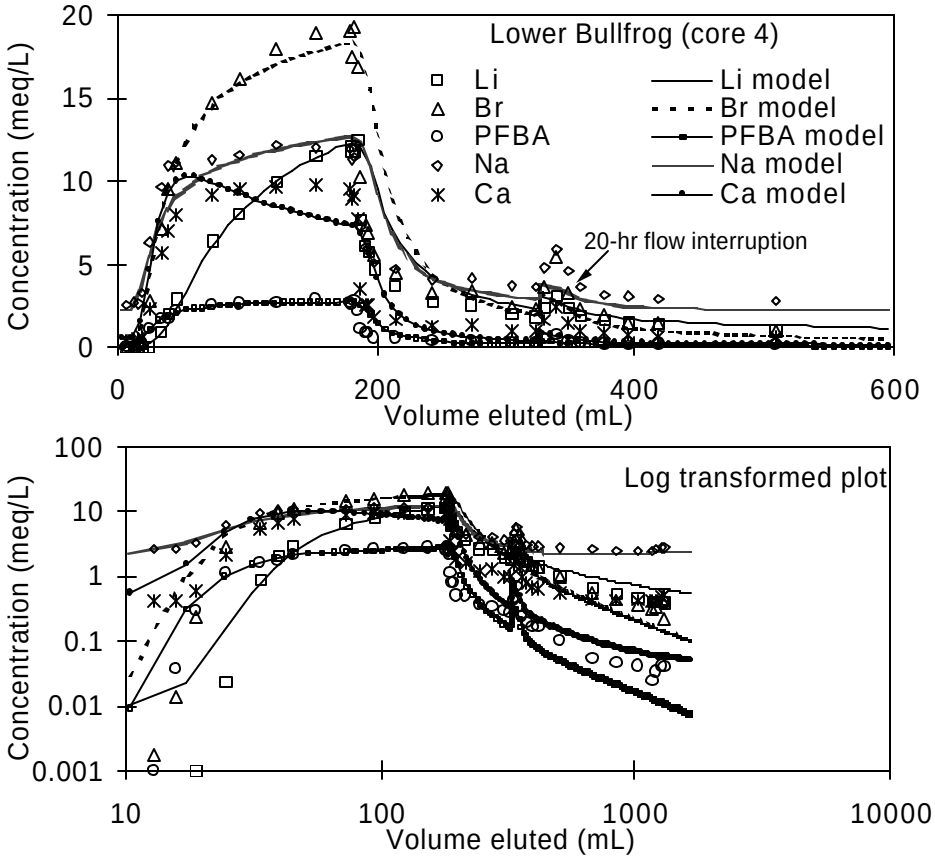

Figure 4.8. Comparison of single-component and ion-exchange model results with Li^+ data, core 4, test 1.

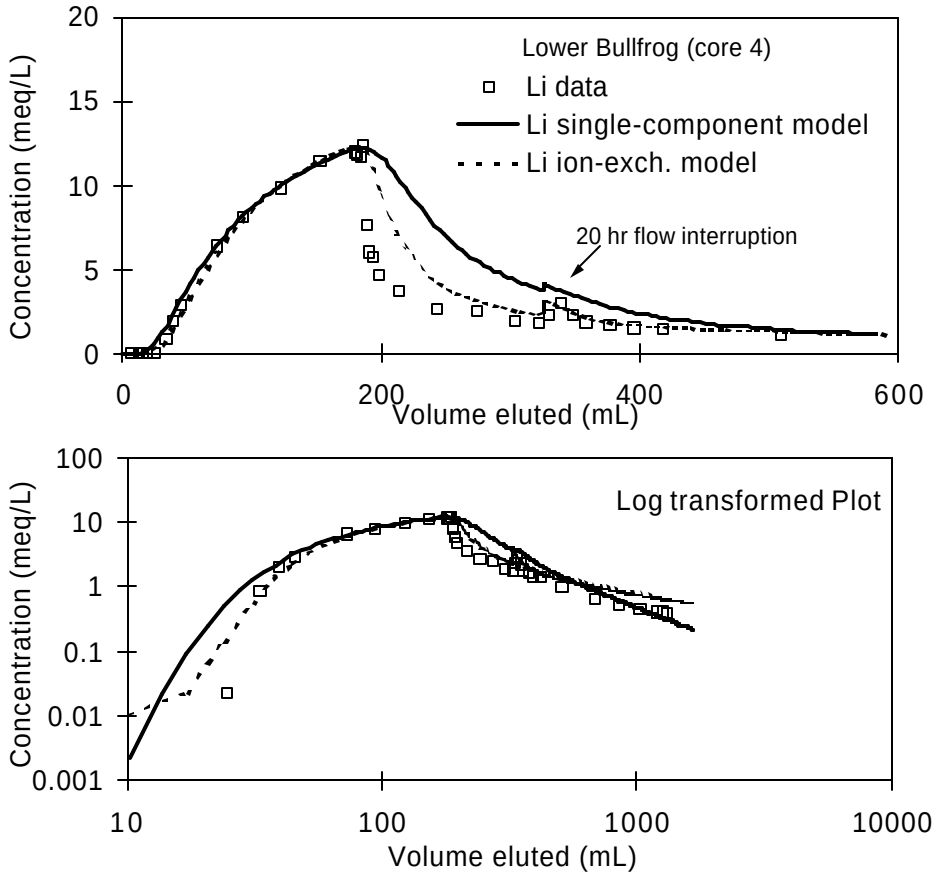

4.4.5. Comparison of Data Collected from Different Methods

Table 4.3 lists the Li^+ partition coefficients (K_D) and CEC values obtained from different experimental methods. The best-fit model results for the CEC were greater than that measured in the CEC experiments for core 2 and core 4 (the best-fit model result for core 1 was the same as the measured value). This result may be due to the geometry difference between the fractured tuff cores and the CEC samples. For the CEC tests, the tuff samples were crushed and sieved to a particle size fraction of 0.075 – 0.5 mm [*Anghel et al.*, 2000] and 30 mL of lithium acetate solution was mixed with 5 g of tuff.

Assuming a particle density r_p of 2.65 g mL^{-1}, the porosity n_m of the solid-solution mixtures was 0.94 using the relationship $n_m = V/(V+M/r_p)$, where V is the volume of tracer solution and M is the mass of solids. Conversely, the matrix porosities of the intact tuff cores were 0.14 to 0.30 (Tables 4.1 and 4.2). Thus, the samples in the fractured tuff core experiments provided a large surface area relative to the volume of solution added to the sample and thus more ion exchange sites for Li^+. If this hypothesis were correct, all four rock types would show the same pattern of the best-fit model result being greater than the measured value of CEC. It is not clear why the fitted value of CEC was less than the measured value for core 3. Based on a single-component (K_D) model, core 3 exhibited the least amount of sorption capacity for Li^+ (K_D = 0.037 L kg^{-1}) in the fractured core tracer test, which was much less than that measured in batch sorption experiments (K_D = 0.43 L kg^{-1}). It is possible that during the tracer test in core 3, the tracer solution did not achieve complete equilibrium with the tuff material, as opposed to batch tests in which the tuff sample was well mixed with the tracer solution. The diffusive mass transfer coefficient was quite large (Table 4.2) for core 3, and we infer that this limited the residence time of solutes in the porous matrix.

Table 4.3. Comparison of Li^+ sorption data obtained from different experiments.

	Li^+ Partition coefficient, K_D (L kg^{-1})		Cation exchange capacity, *CEC* (meq kg^{-1})	
	Batch tests[a]	Tracer tests	CEC tests[b]	Tracer tests
Core 1, Test 1	0.078	0.15	19.9	19.9
Core 1, Test 2		0.20		19.9
Core 2	0.26	0.20	43.2	129.6
Core 3	0.43	0.037	31.9	3.19
Core 4	1.7	0.95	179.7	270.

[a]*Callahan* [2001].

[b]*Anghel et al.* [2000].

4.5. Conclusions

To model Li^+ transport in fractured tuff cores, a retardation factor approach was initially employed. While the single-component retardation model explained the rising front of the Li^+ BTC, it failed to approximate the entire Li^+ BTC, especially for volcanic tuff cores of high cation exchange capacity (CEC). By including ion exchange equilibria, the model fits more accurately matched the Li^+ BTC, and the Na^+ and Ca^{2+} BTC were also matched fairly well for all the experiments. Transport data for Na^+ and Ca^{2+} were used to constrain the model to obtain the best-fit results for $K_{Li\backslash Na}$, $K_{Li\backslash Ca}$, and CEC, unlike previous crushed tuff column tests where only Li^+ data were obtained [*Callahan et al.*, 2001]. The ion exchange model specifically accounted for the concentration of each cation in the fractured tuff cores. This approach is superior to single-component models that infer sorption isotherm parameters from the transport behavior of a reactive solute, e.g., Freundlich and Langmuir sorption equations [*Reimus et al.*, 1999] because the ion exchange equations more accurately describe the fundamental processes that affect Li^+ transport.

Using multiple solutes in tracer tests in fractured tuff provides information on the hydrodynamic dispersion within fractures, diffusive mass transfer between water in the fractures and water in the porous matrix, and the retardation behavior of reactive solutes, all from a single experiment. However, injecting high concentrations of chemicals into a system with a low ionic-strength water can drastically alter the transport behavior of cations compared to their behavior under low-concentration injection conditions. The traditional approach of estimating a retardation coefficient from tracer data is often used

to predict the behavior of reactive solutes at low concentrations, but using this parameter obtained from high concentration tracer tests can lead to large discrepancies. We have shown that using the ion-exchange approach is necessary to explain the transport behavior of cations at high concentrations and to increase the applicability of tracer test interpretations to low-concentration conditions.

Acknowledgments. Financial support for this work was provided by the U.S. Department of Energy, Office of Civilian Radioactive Waste Management, as part of the Yucca Mountain Site Characterization Project. Thanks to Fred Phillips, Brian McPherson, and John Wilson for their discussions of the data and interpretations, and also to Dale Counce for the sample analyses.

References

Anghel, I., H. J. Turin, and P. W. Reimus, Lithium sorption to Yucca Mountain Tuffs, *Los Alamos Unrestricted Report LA-UR-00-2998*, Los Alamos National Laboratory, Los Alamos, N.M., 2000.

Appelo, C. A. J., Some calculations on multicomponent transport with cation-exchange in aquifers, *Ground Water, 32*(6), 968-975, 1994.

Appelo, C. A. J. and D. Postma, Geochemistry, Groundwater and Pollution, A. A. Balkema, Rotterdam, 1993.

Appelo, C. A. J., A. Willemsen, H. E. Beekman, and J. Griffioen, Geochemical calculations and observations on salt water intrusions, II., *J. Hyd., 120*, 225-250, 1990.

Appelo, C. A. J., J. A. Hendriks, and M. van Veldhuizen, Flushing factors and a sharp front solution for solute transport with multicomponent ion exchange, *J. Hyd., 146*, 89-113, 1993.

Barenblatt, G. I., I. P. Zheltov, and I. N. Kochina, Basic concepts in the theory of seepage of homogeneous liquids in fissured rocks, *J. Appl. Math. Mech. Engl. Transl., 24*, 1286-1303, 1960.

Berkowitz, B., J. Bear, and C. Braester, Continuum models for contaminant transport in fractured porous formations, *Water Resour. Res., 24* (8), 1225-1236, 1988.

Bibby, R., Mass transport of solutes in dual-porosity media, *Water Resour. Res., 17* (4), 1075-1081, 1981.

Bond, W. J., Competitive exchange of K^+, Na^+, and Ca^{2+} during transport through soil, *Aust. J. Soil Res., 35*, 739-752, 1997.

Brusseau, M. L., Q. Hu, and R. Srivastava, Using flow interruption to identify factors causing nonideal contaminant transport, *J. Contam. Hyd., 24*, 205-219, 1997.

Callahan, T. J., Laboratory investigations and analytical and numerical modeling of the transport of dissolved solutes through fractured rock, unpublished Ph.D. dissertation, New Mexico Institute of Mining and Technology, Socorro, 2001.

Callahan, T. J., P. W. Reimus, R. S. Bowman, and M. J Haga, Using multiple experimental methods to determine fracture/matrix interactions and dispersion of nonreactive solutes in saturated volcanic rock, *Water Resour. Res., 36*(12), 3547-3558, 2000.

Callahan, T. J., P. W. Reimus, P. C. Lichtner, and R. S. Bowman, Interpreting Asymmetric Transport Patterns of High Concentration Ionic Tracers in Porous Media, in preparation, 2001.

Cerník, M., K. Barmettler, D. Grolimund, W. Rohr, M. Borkovec, and H. Sticher, Cation transport in natural porous media on laboratory scale: multicomponent effects, *J. Contam. Hyd., 16*, 319-337, 1994.

Charbeneau, R. J., Multicomponent exchange and subsurface solute transport: Characteristics, coherence, and the Riemann problem, *Water Resour. Res., 24*(1): 57-64, 1988.

Corapcioglu, M. Y. and S. Wang, Dual-porosity groundwater contaminant transport in the presence of colloids, *Water Resour. Res., 35*, 3261-3273, 1999.

Fuentes, H. R., W. L. Polzer, E. H. Essington, and B. D. Newman, Characterization of reactive tracers for C-Wells field experiments I: Electrostatic sorption mechanism, lithium, *Los Alamos National Laboratory Report LA-11691-MS*, Los Alamos, NM, 1989.

Geldon, A. L., Preliminary hydrogeologic assessment of boreholes UE25c #1, UE25c #2, and UE25c #3, Yucca Mountain, Nye County, Nevada, *U.S. Geol. Surv. Water-Resour. Invest. Rep. 92-4016*, Denver, CO, 85 pp., 1993.

Grisak, G. E. and J. F. Pickens, Solute transport through fractured media. 1. The effect of matrix diffusion, *Water Resour. Res., 16*, 719-730, 1980.

Grisak, G. E., J. F. Pickens, and J. A. Cherry, Solute transport through fractured media. 2. Column study of fractured till, *Water Resour. Res., 16*, 731-739, 1980.

Hull, L. C., J. D. Miller, and T. M. Clemo, Laboratory and simulation studies of solute transport in fracture networks, *Water Resour. Res., 23*, 1505-1513, 1987.

Jardine, P. M., W. E. Sanford, J.-P. Gwo, O. C. Reedy, D. S. Hicks, J. S. Riggs, and W. B. Bailey, Quantifying diffusive mass transfer in fractured shale bedrock, *Water Resour. Res., 35*, 2015-2030, 1999.

Maloszewski, P. and A. Zuber, Interpretation of artificial and environmental tracers in fissured rocks with a porous matrix, in *Isotope Hydrology*, IAEA, Vienna, Austria, 1983.

Maloszewski, P. and A. Zuber, On the theory of tracer experiments in fissured rocks with a porous matrix, *J. Hyd., 79*, 333-358, 1985.

Maloszewski, P. and A. Zuber, Mathematical modeling of tracer behavior in short-term experiments in fissured rocks, *Water Resour. Res. 26*, 1517-1528, 1990.

Maloszewski, P. and A. Zuber, Tracer experiments in fractured rocks: Matrix diffusion and the validity of models, *Water Resour. Res., 29*, 2723-2735, 1993.

Maloszewski, P., A. Herrmann, and A. Zuber, Interpretations of tracer tests performed in fractured rock of the Lange Bramke basin, Germany, *Hydrogeol. J., 7*, 209-218, 1999.

Mansell, R. S., S. A. Bloom, and W. J. Bond, A tool for evaluating a need for variable selectivities in cation transport in soil, *Water Resour. Res., 29*(6): 1855-1858, 1993.

Neretnieks, I., Diffusion in the rock matrix: An important factor in radionuclide retardation? *J. Geophys. Res., 85*, 4379-4397, 1980.

Ostensen, R. W., Tracer tests and contaminant transport rates in dual-porosity formations with application to the WIPP, *J. Hyd., 204*, 197-216, 1998.

Reimus, P. W. and M. J. Haga, Analysis of tracer responses in the BULLION forced-gradient experiment at Pahute Mesa, Nevada, *Los Alamos National Laboratory Report LA-13615-MS*, Los Alamos, NM, 1999.

Reimus, P. W., A. Adams, M. J. Haga, A. Humphrey, T. Callahan, I. Anghel, and D. Counce, Results and interpretation of hydraulic and tracer testing in the Prow Pass Tuff at the C-Holes, *Yucca Mountain Project Milestone SP32E7M4*, Los Alamos National Laboratory, Los Alamos, NM, 1999.

Tang, D. H., E. O. Frind, and E. A. Sudicky, Contaminant transport in fractured porous media: Analytical solution for a single fracture, *Water Resour. Res., 17*, 555-564, 1981.

Tsang, Y. W., Study of alternative tracer tests in characterizing transport in fractured rocks, *Geophys. Res. Letters, 22* (11), 1421-1424, 1995.

Valocchi, A. J., R. L. Street, and P. V. Roberts, Transport of ion-exchanging solutes in groundwater: Chromatographic theory and field simulation, *Water Resour. Res., 17*, 1517-1527, 1981.

Valocchi, A. J., P. V. Roberts, G. A. Parks, and R. L. Street, Simulation of the transport of ion-exchanging solutes using laboratory-determined chemical parameter values, *Ground Water, 19*, 600-607, 1981.

Vulava, V. M., Cation competition in soil materials: Adsorption equilibria and transport, unpublished Ph.D. dissertation, Swiss Federal Institute of Technology (ETH), Zurich, Switzerland, 1998.

Wallach, R. and J.-Y. Parlange, Modeling transport in a single crack by the dual-porosity concept with a boundary layer at the interface, *J. Contam. Hyd., 34*, 121-138, 1998.

Wallach, R. and J.-Y. Parlange, Applying the boundary layer concept to model transport of dissolved chemicals in preferential flow paths, *Water Resour. Res., 36*, 2845-2851, 2000.

5. On the Relationship Between Diffusive Mass Transfer and Scale in Fractured Media

(In preparation for submission to *Journal of Contaminant Hydrology*)

Timothy J. Callahan[1,2], Paul W. Reimus[1], and Robert S. Bowman[2]

[1]Environmental Science and Waste Technology Group, Los Alamos National Laboratory, Los Alamos, NM 87545

[2]Department of Earth and Environmental Science, New Mexico Institute of Mining and Technology, Socorro, NM 87801

Abstract. The objective of this study was to determine whether matrix diffusion parameters of fractured rock derived from lab tests are applicable at the field scale. We performed transport experiments with nonreactive anion tracers in fractured rock cores at different flow velocities. We observed that the characteristic times of diffusion for the tracers were larger for tests conducted at slower velocities. This relationship between the characteristic time of diffusion and flow velocity was apparently due to the larger relative importance of free-water solute diffusion in fractures at small time scales. For longer-duration laboratory experiments and field experiments, diffusive mass transfer was dominated by diffusion into the unfractured porous matrix, Because of the influence of free-water diffusion, caution must be exercised when applying laboratory-derived diffusive mass transport parameters in fractured media to larger scales. These results emphasize that studying pollutant transport over a range of scales will help determine the relative importance of different transport mechanisms at different scales in heterogeneous systems such as fractured porous rock.

5.1. Introduction

Over the past several years, numerous laboratory and field experiments have been conducted in which solute transport processes were studied in saturated, fractured volcanic tuff at the Nevada Test Site (NTS). One objective of this work was to determine the influence of matrix diffusion on solute transport. Matrix diffusion can significantly retard the movement of solutes through fractured rock groundwater systems [*National Research Council*, 1996]; accounting for this process is critical in assessing potential radionuclide migration at the NTS.

Laboratory-derived transport parameters are often used to predict the migration of contaminants at field sites. Our objective was to compare the transport behavior of solutes in fractured rock at different time and length scales, specifically to determine the relationship between diffusive mass transfer and scale of experiment. In this study, tracer transport data were obtained from fractured volcanic tuff cores from the C-Wells tracer site near Yucca Mountain, Nevada [*Reimus et al.,* 1999; *Callahan et al.*, 2000]. The cores were 0.11 m to 0.22 m in length and the tracer experiments were conducted at average residence times ranging from less than one hour to 150 hours. It was previously shown that diffusive mass transfer strongly influenced tracer transport in these cores [*Callahan et al.*, 2000]. However, *Callahan et al.* [2000] showed that the calculated diffusive mass transfer coefficient, $MTC = n_m^2 D_m / B^2$ (where B is the fracture aperture, n_m is the porosity of the unfractured matrix, and D_m is the effective diffusion coefficient of a solute in the matrix) was larger for tests conducted at shorter time scales. Here we define the characteristic time of diffusion as the inverse of the diffusive mass transfer coefficient. The characteristic time of diffusion is the time required for a given fraction of solute

mass to diffuse from the fracture into the porous matrix; $t_D = B^2/(n_m{}^2 D_m)$. The characteristic time of advection is the mean residence time of a solute in the fracture; $t = L/v$, L is the flow length and v is the average linear velocity of the solute.

In this study, we examine scaling of diffusive mass transfer as a function of advective time in systems of fixed geometry (the laboratory experiments), and we also examine this scaling behavior as it is extended to field-scale tracer tests in which the fracture geometry is largely unknown and distance scales are much larger than in the laboratory tests. We propose that transport of solute tracers in fractured volcanic rocks over short time scales is influenced by small-scale heterogeneities in the fractures (where diffusion occurs within stagnant water), whereas at larger scales, this process will have less importance relative to diffusion into the porous rock matrix (henceforth referred to as "matrix diffusion").

The conceptual model we used to describe transport in heterogeneous porous media such as fractured tuff is the dual-continuum, or "dual-porosity" model [*Tsang*, 1995; *Lichtner*, 2000], in which regions of flowing and nonflowing water are defined, and diffusive communication between these continua is described using either a mass transfer coefficient [e.g., *Maraqa et al.*, 1999; *Callahan et al.*, 2000] or a characteristic time of diffusion which is essentially a diffusion time constant [*Becker and Shapiro*, 2000]. This diffusive mass transfer is often modeled as a first-order rate process, such as in the transport parameter estimation code CXTFIT (version 2.0) [*Toride et al.*, 1995]. Previous researchers have discussed apparent relationships between pore water velocity and mass transfer rates in heterogeneous porous media [*van Genuchten and Wierenga*, 1977; *Nkedi-Kizza et al.*, 1983; *DeSmedt and Wierenga*, 1984; *DeSmedt et al.*, 1986;

Schulin et al., 1987; *Herr et al.*, 1989; *Brusseau et al.*, 1991; *Fischer et al.*, 1996; *Bajracharya and Barry*, 1997; *Maraqa et al.*, 1999]; the conclusion from these studies was that mass transfer rates decreased with pore water velocity. These cited studies focused on aggregated porous material in which the heterogeneity of the system was characterized by the fraction of mobile water relative to the total porosity. Our objective was to identify scaling relationships between diffusive mass transfer and advection times by studying the transport of nonreactive ionic tracers in fractured volcanic tuff cores at different velocities, and comparing these data to field tracer data in the same rock units as the laboratory samples.

5.2. Experimental Methods

It is often difficult to separate the effects of matrix diffusion from hydrodynamic dispersion in heterogeneous media if transport data exist for only one tracer [*Carrera et al.*, 1998; *Becker and Shapiro*, 2000; *Callahan et al.*, 2000]. Thus, we used multiple nonsorbing solutes with different diffusion coefficients, pentafluorobenzoate (PFBA) and bromide, in the same tracer test to allow us to separate the effects of diffusion between stagnant and flowing water and dispersion in the flowing water in fractured volcanic tuffs.

The transport of PFBA and Br^- in fractured ash flow tuffs was studied in both laboratory and field experiments. The matrix diffusion coefficients of PFBA and Br^- were determined in diffusion cell tests using unfractured wafers of volcanic tuff samples obtained from the C-Wells tracer test site, near Yucca Mountain, Nevada [*Callahan et al.*, 2000]. For the laboratory fracture experiments, one induced fracture was created in

each of four volcanic tuff cores following the procedure of *Callahan et al.* [2000]. The cores were obtained from the same stratigraphic intervals as the diffusion cell wafers. The fractures were similar to natural fractures but did not have secondary mineral coatings. Cross-well tracer tests were conducted at the C-Wells site near Yucca Mountain, Nevada [*Reimus et al.*, 1999]. For both the lab and field tracer tests, a pulse of tracer solution was injected and followed by a tracer-free groundwater flush. The breakthrough curves were determined by analyzing the effluent for tracers as a function of time.

5.2.1. Diffusion Cell Tests

Nonfractured volcanic tuff wafers, about 0.01 cm long and 0.1 m in diameter, were encased in epoxy and a Plexiglas sleeve for diffusion cell tests, in which matrix diffusion coefficients through the wafers were measured. The diffusion cell apparatus consisted of a smoothly-cut piece of core (rock "wafer") with the perimeter of the wafer encased in a lucite housing. Two water reservoirs were attached to either end of the wafer unit, and one was filled with tracer solution while the other was filled with a synthetic well water consisting of sodium carbonate and sodium bicarbonate that has similar pH, Na^+, and HCO_3^- concentrations as water from well J-13, 4 km east of the C-Wells site [*Fuentes et al.*, 1989; *Callahan et al.*, 2000]. Wafers 1 –3 were from the upper flow zone, the central flow zone, and the lower flow zone, respectively, of the Prow Pass Tuff Member of the Crater Flat Tuff Formation and wafer 4 was from the lower flow zone of the Bullfrog Tuff Member, also a part of the Crater Flat Tuff Formation [*Geldon*, 1993]. The experimental conditions are listed in Table 5.1. PFBA and LiBr were dissolved in the synthetic well water and buffered to a pH of 7.5 – 8.5 using NaOH [*Reimus et al.*, 1999].

Tracer-free synthetic well water contained 2 meq L^{-1} Na^+ and 2 meq L^{-1} HCO_3^- and was flushed through the "clean water" reservoir at varying flow rates that were increased or decreased depending on whether the rate of change of tracer concentrations in the reservoir was large or small, respectively. Advection in the diffusion cell wafers was avoided by orienting the diffusion cell apparatus such that the hydraulic gradient across the wafer was zero [*Callahan et al.*, 2000]. The diffusion of tracers through the wafers was modeled using the diffusion equation described by *Callahan et al.* [2000].

Table 5.1. Experimental conditions for the tracer tests in the four diffusion cell wafers.

Experiment	Flush rate	Tracer concentrations (meq L^{-1})		
	(mL hr^{-1})	PFBA	Br^-	Li^+
Wafer 1	0.5 – 8.0	6.3	5.0	5.4
Wafer 2	0.8 – 6.0	5.0	21	22
Wafer 3	1.5 – 3.2	4.8	16	16
Wafer 4	0.5 – 8.0	6.4	4.8	4.6

5.2.2. Laboratory Tracer Tests in Fractured Tuff Cores

Four cores of volcanic tuff 0.1 m to 0.3 m in length and 0.1 m in diameter were obtained from the C-Wells site near Yucca Mountain, Nevada. One fracture was mechanically induced in each core and prepared for column testing following the procedure of *Callahan et al.* [2000]. A pulse of a mixed tracer solution containing PFBA and LiBr dissolved in J-13 well water [*Fuentes et al.*, 1989] and buffered with NaOH to a pH of 7.8 – 8.0 was injected for each of the two tests conducted on each core (the exception is core 1, in which three tests were conducted). The flow rates of the two tests in each core differed by about an order of magnitude in order to study the effects of time

scale on tracer transport. The experimental conditions for the nine tracer tests are listed in Table 5.2.

Table 5.2. Experimental conditions for the tracer tests in the four fractured tuff cores.

Experiment	Matrix porosity, n_m	Q (mL hr^{-1})	Pulse vol. (mL)	Tracer concentrations (meq L^{-1}) PFBA	Br^-	Li^+
Core 1, Test 1	0.27	4.0	59.3	3.00	21.6	27.5
Test 2		4.0	60.7	3.00	21.6	27.5
Test 3		0.5	80.1	3.02	23.4	22.8
Core 2, Test 1	0.14	6.0	71.2	3.61	31.6	31.0
Test 2		0.4	74.0	3.02	23.4	22.8
Core 3, Test 1	0.29	11.0	164	3.02	23.4	22.8
Test 2		0.5	79.0	3.21	24.2	23.7
Core 4, Test 1	0.30	5.0	172	3.21	24.2	23.7
Test 2		0.5	162	3.00	21.6	27.5

A dual-porosity model was used to describe transport through the fractured tuff cores [*Callahan et al.,* 2000]. The use of this model was supported by the relatively high porosity of the tuffs (0.14 – 0.30) and the fact that the permeability of the fractures was at least five orders of magnitude greater than that of the porous matrix. The governing equations describing the transport of nonreactive tracers in fractured dual-porosity media are

$$\frac{\partial C_f}{\partial t} = D_f \frac{\partial^2 C_f}{\partial x^2} - v_f \frac{\partial C_f}{\partial x} + \frac{n_m D_m}{b n_f} \frac{\partial C_m}{\partial y}\bigg|_{y=b} \tag{5.1}$$

$$\frac{\partial C_m}{\partial t} = D_m \frac{\partial^2 C_m}{\partial y^2}, \tag{5.2}$$

where C_f [M solute M^{-1} solid] and C_m [M solute L^{-3} liquid] are the solute concentrations in the solid and liquid phases, respectively, D_f [L^2 T^{-1}] is the hydrodynamic dispersion of

solute in the fracture, v_f [L T^{-1}] is the average linear velocity of solute in the fracture, n_m [-] is the porosity within the matrix, b [L] is the mean half-aperture of the fracture, n_f [-] is the porosity within the fractures (n_f = 1 for open fractures), x [L] is the direction of flow in the fracture, D_m [L^2 T^{-1}] is the effective diffusion coefficient of solute in the matrix, and y [L] is the direction of diffusion between the fracture and matrix [*Callahan et al.*, 2000]. The solution to (5.1) and (5.2) in the Laplace domain using the boundary conditions given by *Tang et al.* [1981] is [*Callahan et al.*, 2000]

$$\overline{C_f}(x) = \exp\left[\frac{xv_f}{2D_f}\left(1-\sqrt{1+\frac{4D_f}{v_f^2}s+\frac{4D_f n_m}{v_f^2 b}\sqrt{D_m s}}\right)\right], \tag{5.3}$$

Defining the dimensionless Peclet number as $Pe = \frac{xv_f}{D_f}$ and the characteristic time of advection, or the solute mean residence time as $t = \frac{x}{v_f}$ [T], (5.3) can be rewritten

$$\overline{C_f}(x) = \exp\left[\frac{Pe}{2}\left(1-\sqrt{1+\frac{4t}{Pe}\left\{s+\frac{n_m}{b}\sqrt{D_m s}\right\}}\right)\right]. \tag{5.4}$$

where s [T^{-1}] is the transform variable for Laplace space. We define the lumped parameter $t_D = \frac{B^2}{n_m^2 D_m}$ [T] as the characteristic time of diffusion in the system. The characteristic time of diffusion was defined similarly by *Becker and Shapiro* [2000]. The total aperture $B = 2b$ is used instead of the half-aperture.

The Reactive Transport Laplace Transform Inversion code (RELAP), described by *Reimus and Haga* [1999], was used to simultaneously fit the responses of two nonreactive tracers (PFBA and Br^-) in the same medium using (5.4). Fitting the responses of tracers of different diffusion coefficients injected simultaneously allowed us to

successfully separate the effects of hydrodynamic dispersion and diffusion in the system. To do this, we assumed that the two tracers had the same residence time and Peclet number, so the difference in their response was due to their different characteristic times of diffusion, τ_D.

5.2.3. Field Tracer Tests

Tracer tests were conducted at the C-Wells complex in southern Nevada between 1996 and 1999. Descriptions of the experiments are given by *Reimus et al.* [1999]. The test objectives included obtaining estimates of fracture porosity, longitudinal dispersivity, and diffusive mass transfer coefficients for performance assessment models of the potential high-level radioactive waste repository at Yucca Mountain, Nevada. PFBA and Br^- were used as nonsorbing solute tracers in each field test. The laboratory diffusion cell and fractured rock core tracer experiments were conducted to determine the applicability of laboratory-derived parameters to field-scale transport. Transport in the field tests was described using (5.1) and (5.2); the interpretation procedure was the same as that used by *Callahan et al.* [2000].

5.3. Results and Discussion

5.3.1. Diffusion Cell Tests

The results from the diffusion cell tests are listed in Table 5.3. The diffusion coefficients were roughly proportional to the log of the matrix permeability, which was measured using a falling head method [*Callahan et al.*, 2000].

Table 5.3. Molecular diffusion coefficients for PFBA and Br^- measured in the diffusion cell wafers.

Experiment	Permeability of matrix (m^2)	Diffusion coefficient in matrix ($m^2\ s^{-1}$)[a]	
		PFBA	Br^-
Wafer 1	4.72×10^{-15}	1.9×10^{-10}	6.0×10^{-10}
Wafer 2	7.76×10^{-19}	0.13×10^{-10}	0.4×10^{-10}
Wafer 3	4.49×10^{-16}	1.1×10^{-10}	3.0×10^{-10}
Wafer 4	9.37×10^{-17}	0.35×10^{-10}	1.0×10^{-10}

5.3.2. Fractured Tuff Core Tests

The modeling results for the fractured tuff core tracer tests are provided in Table 5.4. In general, the characteristic time of diffusion was larger for the longer-term tests. Also, the diffusion coefficients measured in the diffusion cell tests were smaller than those calculated from the tracer transport tests in the fractured tuff cores except for test 3 in core 1 (Table 5.5).

Table 5.4. Modeling parameters obtained from RELAP for the fractured rock core tests.

Experiment	τ (hr)	Pe (-)	τ_D (Br^-) (hr)
Core 1, Test 1	8.2	3.0	18.7
Test 2	6.5	3.9	15.0
Test 3	74.0	5.1	74.6
Core 2, Test 1	2.0	15	31.5
Test 2	32.6	9.8	179
Core 3, Test 1	0.8	18	5.46
Test 2	30.0	3.3	13.6
Core 4, Test 1	4.2	46	13.0
Test 2	149.0	7.0	96.5

Table 5.5. Model parameter results and estimates of effective surface area in the fractured cores.

Experiment	τ (hr)	B (m)	D_m (Br^-) ($m^2\ s^{-1}$)	D_m^* (Br^-)[a] ($m^2\ s^{-1}$)	A[b] (m^2)	A_{eff}[c] (m^2)
Core 1, Test 1	8.2	2.12×10^{-3}	9.0×10^{-10}	6.0×10^{-10}	0.031	0.019
Test 2	6.5	1.96×10^{-3}	9.6×10^{-10}			0.019
Test 3	74.0	2.56×10^{-3}	2.8×10^{-10}			0.011
Core 2, Test 1	2.0	0.72×10^{-3}	2.4×10^{-10}	0.4×10^{-10}	0.033	0.041
Test 2	32.6	0.88×10^{-3}	0.63×10^{-10}			0.019
Core3, Test 1	0.8	0.82×10^{-3}	4.13×10^{-10}	3.0×10^{-10}	0.022	0.013
Test 2	30.0	1.26×10^{-3}	3.9×10^{-10}			0.014
Core 4, Test 1	4.2	1.00×10^{-3}	2.4×10^{-10}	1.0×10^{-10}	0.041	0.033
Test 2	149.0	3.40×10^{-3}	3.75×10^{-10}			0.042

[a]Molecular diffusion coefficients measured in diffusion cell wafers (Table 5.3).

[b]Surface area of fracture, the product of the length and width of the fractured cores.

[c]Effective surface area of fracture, determined by using the D_m^* value from the diffusion cell tests in the τ_D calculation (Table 5.4) and the effective fracture volume for each test, $Q^*\tau$.

Cussler [1984] and *Hu* [2000] state that molecular diffusion coefficients vary with concentration, and it should be noted that the tracer concentrations for the diffusion cell and fractured rock core tests were within an order of magnitude (Table 5.1, Table 5.2). Assuming that the small difference in tracer concentration did not drastically affect the diffusion process in the two methods, the diffusion coefficients obtained from the diffusion cell tests probably better reflect the true bulk values in the porous matrix of these rock types because diffusion through the porous medium was the only transport mechanism in the wafers.

Callahan et al. [2000] hypothesized that the diffusive mass transfer coefficient was larger for the shorter-term laboratory tests because of either free water diffusion

within the fractures during the short-term tests, which was interpreted as matrix diffusion, or a smaller effective fracture aperture than that deduced from B = Q τ/Lw (i.e., a smaller ratio of fracture volume to surface area, or smaller value of B). It is possible that free water diffusion within the fracture was less important at larger time scales, and the characteristic time of diffusion was therefore a function of "true" matrix diffusion due to the solutes accessing a larger volume of the porous matrix.

The fact that the diffusion cell experiments produced smaller matrix diffusion coefficients than in the fractured rock core tests in the same rock types (Table 5.5) supports the hypothesis that free water diffusion within the fractures was important during the laboratory transport experiments. We inserted the diffusion coefficients measured in the diffusion cell experiments into the expression $t_D = B^2/(n_m{}^2 D_m)$ and solved for the fracture surface area, $A = \frac{t\ Q}{n_m \sqrt{D_m t}}$ [L^2], where $A = V/B$, $V = Qt$; V is the effective volume of the fracture [L^3] and Q [$L^3\ T^{-1}$] is the average volumetric flow rate during the tracer test. The effective fracture surface area was smaller than that based on the length and width of the fractures for each test and for all the cores, except for test 1 on core 2 (Table 5.5). This result suggests the flow was channeled in the fractures during the transport experiments, which would allow diffusion within the adjacent stagnant water ("free water diffusion") to occur. Free water diffusion could have also taken place within voids along the rough walls of the fracture surfaces. To consider the effects of free water diffusion in the fractured tuff cores, we added a third domain to the dual-porosity model.

5.3.2.1. The Triple Porosity Model. If diffusive mass transfer was not a function of experimental time scale, the best-fit model parameters obtained from one tracer test should have fit tracer breakthrough curves obtained from all other tests in the same system. However, this was not the case for the tracer experiments conducted on the fractured tuff cores. Figure 5.1 shows the tracer data and model fits from RELAP for core 4, test 1. Core 4 was investigated because of the poor model fits to the transport data using the dual-porosity model. The model fits assuming dual-porosity conditions match the transport data fairly well. Prior to test 2, the model parameters were applied to the test 2 data (and accounting for the difference in experimental flow rate), which resulted in a poor fit to the data (Figure 5.2). Therefore, it is likely that some process not represented in the dual-porosity model influenced tracer transport during one or both core experiments. We assumed that free water diffusion in the fracture, due to either flow channeling or fracture surface roughness caused the dual-porosity model to be unsatisfactory in describing transport in the cores. This hypothesis was supported from observations of the fracture surfaces upon opening the cores (Figure 5.3; see *Callahan*, [2001] for a description of the photography method). Therefore, a triple-porosity model was used to improve the ability to fit the data from both tests with a single set of diffusion parameters.

Figure 5.1. Transport data and best-fit model results assuming dual-porosity conditions, core 4, test 1.

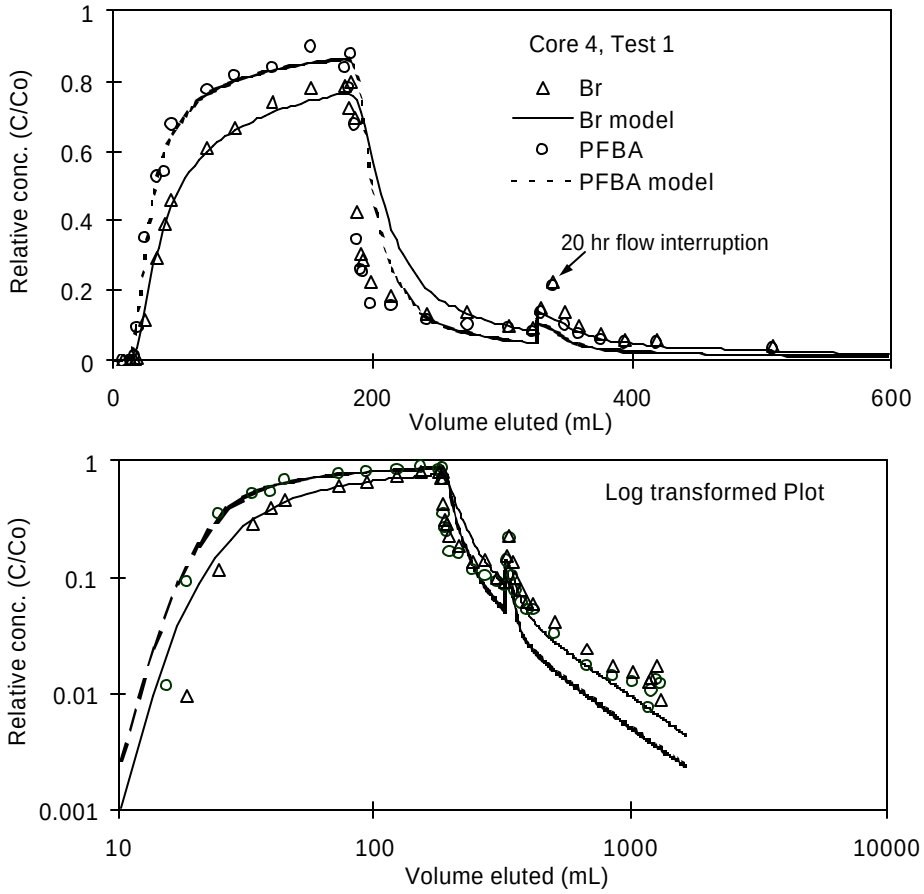

Figure 5.2. Model fits and tracer transport data for core 4, test 2 using the dual-porosity parameter estimates obtained for test 1 and adjusted for the slower flow rate. The transport properties were Pe = 46, τ = 4.2 hr, and τ_D = (B = 1.0 x 10^{-3} m, n_m = 0.30, D_m (Br^-) = 2.4 x 10^{-10} m^2 s^{-1}).

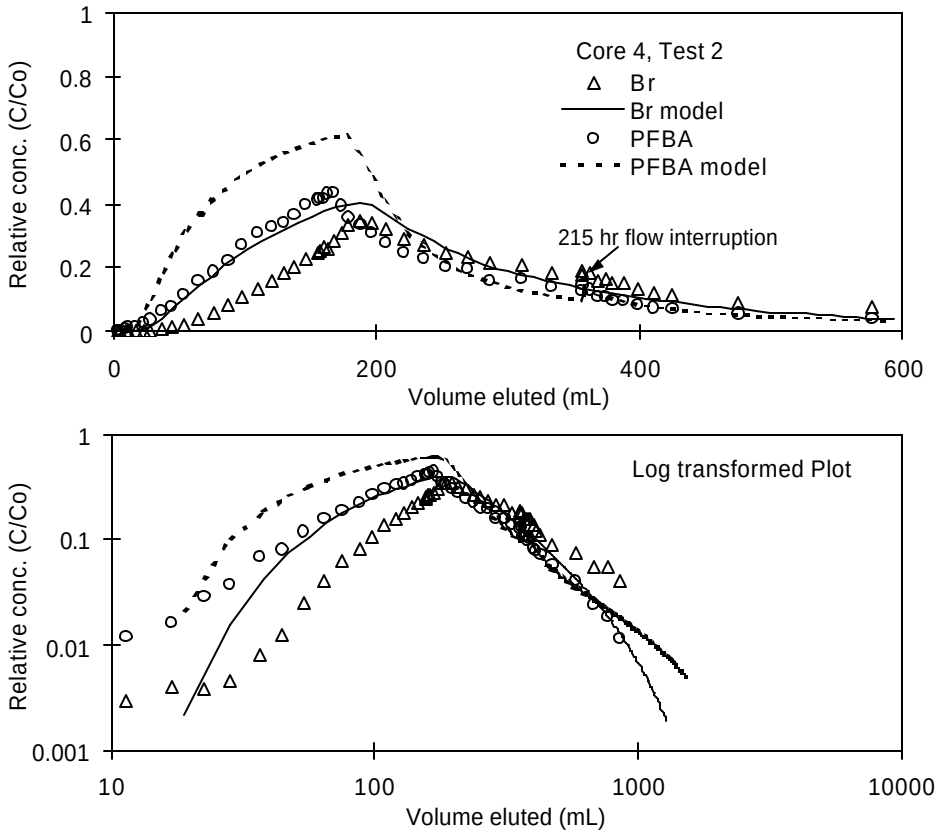

Figure 5.3. Photograph of core 4 under ultraviolet (UV) light. Previous to opening, a 40-mL solution of latex microspheres, each sphere containing fluorescein, was injected into the fractured cores (oriented such that the fractures were parallel to the bench top) and the microspheres were allowed to settle onto the lower surface of the fracture (flow direction was left to right). The light-colored spots indicate the presence of latex microspheres (10^{-6}m avg diam.). Length of core is 0.22 m, diameter is 0.1 m.

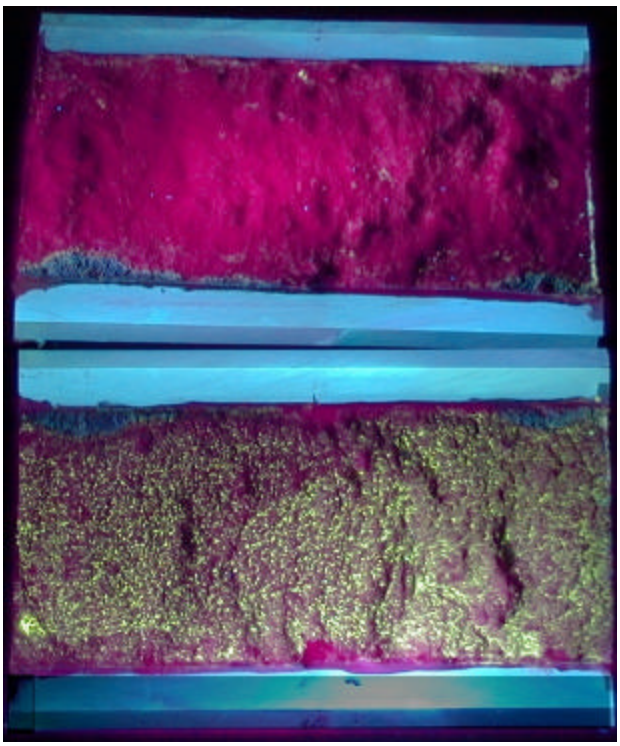

The triple-porosity model is an extension of the dual-porosity model and can account for the presence of a transition layer (Figure 5.4). It can also qualitatively approximate the effects of flow channeling in a fracture. This approach is similar to that assumed in a numerical study by *Grenier et al.* [1998], who considered flow channeling in a fracture with diffusive mass transfer between all three domains of a triple-porosity system. For this study, the Reactive Transport (RETRAN) code [*Reimus et al.*, 1999] was

adapted to account for a third domain consisting of nodes that were assigned separate porosity values and matrix diffusion coefficients. We added a third equation to (5.1) and (5.2) to account for mass transfer in the transition layer

$$\frac{\partial C_l}{\partial t} = D_l \frac{\partial^2 C_l}{\partial y^2}, \tag{5.5}$$

Figure 5.4. Triple-porosity model describing solute transport in heterogeneous geologic media. This model can approximate a system in which a transition layer exists between the advecting water in the fracture and the porous matrix.

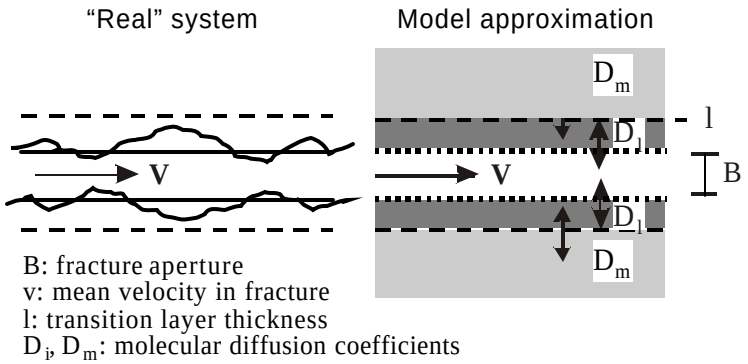

A transition layer 0.4 cm thick was added as a third continuum in the numerical code. For core 4, the layer was assigned a matrix diffusion coefficient (D_m) equal to 6.0 x 10^{-10} m^2 s^{-1} for Br^- and 2.0 x 10^{-10} m^2 s^{-1} for PFBA and a porosity of 0.70. For the bulk matrix, we assumed the corresponding values of 1.0 x 10^{-10} m^2 s^{-1} for Br^- and 0.33 x 10^{-10} m^2 s^{-1} for PFBA; these were the values determined from the diffusion cell experiments on a separate sample of core 4. The bulk matrix porosity was 0.30, the same as that measured in independent porosity measurements [*Callahan et al.*, 2000]. The values for Peclet number and the characteristic time of advection from test 1 in core 4 were used to model test 2 (the time of advection was adjusted in proportion to the different flow rates).

These values provided the best visual fit to the test 2 tracer data (Figure 5.5) while having the least effect on the fits to Br^- and PFBA in test 1. The improvement offered by the triple-porosity model is seen by comparing Figure 5.5 to Figure 5.2.

Using the transport parameters determined for test 1, the triple-porosity fits to the test 2 data are qualitatively better than those obtained assuming dual-porosity conditions. It is possible that it would be more appropriate to model the fractures as having a series of transition layers, each having unique diffusive mass transfer properties. Modeling multi-rate diffusion has been attempted by others to explain and predict transport behavior in heterogeneous media [*Haggerty and Gorelick*, 1995; *Haggerty et al.*, 2000; *Fleming and Haggerty,* 2001; *Haggerty et al.*, 2001; *McKenna et al.*, 2001]. These conceptual models use a series of diffusion coefficients as solute is transported through media containing a large size distribution of pores. The triple-porosity model described here is a simple expansion of the dual-porosity model, and describes diffusion through a series of domains, rather than in parallel. We feel this method is the most realistic and best constrained concept for the fractured tuff cores.

Figure 5.5. Triple-porosity model fits and tracer data for core 4, test 2 using parameter estimates obtained for test 1 and adjusted for the slower flow rate. We assumed a transition layer 0.4 cm thick between the fracture and matrix domains. The properties of the transition layer were $n_l = 0.70$ and $D_l = 6.0 \times 10^{-10}$ m^2 s^{-1} and 2.0×10^{-10} m^2 s^{-1} for Br^- and PFBA, respectively (bulk matrix properties were $n_m = 0.30$, $D_m = 1.0 \times 10^{-10}$ m^2 s^{-1} for Br^- and 0.33×10^{-10} m^2 s^{-1} for PFBA).

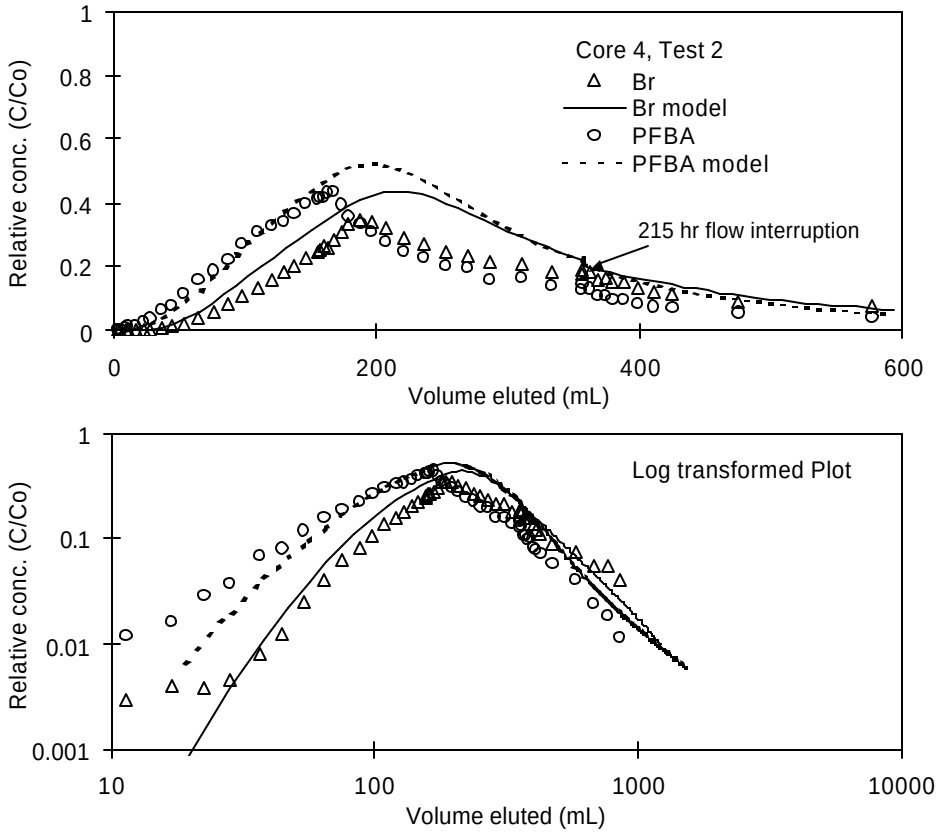

5.3.3. Field Tracer Tests

The fractured tuff cores in the laboratory provided simplified systems for solute transport in fractured rock due to the single-fracture geometry. Comparing the transport results between media of much different geometries introduces additional uncertainties associated with the application of the dual-continuum model. Table 5.6 lists the transport

parameters obtained from the field tracer data. The variability and of the fracture apertures in the field and the uncertainty of travel distances in the fracture network were undoubtedly much greater than in the single-fracture tuff cores. The effective fracture aperture(s) in the field were probably larger than in the fractured tuff cores due to the presence of multiple fractures as observed from downhole televiewers at the C-Wells [*Geldon*, 1993]. Large fracture apertures would produce larger characteristic times of diffusion calculated from tracer data. Using the matrix diffusion coefficient for Br^- obtained from diffusion cell tests and matrix porosity values measured on representative samples in the laboratory, the effective fracture aperture for the 1996 test, as determined from τ_D (Table 5.6), was 0.09 cm for Path 1 and 0.3 cm for Path 2. For the 1998 test, the effective fracture aperture was 0.7 cm.

Table 5.6. Modeling parameters obtained from RELAP for the field tracer tests.

Experiment	τ (hr)	Pe (-)	τ_D (Br^-) (hr)
1996 Test, Pathway 1[a]	31 – 37[b]	6 – 9[c]	445
1996 Test, Pathway 2[a]	640 – 995[b]	1.7 – 3[c]	5297
1998 Test	620 – 1230[b]	0.9 – 1.9[c]	1186

[a]Assuming transport through two discrete flow zones in the aquifer [*Reimus et al.*, 1999].

[b]Assuming radial flow (lower bound) or linear flow (upper bound) conditions.

[c]Based on assumption of linear flow (lower bound) or radial flow (upper bound) conditions.

Figure 5.6 shows the relationship between the characteristic time of diffusion and the time of advection for the laboratory and field tracer tests. While it is debatable to extend the laboratory data to field scales, the trend of increased characteristic time of

diffusion with larger time of advection is evident within the laboratory data and appears to extend to the field data.

Qualitative comparison of the lab and field data suggests that the process of diffusive mass transfer in the field tracer tests was influenced predominantly by diffusion within the porous matrix, and that the tracers experienced relatively large fracture apertures compared to the tuff cores. *Carrera et al.* [1998] suggested that at larger scales the relative importance of matrix diffusion will decrease, eventually producing an asymptotic value for the characteristic time of diffusion that is constant for any small flow rate or large travel distance. For this field system, the transport data suggest that this asymmetric value, if it exists, will be obtained for characteristic times of advection than the maximum characteristic time of diffusion calculated, 1230 hr (Table 5.6).

Figure 5.6. Plot of characteristic time of diffusion (τ_D) vs. characteristic time of advection (τ) for tracer tests in fractured volcanic tuffs. The lab data were obtained from tracer tests in four rock cores 0.1 – 0.2 m long. The symbols represent the results for Br^- in multiple-tracer experiments. The field data are for Br^- and indicate a range of τ based on assuming either radial or linear flow conditions as lower and upper bounds, respectively.

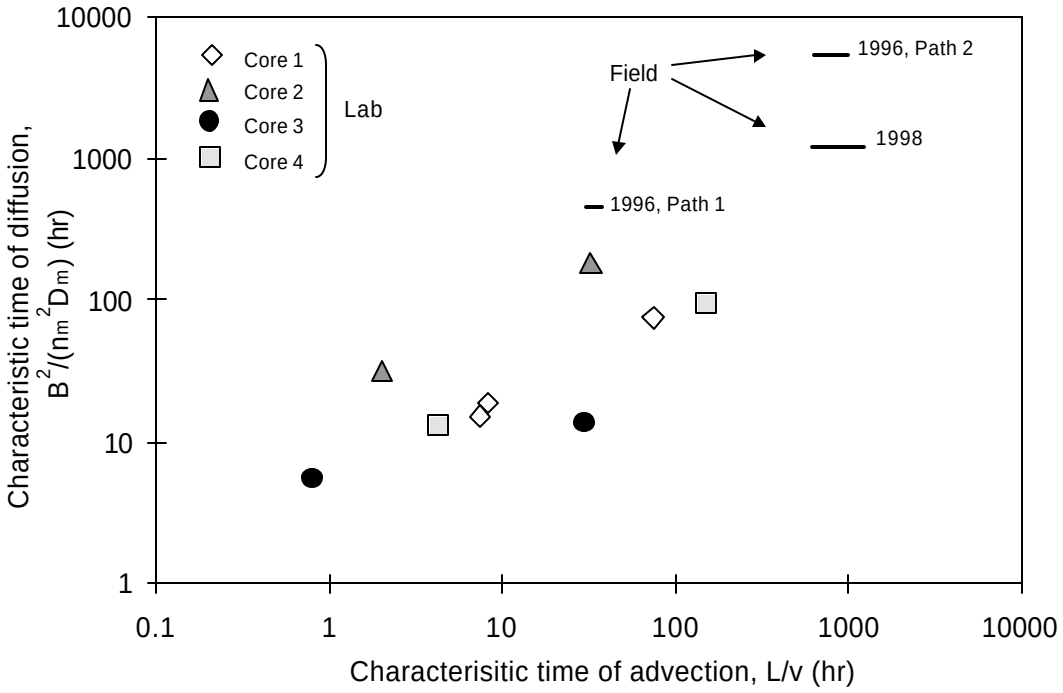

5.4. Conclusions

Transport data for pentafluorobenzoate (PFBA) and bromide were obtained in fractured volcanic tuffs using diffusion cell, fractured tuff core, and field tracer tests. These transport parameters can be applied to field sites with the understanding that certain caveats apply. We found that (a) the characteristic time of diffusion was larger for tracer tests conducted at larger time scales for the laboratory fractured tuff cores and (b) matrix diffusion coefficients calculated from tracer data in the fractured tuff cores were

larger than those determined from both the diffusion cells and the field tracer experiments. We hypothesized that this relationship between the characteristic time of diffusion and time scale was due to either flow channeling in the fractures or the surface roughness of the fractures, both which would result in a bias toward smaller characteristic times of diffusion in the fractures at shorter time scales. For three of the four cores, the effective fracture surface area calculated assuming that the diffusion coefficients obtained from the diffusion cells applied to the matrix in the fractured cores was 20 % to 41 % smaller than the measured fracture surface area assuming a constant aperture (i.e., length by width). This result supports the flow channeling hypothesis. The effective surface area of a fourth core was 24 % larger than the measured surface area. However, it is likely that the total surface area of each tuff core was much larger than that estimated from the length and width because of the roughness. In the longer-term core tests and the field tests, molecular diffusion within stagnant water in the fracture was probably less important, and the diffusive mass transfer process was mainly due to matrix diffusion.

These results suggest that diffusive mass transfer controlled the migration of solutes in fractured media but at short time scales, the diffusion mechanism was strongly influenced by diffusion in stagnant water within the fractures of the cores. This free-water diffusion causes an overestimation of diffusive mass transfer for transport in fractured media at larger scales. Thus, tracer transport data obtained from laboratory experiments should be used cautiously when predicting movement of pollutants at larger scales.

Acknowledgments. Financial support for this work was provided by the U.S. Department of Energy, Office of Civilian Radioactive Waste Management, as part of the

Yucca Mountain Site Characterization Project. We thank John Wilson, Brian McPherson, and Fred Phillips for their thoughtful discussions of this work and suggestions on interpreting the data, Marc Haga for conducting the diffusion cell experiments, and Dale Counce for the sample analyses.

References

Bajracharya, K. and D. A. Barry, Nonequilibrium solute transport parameters and their physical significance: numerical and experimental results, *J. Contam. Hyd.*, *24*, 185-204, 1997.

Becker, M. W. and A. M. Shapiro, Tracer transport in fractured crystalline rock: evidence of nondiffusive breakthrough tailing, *Water Resour. Res.*, *36*(7), 1677-1686, 2000.

Brusseau, M. L., T. Larsen, and T. H. Christensen, Rate-limited sorption and nonequilibrium transport of organic chemicals in low organic carbon aquifer materials, *Water Resour. Res.*, *27*(6), 1137-1145, 1991.

Callahan, T. J., Laboratory investigations and analytical and numerical modeling of the transport of dissolved solutes through fractured rock, unpublished Ph.D. dissertation, New Mexico Institute of Mining and Technology, Socorro, 2001.

Callahan, T. J., P. W. Reimus, R. S. Bowman, and M. J. Haga, Using multiple experimental methods to determine fracture/matrix interactions and dispersion in saturated fractured volcanic tuff, *Water Resour. Res.*, *36*(12), 3547-3558, 2000.

Carrera, J., X. Sanchez-Vila, I. Benet, A. Medina, G. Galarza, and J. Guimera, On matrix diffusion: Formulations, solution methods, and qualitative effects, *Hydrogeol. J.*, *6*, 178-190, 1998.

Cussler, E. L., Diffusion: Mass Transfer in Fluid Systems, Cambridge Univ. Press, New York, 1984.

DeSmedt, F. and P. J. Wierenga, Solute transfer through columns of glass beads, *Water Resour. Res., 20*, 225-232, 1984.

DeSmedt, F., F. Wauters, and J. Sevilla, Study of tracer movement through unsaturated sand, *J. Hydrol., 85*, 169-181, 1986.

Fischer, U., R. Schulin, M. Keller, and F. Stauffer, Experimental and numerical investigation of soil vapor extraction, Water Resour. Res., 32(12), 3413-3427, 1996.

Fleming, S. W. and R. Haggerty, Modeling solute diffusion in the presence of pore-scale heterogeneity: method development and an application to the Culebra dolomite Member of the Rustler Formation, New Mexico, USA, *J. Contam. Hyd., 48*, 253-276, 2001.

Freeze, R. A. and J. A. Cherry, Groundwater, Prentice-Hall, Inc., Englewood Cliffs, NJ, 1979.

Fuentes, H. R., W. L. Polzer, E. H. Essington, and B. D. Newman, Characterization of reactive tracers for C-Wells field experiments I: Electrostatic sorption mechanism, lithium, *Los Alamos National Laboratory Report LA-11691-MS*, Los Alamos, NM, 1989.

Geldon, A. L., Preliminary hydrogeologic assessment of boreholes UE25c #1, UE25c #2, and UE25c #3, Yucca Mountain, Nye County, Nevada, *U.S. Geol. Surv. Water-Resour. Invest. Rep. 92-4016*, Denver, CO, 85 pp., 1993.

Grenier C., E. Mouche, and E. Tevissen, Influence of variable fracture aperture on transport of non-sorbing solutes in a fracture: a numerical investigation, *J. Contam. Hyd., 35*, 305-313, 1998.

Haggerty, R. and S. Gorelick, Multiple-rate mass transfer for modeling diffusion and surface reactions in media with pore-scale heterogeneity, *Water Resour. Res., 31*(10), 2383-2400, 1995.

Haggerty, R., S. A. McKenna, and L. C. Meigs, On the late-time behavior of tracer test breakthrough curves, *Water Resour. Res., 36*(12), 3467-3479, 2000.

Haggerty, R., S. W. Fleming, L. C. Meigs, and S. A. McKenna, Tracer tests in a fractured dolomite, 2. Analysis of mass transfer in single-well injection-withdrawal tests, *Water Resour. Res., 37*(5), 1129-1142, 2001.

Herr, M., G. Schäfer, and K. Spitz, Experimental studies of mass transport in porous media with local heterogeneities, *J. Contam. Hyd., 4*, 127-137, 1989.

Hu, P., Diffusion coefficients of hydrologic tracers as measured by a Taylor dispersion apparatus, unpublished M.S. thesis, New Mexico Institute of Mining and Technology, Socorro, 2000.

Lichtner, P. C., Critique of dual continuum formulations of multicomponent reactive transport in fractured porous media, Dynamics of Fluids in Fractured Rock, B. Faybishenko, P. A. Witherspoon, and S. M. Benson (eds.), *Geophys. Mon. 122*, 281-298, Amer. Geophys. Union, 2000.

Maraqa, M. A., R. B. Wallace, and T. C. Voice, Effects of residence time and degree of water saturation on sorption nonequilibrium parameters, *J. Contam. Hyd., 36*, 53-72, 1999.

McKenna, S. A., L. C. Meigs, and R. Haggerty, Tracer tests in a fractured dolomite, 3. Double-porosity, multiple-rate mass transfer processes in convergent flow tracer tests, *Water Resour. Res., 37*(5), 1143-1154, 2001.

National Research Council, Committee on Fracture Characterization and Fluid Flow, Rock Fractures and Fluid Flow: Contemporary Understanding and Applications, National Academy Press, Washington, D.C., 1996.

Nkedi-Kizza, P., J. W. Biggar, M. Th. van Genuchten, P. J. Wierenga, H. M. Selim, J. M. Davidson, and D. R. Nielsen, Modeling tritium and chloride 36 transport through an aggregated oxisol, *Water Resour. Res., 19*, 691-700, 1983.

Reimus, P. W. and M. J. Haga, Analysis of tracer responses in the BULLION forced-gradient experiment at Pahute Mesa, Nevada, *Los Alamos National Laboratory Report LA-13615-MS*, Los Alamos, NM, 1999.

Reimus, P. W., A. Adams, M. J. Haga, A. Humphrey, T. Callahan, I. Anghel, and D. Counce, Results and interpretation of hydraulic and tracer testing in the Prow Pass Tuff at the C-Holes, *Yucca Mountain Site Characterization Project Milestone Report SP32E2M4SZ*, Los Alamos National Laboratory, Los Alamos, NM, 1999.

Schulin, R., P. J. Wierenga, H. Fluhler, and J. Leuenberger, Solute transport through a stony soil, *Soil Sci. Soc. Am. J., 51*, 36-42, 1987.

Tang, D. H., E. O. Frind, and E. A. Sudicky, Contaminant transport in fractured porous media: Analytical solution for a single fracture, *Water Resour. Res., 17*, 555-564, 1981.

Toride, N., F. J. Leij, and M. Th. van Genuchten, The CXTFIT code for estimating transport parameters from laboratory or field. Version 2.0, *U.S. Dep. Agric. Res. Rep. No. 138*, 121 pp., 1995.

Tsang, Y. W., Study of alternative tracer tests in characterizing transport in fractured rocks, *Geophys. Res. Letters, 22* (11), 1421-1424, 1995.

van Genuchten, M. Th. and P. J. Wierenga, Mass transfer studies in sorbing porous media: experimental evaluation with tritium, *Soil Sci. Soc. Am. J., 41*, 272-278, 1977.

6. Conclusions and Recommendations for Future Work

6.1. Conclusions

The conclusion from this work is that tracer transport parameters can be used to describe and predict field-scale transport in fractured rock with the following stipulations:

a) the conceptual model can account for the process of tracer diffusion in free water within the fractures; this process is most important for experiments conducted at short-time scales because the ratio of matrix: fracture volume accessed is small,

b) the physically-based ion exchange model is used to interpret cation tracer data obtained after high-concentration pulse injections; the commonly-used linear sorption ("K_D") model does not explain the tracer transport behavior and can underpredict cation retardation.

Transport data from field and laboratory tracer tests in fractured rock indicate a relationship between the diffusive mass transfer and scale. Even for a set of laboratory experiments in the same fractured tuff core, the scale relationship is evident; that is, in longer-term tests the characteristic time of diffusion is larger than in short-term tests. The characteristic time of diffusion is defined as $\tau_D = B^2/(n_m^2 D_m)$, where B is the mean fracture aperture, n_m is the porosity of the matrix, and D_m is the molecular diffusion coefficient of a solute in the porous matrix. It was shown by *Callahan et al.* [2001a] that a triple-porosity model more accurately describes solute transport for a short-term test and provided a qualitatively better fit to longer-term tracer test data in the same fractured tuff core. The triple-porosity concept effectively accounted for flow channeling in the

fracture, which allowed molecular diffusion between the flowing and stagnant water ("free water diffusion") within the fracture. This process influenced the characteristic time of diffusion more for short residence times, whereas in longer-term tests, free water diffusion within the fracture was less important relative to true matrix diffusion. Thus, the value of the characteristic time of diffusion at longer characteristic times of advection more accurately reflected true matrix diffusion.

The importance of multicomponent effects increased with the ratio of the reactive solute lithium to the total concentration of cations in solution. The lithium breakthrough curves in two crushed rock column experiments, in which the Li^+ concentration was about 50 % of the total cations, exhibited asymmetric chromatographic separation with the counterion bromide. In a third column test, the concentration of Li^+ was 22% of the total cations, and the asymmetric ion separation was less pronounced. These results have relevance to field tracer tests in which high concentrations of chemicals are injected into the aquifer to counteract dilution effects in the system. Although transport in fractured media is often complicated by diffusive mass transfer between domains, adding multicomponent equations to transport models can increase their accuracy for modeling ion-exchanging tracers such as Li^+.

The multiple-porosity and multicomponent models discussed above provided more accurate descriptions of solute transport in porous and fractured media. For certain cases, such as short-term experiments or high concentration injections in fractured rock cores, a single-component, dual-porosity conceptual model was insufficient, but by adding equilibrium ion-exchange relationships to describe Li^+ transport under high concentration conditions and a porous transition layer to capture the effects of free water

diffusion at short time scales, more accurate interpretations to the transport data were obtained. These results are vital for proper interpretation of laboratory-derived transport data, and for appropriate application of laboratory-derived transport parameters such as diffusive mass transfer and retardation coefficients to field scales. However, the large difference between lab and field geometries must be accounted for when attempting to scale up lab transport data. For transport in saturated, fractured tuff, lab data tended to overestimate the rate of diffusive mass transfer compared to field mass transfer rates in the same rock units.

6.2. Recommendations for Future Work

The following recommendations are listed in order of relative importance. The discussion of applying lab-derived diffusion parameters is followed by one on applying tracer data obtained under high-concentration conditions to lower concentration situations.

First, advancing the state of the art on multiple-porosity and multiple-rate conceptual models used to describe transport through heterogeneous media such as fractured rock is of paramount importance. Stochastic methods are often used to predict a wide range of possible situations when studying contaminant transport issues. However, the importance of the physical mechanisms at work are often overlooked. The models developed in this work can be tested against other methods using the exceptionally high-quality data sets produced here. Also, magnetic resonance imaging techniques can be used to visualize solute transport in heterogeneous media. Such a method may be feasible concurrent with traditional tracer tests. The uncertainty often associated with point-to-

point tracer tests may be reduced by actually seeing where and how the tracer mass moves within the system during tracer experiments.

As for the multicomponent effects discussed previously, the ion-exchange approach would be greatly improved if ion-exchange coefficient data were generated at a variety of concentrations. Usually, one bulk value is assumed for each ion-exchange coefficient; *Vulava* [1998] has shown that ion-exchange coefficients are a function of the concentrations of each cation in solution. Thus, the traditional batch sorption experiment is an oversimplified method that provides only a cursory gauge of the transport behavior of reactive solutes in geologic media.

6.2.1. Triple-Porosity Effects

There have been many laboratory studies using visualization techniques to study both one-phase and two-phase flow through fractures or fracture replicas [*Persoff and Pruess*, 1995; *Glass et al.*, 1995; *Tidwell et al.*, 1995; *Brown et al.*, 1998; *Dijk et al.*, 1999; *Detwiler et al.*, 1999; *Su et al.*, 1999; *Detwiler et al.*, 2000; *O'Hara et al.*, 2000]. Variable or rough-walled fractures have been shown to influence contaminant transport, but the extension of these data to the field is limited to inferences of larger-scale heterogeneity, for example, the relationship between fracture network geometry and fluid flow patterns [*Odling et al.*, 1999]. Previous research was conducted at the Chalk River site, Ontario [*Raven et al.*, 1988] in which stagnant water regions in a fracture were inferred from field tracer data. In addition, *Dijk et al.* [1999] used a nuclear magnetic resonance (NMR) technique to view water flow in a natural fracture. They observed regions where the flow velocity was not in the direction of the overall hydraulic gradient,

assumed to be a result of aperture variations in the fractures. However, *Dijk et al.* [1999] did not measure solute concentrations in their study. It would be informative to determine concentration gradients within the fracture, especially in these regions of heterogeneous flow. Diffusive mass transfer in free water in these fracture regions may be quite large compared to that within a tortuous porous matrix. At this time, there is no proven method of practically and accurately measuring concentration gradients within fractures. Imaging studies of flow in fractures and fracture networks have been used to produce flow field predictions [*Thompson*, 1991; *Brown et al.*, 1998], thus providing information on the flow patterns in fractures that could then be used to predict solute distributions in the fractures.

6.2.1.1. Magnetic Resonance Imaging of Transport Through Fractures. As mentioned above, *Dijk et al.* [1999] used a nuclear magnetic resonance (NMR) imaging technique to visualize flow through fractures. The NMR procedure provides an accurate representation of the fracture geometry similar to the fracture cast technique. This procedure has the advantage of being noninvasive, so flow experiments as well as tracer experiments could be conducted during or after imaging flow.

The values of the characteristic time of diffusion for bromide in the fractured tuff cores from the C-Wells site were related to solute residence time of the tracer test [*Callahan et al.*, 2001a]. Diffusive mass transfer is a function of the surface area between the water in the fracture and the porous matrix. If the effective surface area is different during short-term tests than during longer-term tests due to flow channeling, data obtained from fracture casting and NMR techniques should verify this phenomenon.

6.2.1.2. Fracture Cast Imaging. The aperture variability of rock fractures can be measured by creating dyed silicone casts of rock fractures, photographing the casts on a light table, and using computer software to correlate the amount of light transmitted to cast thickness [*Reimus*, 1995; A. I. Abdel-Fattah, pers. comm., 2001]. Along with the dyed silicone fracture casts, silicone "wedges" of known thickness must be created, providing the calibration necessary for the cast thickness calculation. A charge-coupled device (CCD) camera can be used to photograph the calibration wedges and the fracture cast. Image-processing software can then be used to generate a representation of the fracture aperture with light transmittance as a function of position being inversely related to cast thickness (and thus, fracture aperture).

Once the aperture geometry for the fractured rock core is known, it can be incorporated into a numerical flow model. Interpretation of the transport data would be more computationally intensive with a variable fracture aperture representation, but the calculated flow field should, in theory, provide a more accurate representation of flow patterns in the fracture. However, creating fracture casts requires open rock fractures and may irreversibly alter the surface characteristics of the fractures, especially by increasing the hydrophobicity of the fracture surfaces. Therefore, tracer experiments should be conducted in the cores prior to casting.

6.2.2. Multicomponent Effects

For the case of a cation M^{i+} undergoing ion exchange in a hydrogeologic system, the effects of chromatographic separation of the ions should be important only at high values of the M: total cations ratio, for example near the injection well in a cross-well

tracer experiment [*Callahan et al.*, 2001b; 2001c]. It was shown that, for tracer tests in columns of crushed tuff where the concentration of the cation tracer (Li^+) exceeded two-thirds of the total cation equivalents in solution, the apparent retardation of Li^+ relative to the counteranion (Br^-) was less than predicted using a linear isotherm ("K_D") model. Because the solutes were dissolved in solution as LiBr, the high ionic concentration of the nonreactive Br^- had to be balanced by the same number of equivalents of cations. The resident concentrations of Na^+ and Ca^{2+} in the system were too low to balance the Br^- charge, and thus a significant proportion of Li^+ transported along with Br^- in solution.

The injection of large masses and hence high concentrations of chemicals is often necessary in field tracer tests in order to obtain analytically-detectable concentrations at the measurement points due to dilution effects in the injection and production wells and the aquifer. Interpreting the transport data of a reactive solute using a retardation factor approach may be inadequate, especially for media having high sorptive capacities. The data obtained from core 4 were not modeled correctly using a single-component dual-porosity model based on *Tang et al.* [1981] and *Maloszewski and Zuber* [1985]. The data were more accurately interpreted by adding ion exchange equilibria relationships to the applicable transport model.

6.2.2.1. Exchange Coefficients vs. Concentration. Cation exchange coefficients were calculated for $Li^+\backslash Na^+$ and $Li^+\backslash Ca^{2+}$ in single- and dual-continua media [*Callahan et al.*, 2001b, 2001c]. Because the values of these coefficients were determined by minimizing the sum-of-squares differences between the data and the model fits to the data, they are concentration-averaged over the entire transport experiment.

The model is calibrated on two equilibrium constants for Li^+ exchanging with either a monovalent cation or a divalent cation. Batch sorption data for this ternary system would help validate and constrain model calibrations. Typical batch sorption experiments usually focus on solute partitioning as a function of the concentration of only one solute. The sorption of Li^+, which is assumed to undergo ion exchange on the volcanic tuffs, is also a function of the concentrations of the other cations in solution (e.g., Ca^{2+} and Na^+). An experimental program that involves varying the concentrations of all three cations in batch sorption tests would provide data for Li^+ sorption that could be inserted directly into the transport model.

An example test procedure is described as follows. For each rock type, the sorption of Li^+ should be measured in reactor cells using four starting concentrations of Li^+; 1, 10, 100, and 1000 mg L^{-1}. At each initial Li^+ concentration, the concentration of one co-cation would be held constant while varying the concentration of the other, and then vice-versa. An example test protocol is shown in Table 6.1. Na^+ and Ca^{2+} would used because these ions are the main exchangers for Li^+ in groundwater from the C-Wells, as well as water from well J-13, near the C-Wells site, which was used as a surrogate groundwater in the transport experiments of this study. Any similar test matrix could be used for other groundwater systems, depending on the cation chemistry. A similar approach was used by *Vulava* [1998] in his dissertation research on competitive sorption of cations on soils. He showed successfully that the sorption thermodynamics for each cation is dependent not only on its concentration but on the concentrations of the other cations in the system.

Table 6.1. Experimental protocol to measure exchange coefficients as a function of cation concentration.

Li^+	Na^+	Ca^{2+}	Li^+	Na^+	Ca^{2+}	Li^+	Na^+	Ca^{2+}
1	1	1	1	10	1	1	100	1
10			10			10		
100			100			100		
1000			1000			1000		
1	1	10	1	10	10	1	100	10
10			10			10		
100			100			100		
1000			1000			1000		
1	1	100	1	10	100	1	100	100
10			10			10		
100			100			100		
1000			1000			1000		

6.2.2.2. Varying the Injection Concentration of a Reactive Tracer. A series of tracer experiments in a fractured rock core could be conducted where the injection concentration is varied between tests. The experiments would begin with a low concentration test (ionic strength of injectate about an order of magnitude less than that of the groundwater). This would be followed by tests of successively higher concentrations, concluding with a test in which the ionic strength of the injectate is two to three orders of magnitude greater than background. This approach is preferable to starting with a high concentration test, which could complicate interpretation of transport data due to high background concentration effects. This test matrix would indicate the critical concentration at which the single-component dual-porosity model no longer describes reactive tracer transport.

References

Brown, S., A. Caprihan, and R. Hardy, Experimental observation of fluid flow channels in a single fracture, *J. Geophys. Res., 103* (B3), 5125-5132, 1998.

Callahan, T. J., P. W. Reimus, and R. S. Bowman, Influence of Solute Residence Time on Matrix Diffusion in Saturated, Fractured Volcanic Tuffs, in preparation, 2001a.

Callahan, T. J., P. W. Reimus, P. C. Lichtner, and R. S. Bowman, Interpreting Asymmetric Transport Patterns of High Concentration Ionic Tracers in Porous Media, in preparation, 2001b.

Callahan, T. J., P. W. Reimus, P. C. Lichtner, and R. S. Bowman, Multicomponent Effects on the Transport of Cations Undergoing Ion Exchange in Saturated, Fractured Rock, in preparation, 2001c.

Detwiler, R. L., S. E. Pringle, and R. J. Glass, Measurement of fracture aperture fields using transmitted light: An evaluation of measurement errors and their influence on simulations of flow and transport through a single fracture, *Water Resour. Res., 35,* 2605-2617, 1999.

Detwiler, R. L., H. Rajaram, and R. J. Glass, Solute transport in variable-aperture fractures: An investigation of the relative importance of Taylor dispersion and macrodispersion, *Water Resour. Res., 36*(7), 1611-1625, 2000.

Dijk, P., B. Berkowitz, and P. Bendel, Investigation of flow in water-saturated rock fractures using nuclear magnetic resonance imaging (NMRI), *Water Resour. Res., 35,* 347-360, 1999.

Glass, R. J., M. J. Nicholl, and V. C. Tidwell, Challenging models for flow in unsaturated, fractured rock through exploration of small-scale processes, *Geophys. Res. Lett., 22*(11), 1457-1460, 1995.

Maloszewski, P. and A. Zuber, On the theory of tracer experiments in fissured rocks with a porous matrix, *J. Hyd., 79,* 333-358, 1985.

Odling, N. E., P. Gillespie, B. Bourgine, C. Castaing, J. P. Chiles, N. P. Christensen, E. Fillion, A. Genter, C. Olsen, L. Thrane, R. Trice, E. Aarseth, J. J. Walsh, and J. Watterson, Variations in fracture system geometry and their implications for fluid flow in fractured hydrocarbon reservoirs, *Petrol. Geosci., 5*(4), 373-384, 1999.

O'Hara, S. K., B. L. Parker, P. R. Jørgensen, and J. A. Cherry, Trichloroethylene DNAPL flow and mass distribution in naturally fractured clay: Evidence of aperture variability, *Water Resour. Res., 36*(1), 135-147, 2000.

Persoff, P. and K. Pruess, Two-phase flow visualization and relative permeability measurement in natural rough-walled fractures, *Water Resour. Res., 31,* 1175-1186, 1995.

Raven, K. G., K. S. Novakowski, and P. A. Lapcevic, Interpretation of field tracer tests of a single fracture using a transient solute storage model, *Water Resour. Res., 24,* 2019-2032, 1988.

Reimus, P. W., The use of synthetic colloids in tracer transport experiments in saturated rock fractures, unpublished Ph. D. dissertation, The University of New Mexico, Albuquerque, 1995.

Tang, D. H., E. O. Frind, and E. A. Sudicky, Contaminant transport in fractured porous media: Analytical solution for a single fracture, *Water Resour. Res., 17*, 555-564, 1981.

Thompson, M. E., Numerical simulation of solute transport in rough fractures, *J. Geophys. Res., 96* (B3), 4157-4166, 1991.

Tidwell, V. C., R. J. Glass, and W. Peplinski, Laboratory investigation of matrix imbibition from a flowing fracture, *Geophys. Res. Lett., 22*(12), 1405-1408, 1995.

Vulava, V. M., Cation competition in soil materials: Adsorption equilibria and transport, unpublished Ph.D. dissertation, Swiss Federal Institute of Technology (ETH), Zurich, Switzerland, 1998.